NASA TECHNICAL NOTE

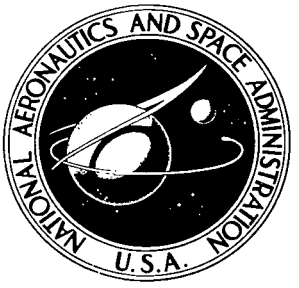

NASA TN D-6256

LOW-SPEED WIND-TUNNEL INVESTIGATION OF A SEMISPAN STOL JET TRANSPORT WING WITH DEFLECTED THRUST AND BLOWING BOUNDARY-LAYER CONTROL

by Robert L. Henderson

Langley Research Center
Hampton, Va. 23365

NATIONAL AERONAUTICS AND SPACE ADMINISTRATION • WASHINGTON, D. C. • JULY 1971

1. Report No.	2. Government Accession No.	3. Recipient's Catalog No.
NASA TN D-6256		

4. Title and Subtitle
LOW-SPEED WIND-TUNNEL INVESTIGATION OF A SEMISPAN STOL JET TRANSPORT WING WITH DEFLECTED THRUST AND BLOWING BOUNDARY-LAYER CONTROL

5. Report Date: July 1971

6. Performing Organization Code:

7. Author(s): Robert L. Henderson

8. Performing Organization Report No.: L-7543

9. Performing Organization Name and Address:
NASA Langley Research Center
Hampton, Va. 23365

10. Work Unit No.: 136-62-02-03

11. Contract or Grant No.:

12. Sponsoring Agency Name and Address:
National Aeronautics and Space Administration
Washington, D.C. 20546

13. Type of Report and Period Covered: Technical Note

14. Sponsoring Agency Code:

15. Supplementary Notes:

16. Abstract

An investigation of the static longitudinal aerodynamic characteristics of a semispan swept wing with an aspect ratio of 3.92 and having deflected thrust and blowing boundary-layer control was performed mainly in a low-speed tunnel with a 3.7-m (12-ft) octagonal test section at the Langley Research Center. Thrust was provided by two pod-mounted ducted fans equipped with 60° exhaust deflection vanes, and boundary-layer control was provided by air blowing through a slot over a full-span plain trailing-edge flap.

17. Key Words (Suggested by Author(s)):
Boundary-layer control
Deflected thrust
STOL configurations

18. Distribution Statement:
Unclassified – Unlimited

19. Security Classif. (of this report)	20. Security Classif. (of this page)	21. No. of Pages	22. Price*
Unclassified	Unclassified	86	$3.00

*For sale by the National Technical Information Service, Springfield, Virginia 22151

LOW-SPEED WIND-TUNNEL INVESTIGATION OF A SEMISPAN STOL JET TRANSPORT WING WITH DEFLECTED THRUST AND BLOWING BOUNDARY-LAYER CONTROL

By Robert L. Henderson
Langley Research Center

SUMMARY

An investigation of the static longitudinal aerodynamic characteristics of a semispan swept wing with an aspect ratio of 3.92 and having deflected thrust and blowing boundary-layer control was performed mainly in a low-speed tunnel with a 3.7-m (12-ft) octagonal test section at the Langley Research Center. Thrust was provided by two pod-mounted ducted fans equipped with 60^{o} exhaust deflection vanes, and boundary-layer control was provided by air blowing through a slot over a full-span plain trailing-edge flap.

The results of the investigation showed that the model gave maximum trimmed lift coefficients of up to 9.85 at a flap setting of 50^{o}, a blowing momentum coefficient of 0.335, and a gross-thrust coefficient of 4.18. Maximum trimmed lift coefficients of up to 7.70 were achieved with the critical engine inoperative and with the model trimmed in roll for a gross-thrust coefficient of 3.17 and a blowing momentum coefficient of 0.206. On the basis of an operational speed margin of 30 percent above the stall speed with one engine out, these maximum lift coefficients would allow a transport aircraft having an engine-out thrust-weight ratio of 0.45 to approach and land at a lift coefficient of from 4.00 to 5.00. Limited lateral data indicated that outboard engine failure would result in large out-of-trim rolling and yawing moments.

INTRODUCTION

There has been much interest recently in the development of a short take-off and landing (STOL) jet transport aircraft. Wind-tunnel models tested to date have demonstrated several concepts designed to produce the high lift necessary for STOL operation while allowing for efficient cruise. In most of these models, engine power is used to lift as well as to propel. Powered lift may be achieved through high-lift devices operated by power or bleed-air taken from the engine, or through some means of thrust deflection. Such powered lift systems may include the use of auxiliary engines or power systems in addition to the main propulsion systems.

Conventional high-lift devices such as mechanical trailing-edge flaps are near their limits in ability to produce lift. Flow separation on the upper surface of the flap results in lift below that predicted by theory for attached flow. However, this flow separation can be prevented through the use of boundary-layer control (BLC), either by removing the boundary-layer air through suction slots or by blowing air over the upper surface of the flap. By such means the theoretical lift of the wing (maximum lift coefficient on the order of 5) can be produced at a relatively low cost in power. Flow attachment is also achieved by the jet-flap concept, in which all of the engine exhaust is directed over a flap. The flattened, deflected exhaust jet gives supercirculation lift and jet reaction lift as well. Although the jet-flap concept is effective in producing lift, the thrust losses due to directing, flattening, and turning the exhaust jet can be rather high in some applications.

Based on simplified analysis it can be shown that the use of boundary-layer control to produce theoretical wing lift in combination with highly deflected engine thrust will allow an aircraft having a thrust-weight ratio of 0.5 to achieve a maximum lift coefficient of about 10. This estimate neglects the effect of jet interference and the effect of out-of-trim moments on engine thrust requirements for trimmed flight. The present investigation was made to provide some basic information on this concept, including a measure of the interference effects for various engine positions.

Tests were conducted with two flap deflections, flaps of two different chords, and four engine positions. Each configuration was tested through an angle-of-attack range for several different values of engine thrust and flap blowing momentum coefficients. Force and moment data were recorded at each angle of attack, and downwash was measured for one configuration at 0° angle of attack. Tests with one engine inoperative were performed to allow estimation of the engine-out characteristics.

SYMBOLS

The longitudinal data are referred to the stability-axis system and the lateral data are referred to the body-axis system. (See fig. 1.) The origin of the axes was located to correspond to the center-of-gravity position (0.285 mean aerodynamic chord).

In order to facilitate international usage of data presented, dimensional quantities are presented both in the International System of Units (SI) and in the U.S. Customary Units. The measurements and calculations were made in U.S. Customary Units. Equivalent dimensions were determined by using the conversion factors given in reference 1.

A aspect ratio, $b^2/2S$

A_e exhaust area, m^2 (ft^2)

b wing span (twice semispan), m (ft)

$\bar{c}$ mean aerodynamic chord, m (ft)

C_D drag coefficient, D/qS

$C_{D,intake}$ engine air intake momentum drag coefficient

C_l rolling-moment coefficient, M_X/qSb

$\Delta C_{l,t}$ theoretical section lift increment due to flap deflection

C_L lift coefficient, L/qS

ΔC_L lift loss due to roll trim

$C_{L,max}$ maximum lift coefficient

$C_{L,trim}$ lift coefficient with pitch trim supplied by a lift load on a tail 3.5 chords aft of the wing

C_m pitching-moment coefficient, $M_Y/qS\bar{c}$

C_n yawing-moment coefficient, M_Z/qSb

C_T thrust coefficient, T/qS

C_μ blowing momentum coefficient, F_R/qS

$C_{\mu,t}$ section blowing momentum coefficient required for theoretical lift

D drag, N (lb)

F_R static jet reaction of flap blowing, N (lb)

F_X force directed along X-axis of model, N (lb)

F_Z	force directed along Z-axis of model, N (lb)
L	lift, N (lb)
M_X	rolling moment, m-N (ft-lb)
M_Y	pitching moment, m-N (ft-lb)
M_Z	yawing moment, m-N (ft-lb)
q	free-stream dynamic pressure, N/m^2 (lb/ft^2)
R	Reynolds number based on $\bar{c}$
S	area of semispan wing, m^2 (ft^2)
T	static thrust, N (lb)
V	velocity, m/sec (ft/sec)
W	weight of aircraft, L, N (lb)
x	chordwise station measured from basic airfoil nose, percent chord
X	body reference axis, wing root chord line
y	distance normal to chord line, percent chord
Y	body reference axis, normal to reflection plane
Z	body reference axis, normal to wing chord plane
α	angle of attack, deg
γ	flight-path angle, $-\tan^{-1}\left(C_D/C_L\right)$, deg
δ_f	flap deflection measured streamwise, deg
ϵ	downwash angle, deg

( )' denotes value before tunnel-wall corrections

Subscripts:

L left wing

R right wing

ext extended chord flap

MODEL AND APPARATUS

The investigation was conducted on a semispan model wing with two pod-mounted engines and a plain trailing-edge flap. Figures 2(a) to 2(c) show photographs of the model mounted on a portion of its reflection plane, and figure 2(d) illustrates the position of the wing and its reflection plane mounted in a low-speed tunnel with a 3.7-m (12-ft) octagonal test section at the Langley Research Center (designated 3.7-m tunnel herein). The reflection plane was mounted on legs bolted to the tunnel floor, and the wing was mounted above the reflection plane by means of a $1\frac{1}{2}$-inch pipe fastened in the wing and extending down through an opening in the reflection plane. The pipe was rigidly mounted to a strain-gage balance which rotated in pitch with the wing.

Sketches of the model appear in figure 3 and dimensional characteristics are given in table I. A three-view drawing of the model including a half-fuselage used in some tests is shown in figure 3(a). Detail sketches of the wing section and blowing system appear in figure 3(b), and the section airfoil coordinates are given in table II.

The flap deflection angle was set by brackets fastened to both the wing and the flap at three locations along the span. High-pressure boundary-layer control air passed through a flexible hose into a tapered blowing tube mounted in the wing just ahead of the flap and was blown rearward through 96 small holes drilled in the tube. The hole diameter was 0.2 percent local wing chord, with 4 percent chord spanwise spacing between holes. The blowing air then impinged on the upper surface of the flap and passed through a small gap between the flap and a flat metal sheet mounted to the wing trailing edge. The flat metal sheet was flexibly mounted so that the gap size was determined by the blowing pressure used (the gap was closed when no blowing pressure was applied). A trailing-edge flap extension nearly doubling the original flap chord was employed during most of the tests. The model engines were ducted fans and were tip-jet driven by compressed air. They were sized to represent high-bypass-ratio turbofan engines capable of providing a thrust-weight ratio of about 0.60 for a representative jet STOL transport.

The two identical nacelles sketched in figure 3(c) were mounted together as a pod in the various positions shown in figure 3(d). The thrust deflection angle was set at 60^{o} by turning vanes which were mounted to each engine exhaust.

In addition to force and moment data obtained through a standard tunnel data acquisition system, some data were also obtained from a free-pivoting balsa vane which measured the downwash at a location representing that of a high horizontal tail. (See fig. 3(a).)

WIND TUNNEL AND CORRECTIONS

The tests were conducted mainly in a 3.7-m tunnel using the setup illustrated in figure 2(d). The reflection plane was 2.44 m (8.00 ft) long and 2.13 m (7.00 ft) wide, and the model was mounted in the center. Because of the unusual shape of the tunnel test section, tests were also made by installing the same apparatus in the 9.1- by 18.3-m (30- by 60-ft) test section of the Langley full-scale tunnel to determine the tunnel-wall corrections experimentally. The following corrections were determined and were applied to all data from the 3.7-m tunnel:

$$\alpha = \alpha' + 0.579C_L'$$

$$C_D = C_D' + 0.0101C_L'^2$$

$$C_L = C_L' - 0.0101C_L'C_D'$$

No blockage corrections were applied.

TESTS

Tests were made for a range of angle of attack, engine thrust coefficient C_T, and flap blowing momentum coefficient C_μ for each of several configurations. The basic configuration was that with the aft engine position and with the extended chord flap deflected 50^{o}. From this configuration, changes were made to determine the individual effects of:

Engine location (forward and far aft)
Reduction in flap chord (short chord flap)
Increased flap deflection to 65^{o} (for either flap chord)
Removal of engine nozzle turning vanes

Raising engine nozzles closer to trailing edge of wing (for far aft engine position)
Inoperative outboard engine
Presence of a fuselage (for the far aft engine position)
Presence of engines (by removing engines)

Engine thrust was set from a static thrust calibration of the engine thrust as a function of rpm, and the values of thrust coefficient given are based on this static thrust calibration for each exit vane configuration. The effect of forward speed on the thrust calibration at constant rpm was not determined experimentally, but simple calculations based on momentum relations would indicate that the engine gross thrust was no more than 3 percent greater than the static thrust for a value of C_T of 4.00 and was no more than 6 percent greater than the static thrust for a value of C_T of 2.00. Similar momentum calculations indicate that the intake momentum drag coefficient was approximately

$$C_{D,intake} = \sqrt{2\frac{A_e}{S} C_T}$$

The thrust deflection angle produced by the exhaust nozzle turning vanes was measured for the static thrust condition and was found to be nearly 60^o for all thrust settings and exit vane configurations.

The BLC blowing momentum was measured under static conditions with the flap in place for each flap configuration. The jet reaction force so measured was used to determine the momentum coefficients presented with the data. Although no exact measurements were made, related tests indicated that the value of the momentum of the air leaving the blowing slot, before skin friction and turning losses over the flap, was nearly 25 percent greater than the measured jet reaction.

Engine-out tests were run with the outboard engine inoperative, as this condition resulted in both lower lift and larger out-of-trim moments than were observed in preliminary tests with the inboard engine inoperative. Differences in the rolling and yawing moments measured for the wing with two engines operative and with one engine operative were used to estimate full-span out-of-trim moments due to engine failure.

Tests in both wind tunnels were run at approximately the following conditions:

$V = 12.2$ m/sec (40 ft/sec)

$q = 85.2$ N/m^2 (1.78 lb/ft^2)

$R = 0.35 \times 10^6$

PRESENTATION OF RESULTS

Results of the investigation are presented in the following figures:

The longitudinal data showed a smooth variation with angle of attack for all configurations, except at the stall. A few tests showed that, as the angle of attack was slowly increased, an angle was reached at which the lift, drag, and pitching moment rapidly became smaller in magnitude. A reduction in angle of attack of approximately 5^o resulted in as rapid an increase in the magnitude of the forces and moments. Tuft studies tended to confirm the conclusion that flow separation near the wing leading edge produced this effect of hysteresis. The dashed lines shown in some data curves at the stall only indicate that hysteresis was observed. The angles of attack for loss of flow attachment and for flow reattachment were not measured, and would likely have different values at full-scale Reynolds numbers in any event.

DISCUSSION OF RESULTS

Preliminary tests were run with a 12.5-percent-chord leading-edge slat having 18^o downward tilt. A Krueger leading-edge flap was used in most of the tests, however, because the Krueger flap gave as much as 10^o higher stall incidence than did the slat for similar thrust and blowing momentum coefficients. Because the higher stall angles were considered more representative of full-scale characteristics, all the data presented were obtained with the Krueger flap on the main part of the wing. (The slat remained on the inboard 10 percent of the wing semispan, however.) The Krueger flap chord was 12 percent of the wing chord at the sweep break, tapering to 18 percent at the wing tip.

Basic Aerodynamic Data

Aft engine position, extended chord flap.- Longitudinal data obtained for the basic model with the aft engine position and the 50^o extended chord flap are presented in figure 4. These data show that increases in either thrust coefficient or blowing momentum coefficient had the effect of increasing the stall incidence slightly and increasing maximum lift substantially. A maximum lift coefficient of about 10.20 was reached for a gross-thrust coefficient of 4.18 and a blowing momentum coefficient of 0.335. Associated with high lift were large nose-down pitching moments which increased with increasing blowing but which were practically unaffected by engine thrust. The addition of a down-load at a tail 3.5 wing chords aft of the center of gravity to provide pitch trim results in a trimmed maximum lift coefficient of about 9.85.

Longitudinal data for the model with the outboard engine inoperative and the 50° extended chord flap are presented in figure 5. These data show that, for given thrust and blowing levels, lift and drag were slightly lower in this condition than in the two-engine case of figure 4. Pitching moments for the two cases are nearly identical. No correction was applied to the drag data for the model with the engine inoperative. The lift loss noted with the outboard engine inoperative was associated with a disturbed region of flow over the upper surface of the wing behind the inoperative engine, as evidenced by tuft studies. It is probable that the reduced span of the engine exhaust resulted in a decrease in the jet-flap effect of the engine exhaust jet as well.

Basic longitudinal data for the model with the aft engine position and the extended chord flap deflected 65° are presented in figure 6. A comparison of these data with the data of figure 4 reveals that, after corrections are applied for the different thrust and blowing momentum coefficients used, changing flap deflection from 50° to 65° had little effect on the aerodynamic characteristics of the model other than to increase drag.

Basic longitudinal data for the model with turning vanes removed from the engine exhaust, and with thrust deflected by the extended chord flap deflected 50°, are presented in figure 7. A comparison of the data of figure 7 with the data of figure 4 shows that removal of the turning vanes was very detrimental to the lift and drag characteristics of this particular configuration.

Aft engine position, short chord flap.- Basic longitudinal data for the wing with the aft engine position and the 50° short chord flap are presented in figure 8. Comparison of these data with those of figure 4 shows that, after corrections for the different thrust and blowing momentum coefficients used, the reduced flap chord resulted in lower lift production, lower drag, and less negative pitching moments. Figure 9 presents basic longitudinal data for the 65° short chord flap and the aft engine position. The lift, drag, and pitching-moment coefficients shown are nearly identical to those of figure 8, indicating that the effects of this increase in flap deflection angle were minor, just as they were for the model with the extended chord flap.

Forward engine position, short chord flap.- Tests on the model with the 50° short chord flap and the forward engine position resulted in the data presented in figure 10. Comparison of this figure with figure 8 shows that the effects of moving the engine forward were to reduce lift slightly for power-on conditions and to cause nose-up pitching moments which increased with increasing thrust. One point of interest in connection with these nose-up pitching moments is that in a conventional configuration the upload at the tail required to give pitch trim might be expected to contribute to speed instability, and the pitching moment changes with throttle setting changes would add to the piloting task. It is expected that the effects of engine position would be the same for the model with the extended chord flap.

Figure 11 presents the data obtained from tests of the model with the short chord flap deflected 65° and the engines in the forward position. Comparison of this figure with figure 10 shows that, again, this increase in the flap deflection had negligible effects on the basic longitudinal data.

Far aft engine position, extended chord flap.- The far-aft-engine configurations were tested in order to determine whether moving the jet exhaust rearward to replace the inboard part of the flap might result in additional lift. The part of the flap directly behind the engines was set at a reduced deflection and its chord extension was removed. Data obtained from tests on the model with the engines in the far aft position (see fig. 3(d)) and the extended chord flap deflected 65° are presented in figure 12. These data may be compared with those of figure 6 after corrections for the different thrust and blowing momentum coefficients used. A slight increase in lift due to thrust is associated with the far aft engine position, but the wing contribution to lift is generally somewhat lower than for the configuration of figure 6. A large nose-down pitching moment due to thrust is apparent in figure 12, so that trimmed lift would be below the levels of figure 6.

Data taken for a similar configuration with the engine exhaust raised nearer the wing chord line (see fig. 3(d)) are presented in figure 13. (Note that the turning vanes in the engine exhaust were also tilted so that the exhaust angle relative to the wing was the same as with the engines not tilted.) Comparison of these data with those of figure 12 shows that raising the engine exhaust and flap trailing edge in this manner produced small increases in lift for similar thrust and blowing levels, but the nose-down pitching moments associated with engine thrust were also larger. The configuration also produced less lift and larger nose-down pitching moments than the configuration of figure 6, which had the aft engine position and the 65° extended chord flap.

Effect of fuselage.- Figure 14 presents uncorrected data on the lift and drag characteristics at an angle of attack of 0° for the configuration of figure 13, both with and without a half-fuselage mounted on the reflection plane. The data show that the effects of the fuselage on the aerodynamic characteristics were apparently small enough to justify the presentation of test data without corrections for the presence of a fuselage, at least for small angles of attack.

Engines removed, short chord flap.- Tests of the model with the short chord flap deflected 50° and the engines removed resulted in the basic longitudinal data presented in figure 15. Comparison of these data with those of figures 8 and 10 shows that for either the forward or the aft engine position, the engines in the stopped condition ($C_T = 0$) caused some loss in maximum lift and an increase in the drag coefficient at low lift coefficients.

Lift Characteristics

Effects of blowing over the flap.- The lift coefficient of the wing at $\alpha' = 0^{\circ}$ is presented as a function of the flap blowing momentum coefficient in figure 16. The data are presented for the configuration with the engines mounted on the wing but inoperative ($C_T = 0$), except for some data taken with the engines removed. The lift produced without blowing was far less than that predicted by application of the theory of reference 2. (See appendix.) Small amounts of blowing produced large gains in lift until the lift coefficient reached the value predicted for attached flow. Beyond this value of momentum coefficient, the lift gains with increased blowing were not as large. However, for the range of momentum coefficients investigated, the lift increment due to increased blowing remained several times larger than the jet reaction lift component of the blowing increment, apparently because of the jet-flap effect of the blowing air sheet.

The blowing momentum coefficient required to bring the flap to its theoretical effectiveness is shown for various levels of the theoretical lift increment due to flap deflection in figure 17. Data in the figure were reduced to sectional form by the method of reference 2. The correlation band shown summarizes the data obtained from other models (refs. 3 and 4) in which the blowing slot width was less than 0.1 percent chord. From this figure it is apparent that the blowing system of the present model was relatively inefficient. Differences in the test conditions (including Reynolds number) from those in references 3 and 4 may explain a part of this inefficiency. Another factor may be the uneven distribution of blowing momentum over the wing span. (See fig. 18.) The blowing slot was not even in size and was not narrow enough to eliminate variations in sectional momentum coefficient caused by the rather large hole spacing (20 hole diameters) along the blowing tube. It is expected that even an approximate tailoring of the blowing momentum to sectional requirements as suggested in reference 5 would result in a substantial reduction in the blowing momentum required to achieve theoretical flap effectiveness.

Effects of deflected thrust.- The lift produced by the wing is supplemented by lift produced by the deflected engine thrust. This thrust is a vector quantity, with components in the lift and drag directions. Additional drag arises from the intake of free-stream air by the engines. Addition of these components to the lift and drag of the wing with engines inoperative is shown by the dashed lines in figure 19. A comparison of these lines with the points shown for engine-on conditions shows that lift and drag may indeed be roughly predicted in this manner. At high angles of attack, some additional lift was obtained because the stall angle was increased by the application of power. Appreciable lift interference due to a jet-flap effect was not evident for either the aft engine position (fig. 19(a)) or for the forward engine position (fig. 19(b)). For both far aft engine positions, the flap chord reduction aft of the engine exhaust led to power-off lift below that shown in figure 6. However, in figures 6, 12, and 13, power-on lift is nearly the same, apparently because of the jet-flap effect of the engine exhaust. Figures 19(c) and 19(d) show the favorable

interference effect of thrust on lift for the far aft engine positions. Similar jet interference effects were noted in reference 6.

A comparison of the lift produced by the present model with that from other powered-lift concepts is presented in figure 20. This figure shows that the internal-flow jet-flap configuration of reference 7 makes very efficient use of thrust to provide lift. The external-flow jet-flap configuration of reference 8 is somewhat less efficient, probably because of the nonuniform blowing along the flap span. The present model shows lift production generally between those of the other models, at least for blowing levels high enough to attach the flow. The lines connecting points of various flap blowing levels and constant engine thrust levels show that considerable lift gains were achieved with increasing blowing. The cost of providing blowing might be expressed either as a loss in lift (e.g., auxiliary compressor weight) or as an increase in engine thrust required (before engine compressor air bleed). Figure 20 and subsequent figures do not include any such correction.

A blowing system similar to that of the present investigation was installed in a full-scale jet transport aircraft. The source of air was compressor bleed from the low-bypass-ratio engines. The data of reference 9 indicate that the blowing momentum was only half the thrust loss due to air bleed from the engines. For high-bypass-ratio turbofans this cost would be larger, the maximum available quantity of bleed air would be small, and the reduction in deflected thrust would reduce the lift produced substantially. In this case, an onboard compressor should be considered as a potential source of BLC air.

Another correction might involve the addition of an assumed thrust loss, due to the turning of the engine exhaust, to the thrust coefficients presented. This loss may be reduced to 5 percent or lower with properly designed turning vanes, as shown in reference 10. No correction has been applied to thrust for such turning losses. For the jet-flap model data presented (refs. 7 and 8), C_{μ} was assumed to be comparable to C_T.

Stability and Trim Characteristics

Longitudinal.- From the basic aerodynamic data of figures 4 to 13, the longitudinal stability and trim characteristics of the wing-alone configuration can be assessed. From these data the longitudinal stability of a complete aircraft configuration can be estimated if the contribution of the horizontal tail is known. However, the contribution of the horizontal tail to pitch stability may be only roughly estimated in this case because data on the variation of downwash at the tail with angle of attack and data on the dynamic pressure at the tail were not obtained. The conditions at the tail might be expected to be similar to those of the external-flow jet-flap model of reference 7, however, in which a high tail was found to be effective in producing both stability and trim. Nevertheless, the contribution

of the tail to stability should be a matter of concern because of the high inboard concentration of powered lift. This concentration might cause the tail to be in the downwash associated with the engine jet sheet. A severe pitchup could occur as it did for the model of reference 11.

The downwash angle was measured for $\alpha' = 0^{o}$ and was found to agree closely with measurements on similar powered-lift models, as shown in figure 21. All the data points in this figure are seen to lie below the values predicted by theory for downwash well behind a wing producing all its lift by circulation. The downwash could be expected to be below the theoretical value for these models because the higher lift coefficients were achieved with the help of deflected thrust. A large nose-down pitching moment is associated with high lift for the models of references 7 and 8. Thrust deflected near the trailing edge of the wing had the same effect on the present model (see figs. 12 and 13). For all engine positions, the pitching moment due to engine thrust was very nearly equal to the thrust multiplied by a moment arm from the thrust line to the assumed center of gravity. If all thrust levels are considered, the aft engine position showed the lowest pitching-moment magnitudes and would therefore make the lowest pitch trim demands on a horizontal tail. The demands on the pilot imposed by pitch trim changes due to engine thrust changes are also light for this engine position, and trimmed lift was as good as with any other configuration.

Lateral.- No information concerning lateral stability could be obtained with a semi-span model, but an approximate indication of the lateral trim problem with one engine inoperative was obtained by averaging data from tests with one engine inoperative with data from tests with both engines operating. Data presented in figures 4 and 5 have been used to synthesize the case presented in figure 22 of a "right wing" with two engines operating and a "left wing" with one engine operating. It might be noted that the engine-out rolling moment shown in figure 22(a) was of approximately the magnitude of the normal force due to outboard engine operation multiplied by the moment arm from the reflection plane to the outboard engine center line and could be kept small by positioning the engines well inboard. The data of figure 22(a) show that trim could be achieved by means of differential blowing over the flaps, although rather large adverse yawing moments were produced. These yawing moments are of a magnitude, however, that could be overcome by the use of a large vertical tail equipped with boundary-layer control over the rudder. Also, roll trim by differential blowing requires a large amount of air in order to maintain lift (fig. 22(b)), and even an improved blowing system would not allow a significant reduction in blowing momentum except at a high cost in lift. Other means of producing roll trim moments without the need for additional blowing air include differential flap deflection, tip spoilers, or raising an outboard portion of the flap as an aileron, with or without continued blowing. An engine-out rolling-moment coefficient of $C_{\ell} = 0.18$ might be trimmed with a lift loss of approximately $\Delta C_L = 0.30$ below the stall by means of wing-tip lift

differential (i.e., spoilers or up-aileron on one tip, with increased blowing on the other tip). Still, the adverse yawing moment due to roll trim might be the factor which determines the type of roll trim used.

Performance

Drag polars for the present model at two levels of flap blowing momentum are presented in figure 23(a) with a drag polar from the data in reference 8. Figure 23(b) presents similar polars for engine-out operation with the models nearly trimmed in roll. The data points were taken from figures 4 and 5. These figures show that for similar thrust levels and flap deflection angles the present model had much less drag, probably because of a better spanwise lift distribution. Lift production is shown to be better than that for the external-flow model, even with the lower flap blowing momentum. The dashed lines in figure 23 show various glide-path angles in steady flight. These intersect the data curves at angles of attack well below the stall angle for a conventional -3° glide-path angle. A STOL approach at -6° glide-path angle may be achieved by raising angle of attack, and the -9° glide-path angle may be reached while maneuvering. The desirable margin of 10° angle of attack below the stall angle is not always maintained, but could be with increased thrust deflection.

A flight envelope (curves of flight-path angle as a function of lift coefficient for various thrust-weight ratios) prepared from the data of figure 4(b) is shown in figure 24. The blowing momentum of these data was approximately sufficient to attach the flow, $C_{\mu} = 0.078$. A blowing momentum coefficient of this magnitude is approximately the maximum bleed air available in approach conditions from representative high-bypass-ratio (6 to 8) engines sized to give a nominal airplane thrust-weight ratio of 0.60. The critical maneuver for this type of aircraft is a wave-off and go-around with full power, at the approach speed, with one engine inoperative. For a four-engine STOL transport with a thrust-weight ratio of 0.60, this corresponds to operation at a thrust-weight ratio of 0.45. Figure 24 shows a maximum lift coefficient of about 7.80 for this thrust-weight ratio, permitting flight at a lift coefficient of 4.60, assuming a 30-percent speed margin above stall speed. It is assumed that the cost of trimming the rolling and yawing moments associated with engine-out flight can be kept small. The flight-path angle of approximately -3° could be raised for wave-off or lowered for a steep STOL approach by changing the thrust deflection angle with very little change in lift. For example, in the case above, a 10° rearward rotation of the exhaust nozzles would be adequate to produce level flight and would cause a lift deficiency of only 4 percent, which could be made up by a 1° increase in angle of attack.

However, the blowing momentum available is not likely to correspond to a constant value of C_{μ} throughout the aircraft flight envelope. Instead, an onboard compressor, for example, might provide a blowing momentum equal to a small constant percentage of the aircraft landing weight. Interpolation of the data in figure 4 allowed a flight envelope

to be found for the case $C_\mu = 0.02C_L$, as presented in figure 25. For engine-out approach, figure 25 shows a maximum lift coefficient of about 9.00 for a thrust-weight ratio of 0.45. Flight at 30 percent above stall speed is then possible at a lift coefficient of 5.30, neglecting the cost of trimming engine-out asymmetries.

Figure 26 presents data from references 7 and 8 and the present study showing the thrust-weight ratio required to fly level at a given lift coefficient. In figures 24, 25, and 26 the thrust-weight ratio $C_T/C_{L,trim}$ is a measure of the engine size, for which the closest equivalent is $C_\mu/C_{L,trim}$ in jet-flap investigations. The points shown in figure 26 were obtained from data near an angle of attack of 0^o for similar flap and thrust deflection angles. Reduced data from figure 4 show that under high-lift conditions the present model requires far more thrust than the internal flow jet-flap model of reference 7, but somewhat less thrust than the external-flow model of reference 8.

SUMMARY OF RESULTS

A wind-tunnel investigation of a semispan wing with deflected engine thrust and blowing boundary-layer control gave the following results:

1. The configuration gave maximum trimmed lift coefficients of up to 9.85 at a 50^o flap setting, a blowing momentum coefficient of 0.335, and a gross thrust coefficient of 4.18.

2. The induced lift due to engine operation was small but generally favorable. More rearward engine positions resulted in slight increases in lift production, but trimmed lift would be lower because of the increased down-load on the tail required for trim.

3. The drag induced by lift of the model was significantly lower than that of some STOL concepts, evidently because of a more uniform spanwise lift distribution.

4. Pitching and rolling moments due to engine operation were essentially equal to the forces due to engine operation multiplied by the appropriate moment arms from the engine exhaust to the assumed center of gravity.

5. For the aft engine position, there was negligible pitching moment due to engine thrust. Since there was little, or no, advantage to having the engines in a different location, the aft position seems favorable in that it minimizes tail design requirements as well as piloting problems.

6. The rather large rolling moments due to engine failure on an aircraft based on the present concept could be trimmed by increased blowing on the engine-out wing, but the resulting adverse yawing moment would require that a conventionally sized vertical tail be equipped with blowing on the rudder in order to provide yaw trim.

Langley Research Center,
National Aeronautics and Space Administration,
Hampton, Va., May 13, 1971.

APPENDIX

THEORETICAL FLAP EFFECTIVENESS

The increment in lift due to flap deflection in two-dimensional incompressible inviscid flow may be found (as a function of flap chord and deflection) by exact theory, as described in reference 2. The corrections for aspect ratio, flap span, sweep, and taper are included in the following formula:

$$\Delta C_L = -a\left(\Delta\alpha_{0_L}\right)_{wing} \approx \left(-\Delta\alpha_{0_L}\right)_{section} \frac{S_f}{S} \frac{a_0 \cos \Lambda}{1 + \frac{18.24}{A}(1 + \tau)a_0}$$

where

$\Delta\alpha_{0_L}$ theoretical change in angle of attack for zero lift

a_0 two-dimensional lift-curve slope

a three-dimensional lift-curve slope

Λ sweep of quarter-chord line

S_f flapped wing surface

τ Glauert correction factor for taper and aspect ratio

For $\frac{S_f}{S} = 0.86$, $\cos \Lambda = 0.91$, $A = 7.84$, and $\tau = 0.015$, the 50^o deflection of a 22.5-percent-chord flap gives $\left(-\Delta\alpha_{0_L}\right)_{section} = 28.5^o$ and $a_0 = 0.1062$, giving $\Delta C_L = 1.89$. The 65^o deflection of a 22.5-percent-chord flap gives $\left(-\Delta\alpha_{0_L}\right)_{section} = 36.5^o$ and $a_0 = 0.1044$, giving $\Delta C_L = 2.40$. At 0^o angle of attack and 0^o flap deflection, the wing lift coefficient was measured as 0.32 with the short-chord flap and the leading-edge slat (rather than the Krueger flap, which reduced lift at low angles of attack when no flap blowing was applied). Thus, the lift coefficients to be expected from the wing at 0^o angle of attack and 50^o and 65^o flap deflections are 2.21 and 2.72, respectively. These are given in figure 16 as dashed lines which cross the curves of lift plotted against blowing momentum coefficient for the short chord flap deflected 50^o and 65^o at $C_\mu = 0.069$ and 0.127, respectively. The extended chord flap for the same deflections and blowing momentum coefficients shows lift coefficients of approximately 2.78 and 3.22, respectively.

REFERENCES

1. Mechtly, E. A.: The International System of Units – Physical Constants and Conversion Factors (Revised). NASA SP-7012, 1969.

2. De los Santos, S. T.; Chaplin, H. R.; and Harkleroad, E. L.: Correlation of Wind-Tunnel Measurements on the Basis of Blowing Momentum Required to Produce Theoretical Flap Effectiveness on Airplane Models Equipped With Boundary-Layer-Control Devices. Aero Rep. 891, David W. Taylor Model Basin, Navy Dep., Dec. 1955.

3. Van den Berg, B.: Windtunnel Investigation With a Two-Dimensional Airfoil on the Effect of Blowing Over a Flap and Over a Control Surface. Rep. MP. 215, Nat. Lucht- Ruimtevaartlab. (Amsterdam), Sept. 1962.

4. Eyre, R. C. W.; and Butler, S. F. J.: Low Speed Wind Tunnel Tests on an A.R.8 Swept Wing Subsonic Transport Research Model With B.L.C. Blowing Over Nose and Rear Flaps for High-Lift. Tech. Rep. 67112, Brit. R.A.E., May 1967.

5. Johnston, G. W.: Recent Advances in STOL Aircraft Design and Operation. AIAA Paper No. 64-183, May 1964.

6. Carter, Arthur W.: Effects of Jet-Exhaust Location on the Longitudinal Aerodynamic Characteristics of a Jet V/STOL Model. NASA TN D-5333, 1969.

7. Turner, Thomas R.: Low-Speed Investigation of a Full-Span Internal-Flow Jet-Augmented Flap on a High-Wing Model With a 35^{o} Swept Wing of Aspect Ratio 7.0. NASA TN D-434, 1960.

8. Freeman, Delma C., Jr.; Parlett, Lysle P.; and Henderson, Robert L.: Wind-Tunnel Investigation of a Jet Transport Airplane Configuration with an External-Flow Jet Flap and Inboard Pod-Mounted Engines. NASA TN D-7004, 1970.

9. Gratzer, L. B.; and O'Donnell, T. J.: The Development of a BLC High-Lift System for High-Speed Airplanes. AIAA Paper No. 64-589, Aug. 1964.

10. Scherrer, Richard: Synthesis of Future High Lift Systems. [Preprint] 700811, Soc. Automot. Eng., Oct. 1970.

11. Parlett, Lysle P.; and Shivers, James P.: Wind-Tunnel Investigation of an STOL Aircraft Configuration Equipped With an External-Flow Jet Flap. NASA TN D-5364, 1969.

TABLE I.- DIMENSIONS OF MODEL

Wing:		
Area, m^2 (ft^2)	0.521	(5.61)
Semispan, cm (in.)	142.88	(56.25)
Semispan aspect ratio	3.92	
Length of mean aerodynamic chord, cm (in.)	39.12	(15.40)
Location of quarter chord of mean aerodynamic chord, reference to root chord leading edge, cm (in.)	34.70	(13.66)
Spanwise location of mean aerodynamic chord, cm (in.)	59.44	(23.40)
Root chord, cm (in.)	50.80	(20.00)
Tip chord, cm (in.)	19.05	(7.50)
Break station chord, cm (in.)	50.80	(20.00)
Spanwise station of break station, cm (in.)	14.22	(5.60)
Sweep of quarter-chord line:		
Inboard panel, deg	0	
Outboard panel, deg	25.00	
Dihedral, deg	0	
Geometric twist, deg	0	
Basic airfoil	NACA 65_1-412	
Flap:		
Break station chord, cm (in.)	15.24	(6.00)
Tip chord, cm (in.)	5.72	(2.25)
Hinge-line station, percent chord	77	
Sweep of hinge line, deg	17.5	
Flap leading-edge radius at break, cm (in.)	2.59	(1.02)
Flap leading-edge radius at tip, cm (in.)	0.965	(0.38)
Length of flap extension at break, cm (in.)	13.97	(5.50)
Length of flap extension at tip, cm (in.)	5.23	(2.06)
Flap extension angle, referenced to chord line, deg	16.7	
Gap station on upper surface, percent chord	77	
Blowing tube inside diameter, percent chord	2.0 to 2.5	
Blowing hole spacing along tube, percent chord	4.0	
Blowing hole diameter, percent chord	0.20	
Blowing jet inclination to chord line, deg	0 (approx.)	
Blowing jet inclination to reflection plane, deg	0 (approx.)	
Krueger flap length, percent chord (root)	12	
Krueger flap length, percent chord (tip)	18	
Krueger flap deflection from wing, deg	110	
Nose radius of inboard half-span, cm (in.)	0.63	(0.25)
Nose radius of outboard half-span, cm (in.)	0.31	(0.12)

TABLE I.- DIMENSIONS OF MODEL – Concluded

Engines:		
Inlet diameter, cm (in.)	15.24	(6.00)
Exit width, cm (in.)	19.30	(7.60)
Exit area, cm^2 ($in.^2$)	331.00	(51.30)
Vane stagger, deg	45	
Vane spacing, cm (in.)	1.02	(0.40)
Length, inlet face to exit center, cm (in.)	32.00	(12.60)
Inboard engine center line to wing root, cm (in.)	25.91	(10.20)
Outboard engine center line to wing root, cm (in.)	50.29	(19.80)
Inlet location, below wing chord plane:		
Forward, cm (in.)	17.14	(6.75)
Aft, cm (in.)	12.70	(5.00)
Far aft, cm (in.)	11.43	(4.50)
Far aft and tilted, cm (in.)	13.97	(5.50)
Exit center location aft of pitch center:		
Forward, cm (in.)	-6.25	(-2.46)
Aft, cm (in.)	6.45	(2.54)
Far aft, cm (in.)	19.15	(7.54)
Far aft and tilted, cm (in.)	19.15	(7.54)
Exit center height below wing chord line:		
Forward, cm (in.)	19.94	(7.85)
Aft, cm (in.)	15.49	(6.10)
Far aft, cm (in.)	14.22	(5.60)
Far aft and tilted, cm (in.)	7.62	(3.00)
Downwash vane:		
Location aft of root leading edge, cm (in.)	172.00	(67.70)
Height above wing chord plane, cm (in.)	39.12	(15.40)
Distance from reflection plane, cm (in.)	28.58	(11.25)
Reflection plane length, cm (in.)	243.8	(96.00)
Reflection plane width, cm (in.)	213.4	(84.00)

TABLE II.- AIRFOIL COORDINATES FOR WING AND FLAP

Wing (with Krueger flap and slat removed)			Flap (no deflection)		
x, percent chord	y_{Upper}, percent chord	y_{Lower}, percent chord	x, percent chord	y_{Upper}, percent chord	y_{Lower}, percent chord
3.50	-0.55	-0.55	72.00	0	0
4.00	.50	-1.80	72.50	1.50	-1.45
5.00	1.55	-2.00	73.00	2.40	-1.40
7.50	3.25	-2.40	74.00	3.40	-1.30
10.00	4.30	-2.60	77.00	4.50	-1.00
12.50	5.35	-2.95	82.00	4.60	-.50
15.00	5.75	-3.03	87.00	3.85	-.05
20.00	6.57	-3.35	92.00	2.50	.15
30.00	7.66	-3.76	100.00	0	0
40.00	8.14	-3.86			
50.00	7.96	-3.55	Flap extension		
60.00	7.09	-2.79	100.00	0	
70.00	5.70	-1.78	126.34	-7.90	
80.00	3.95	-.74			
90.00	1.98	.09	Hinge line		
100.00	0	0	76.85	-0.20	

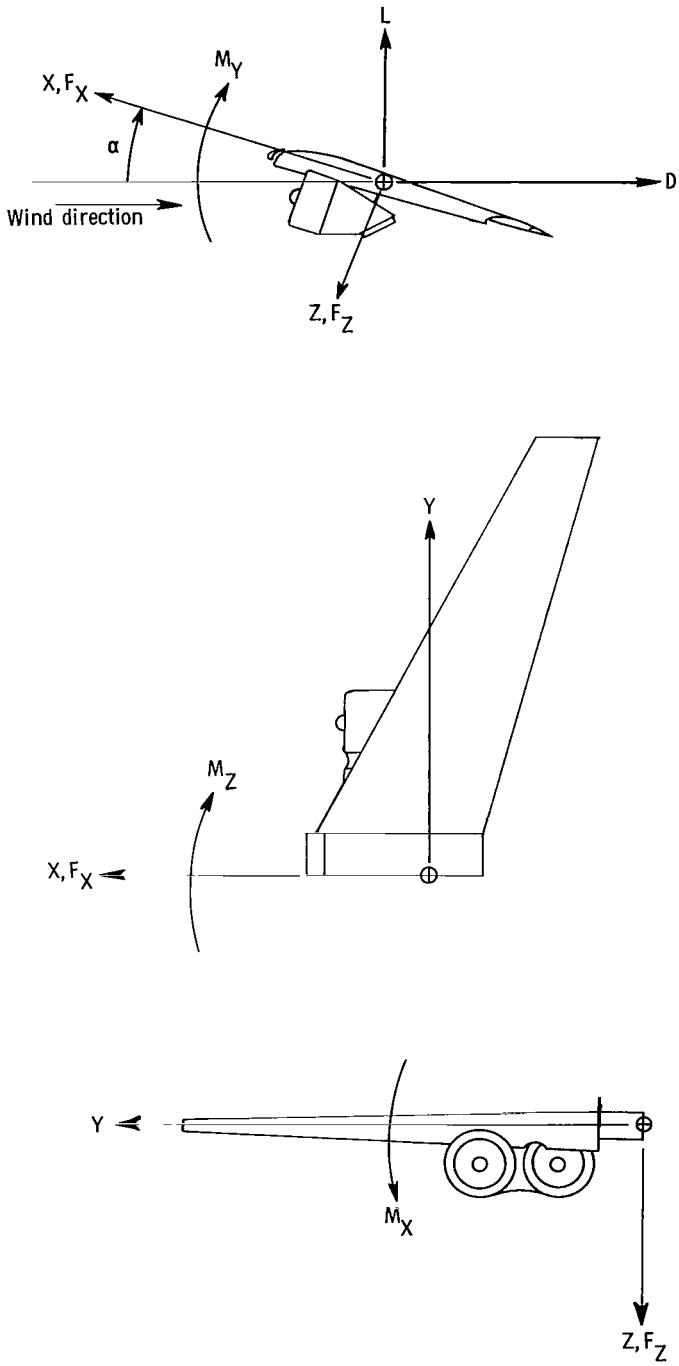

Figure 1.- Axis system used in presentation of data. Arrows indicate positive directions of forces and moments.

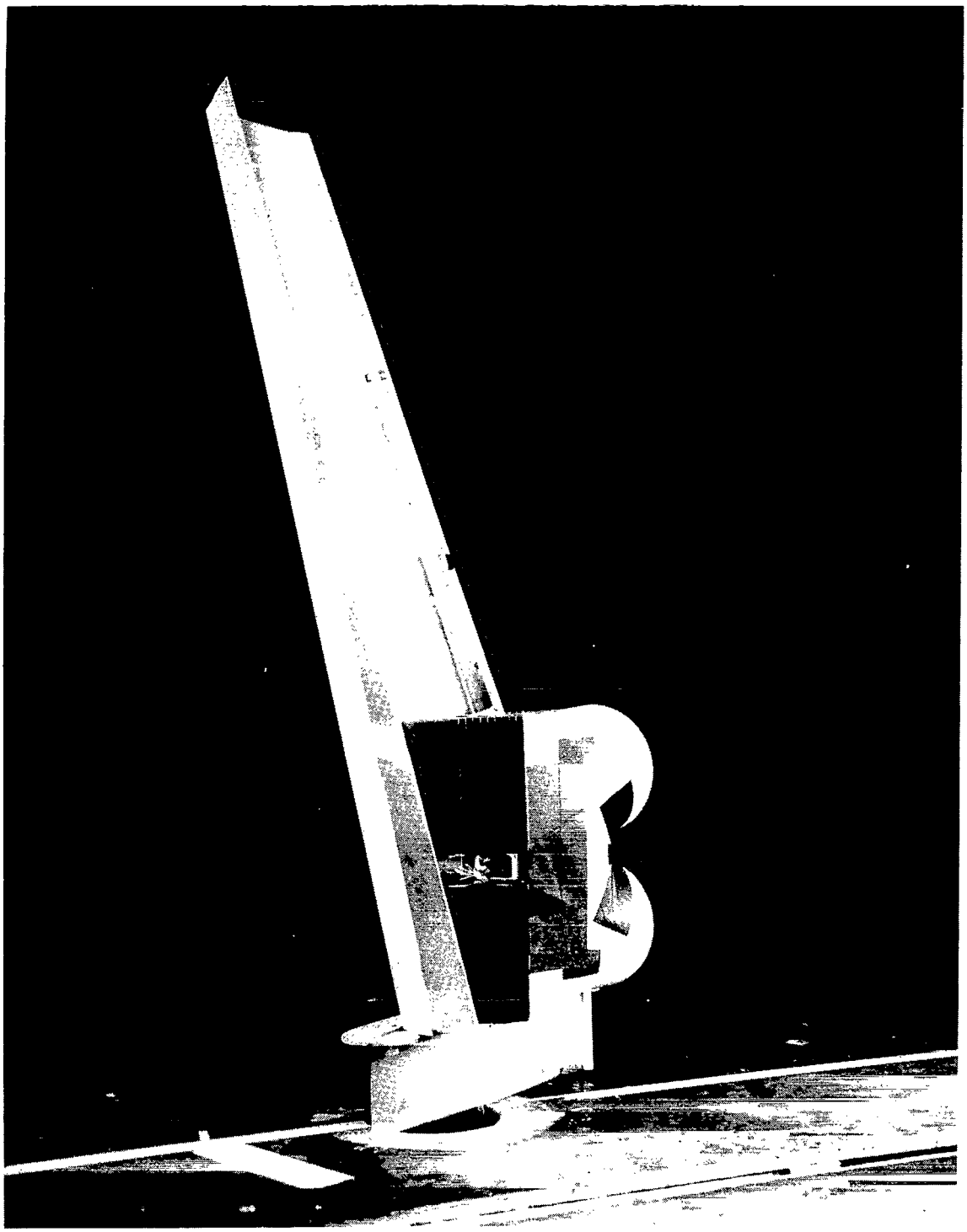

L-70-5541

(a) View from behind and below wing.

Figure 2.- The model on the reflection plane.

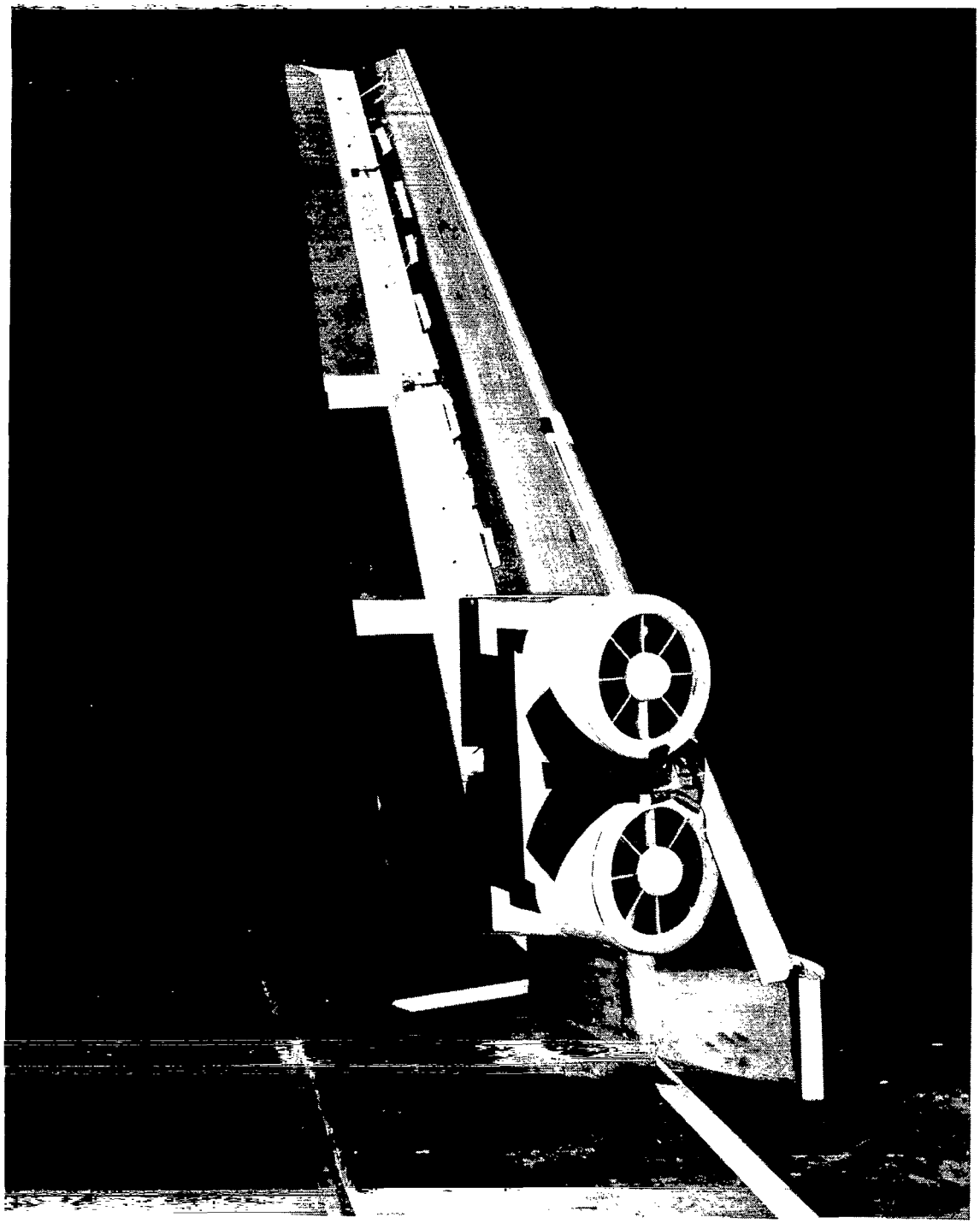

L-70-5542

(b) View from ahead and below wing.

Figure 2.- Continued.

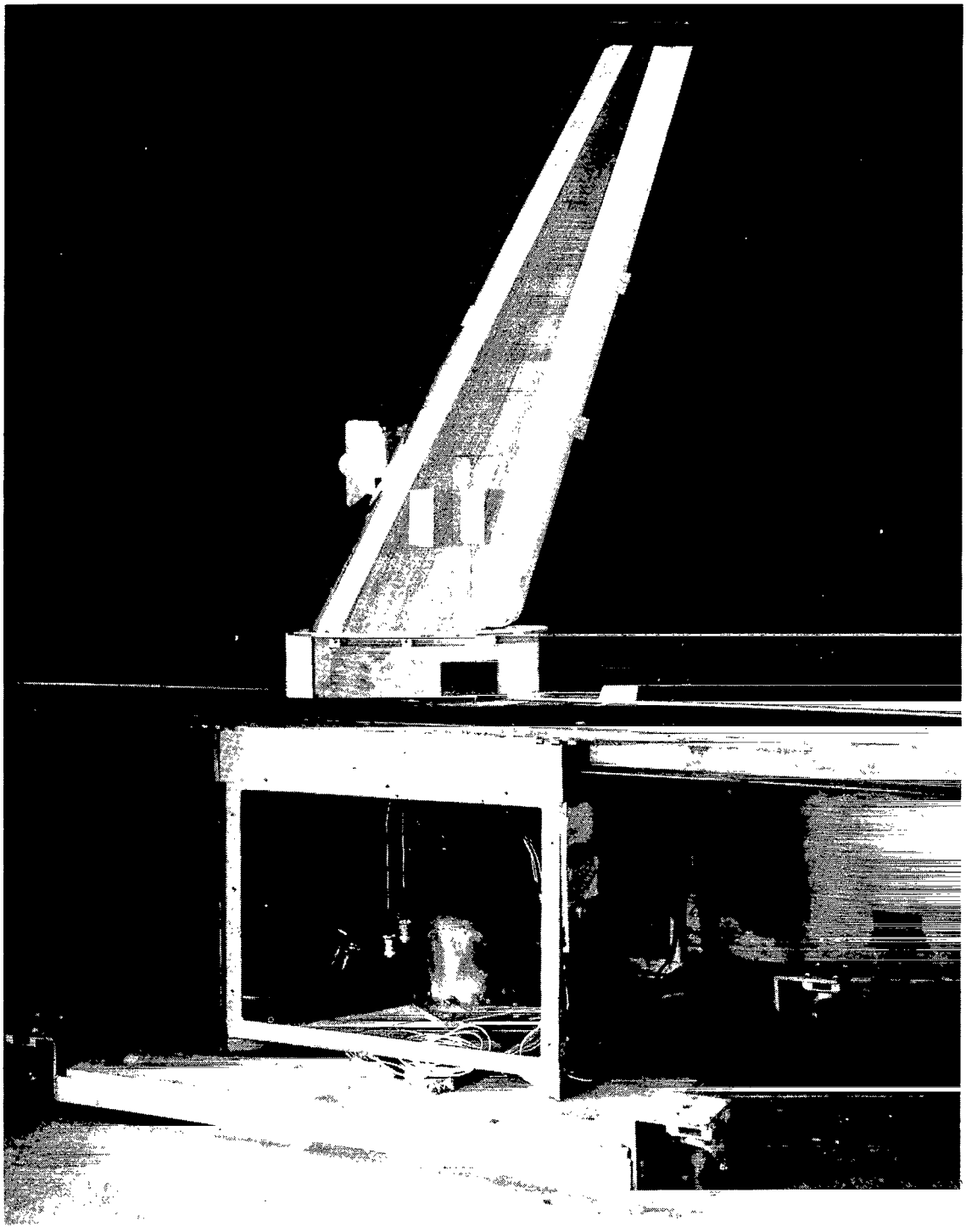

L-70-5540

(c) View from above wing, showing equipment beneath reflection plane.

Figure 2.- Continued.

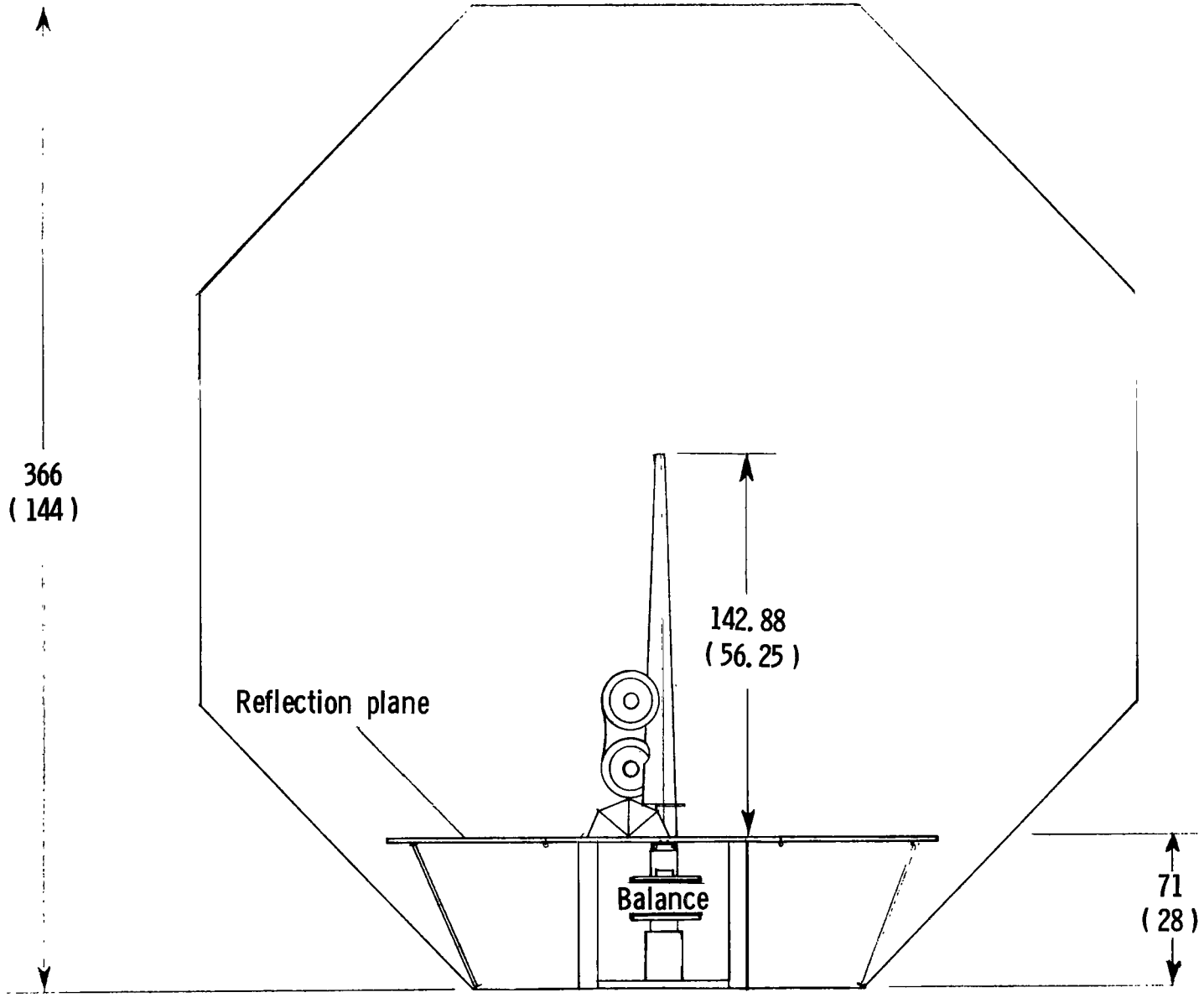

(d) Sketch of set-up in 3.7-m tunnel. Front view; dimensions given are in centimeters (inches).

Figure 2.- Concluded.

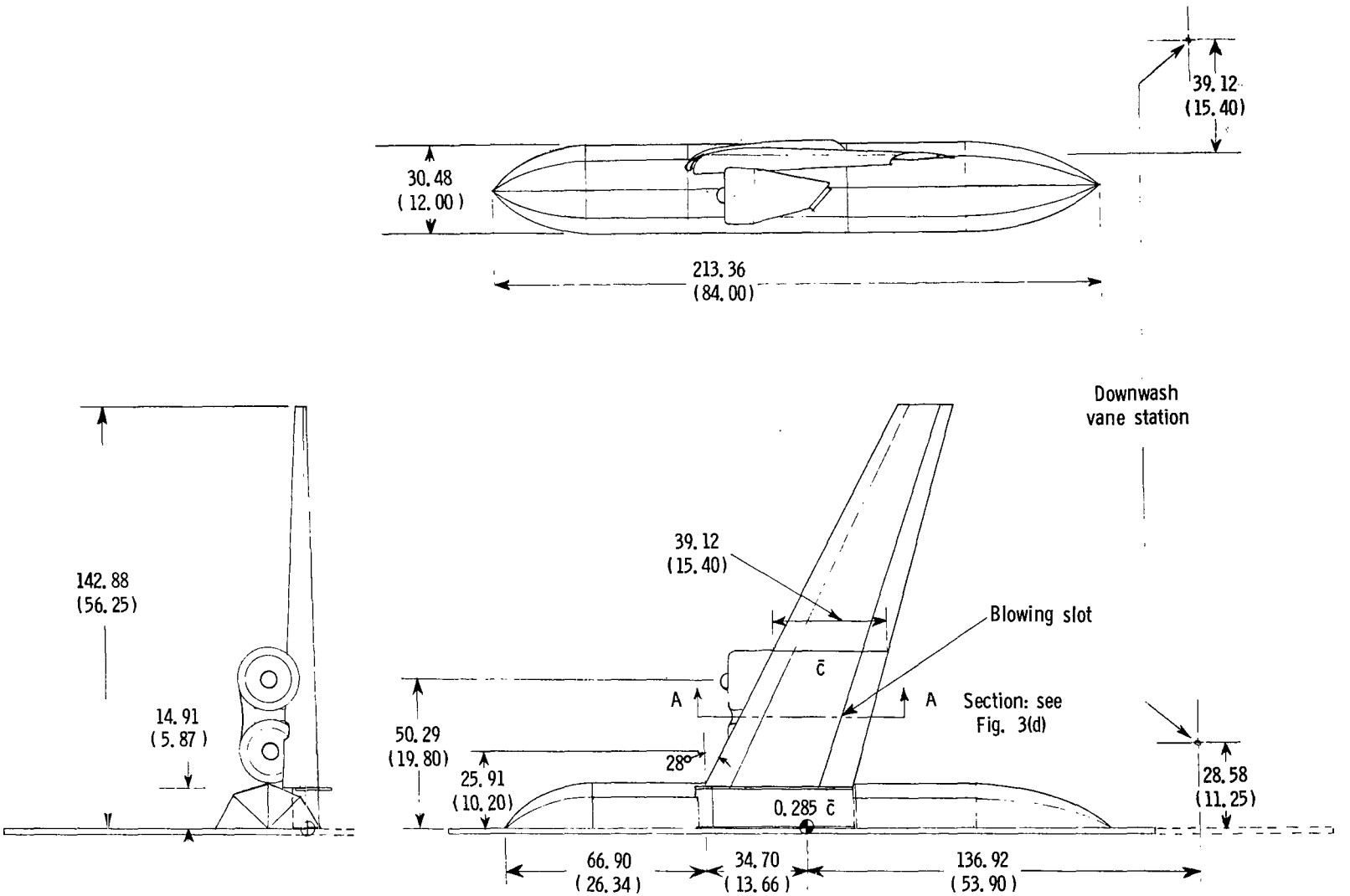

(a) Three-view drawing of model.

Figure 3.- Sketches of the basic model. Dimensions given are in centimeters (inches).

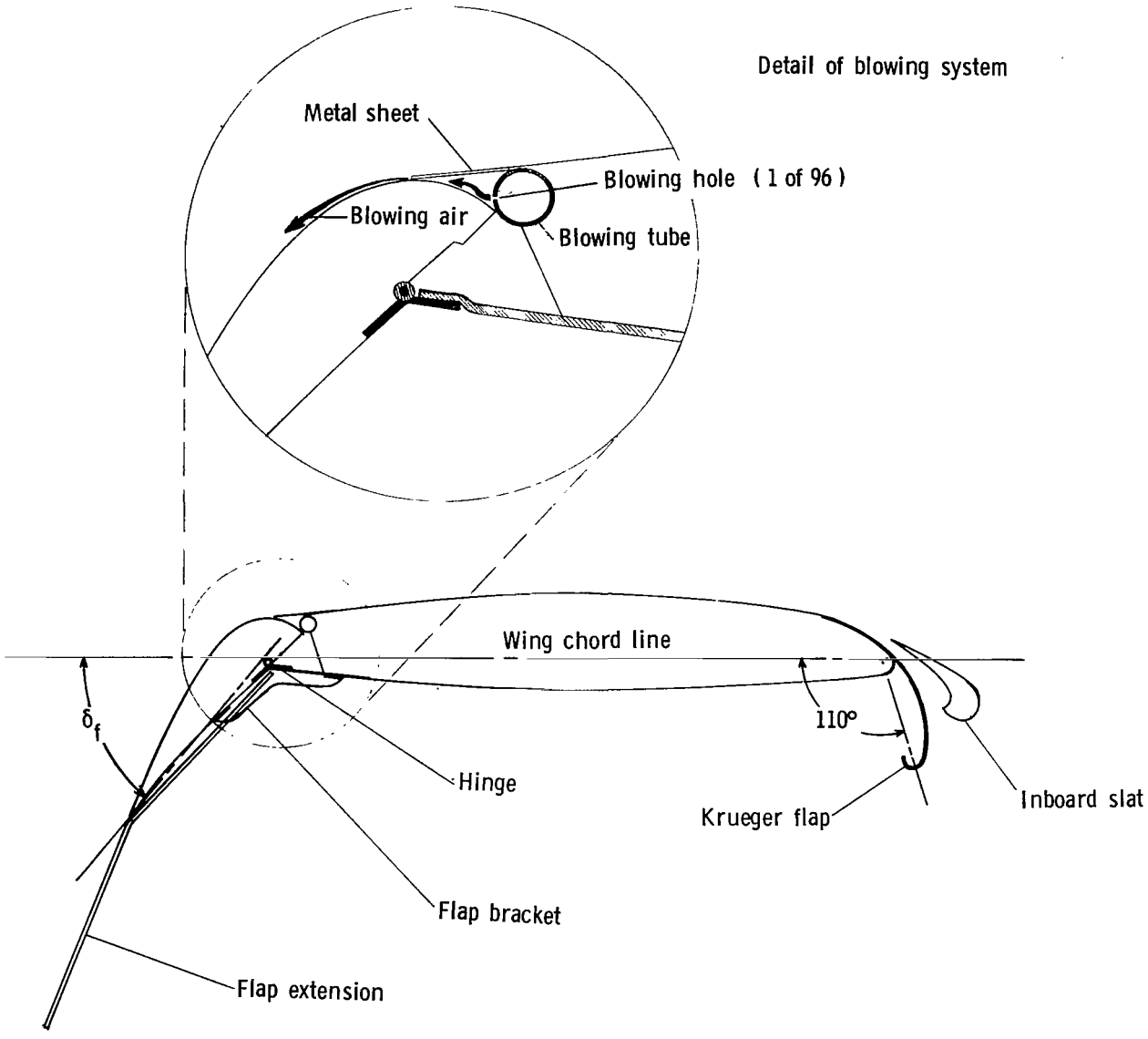

(b) Wing section detail.

Figure 3.- Continued.

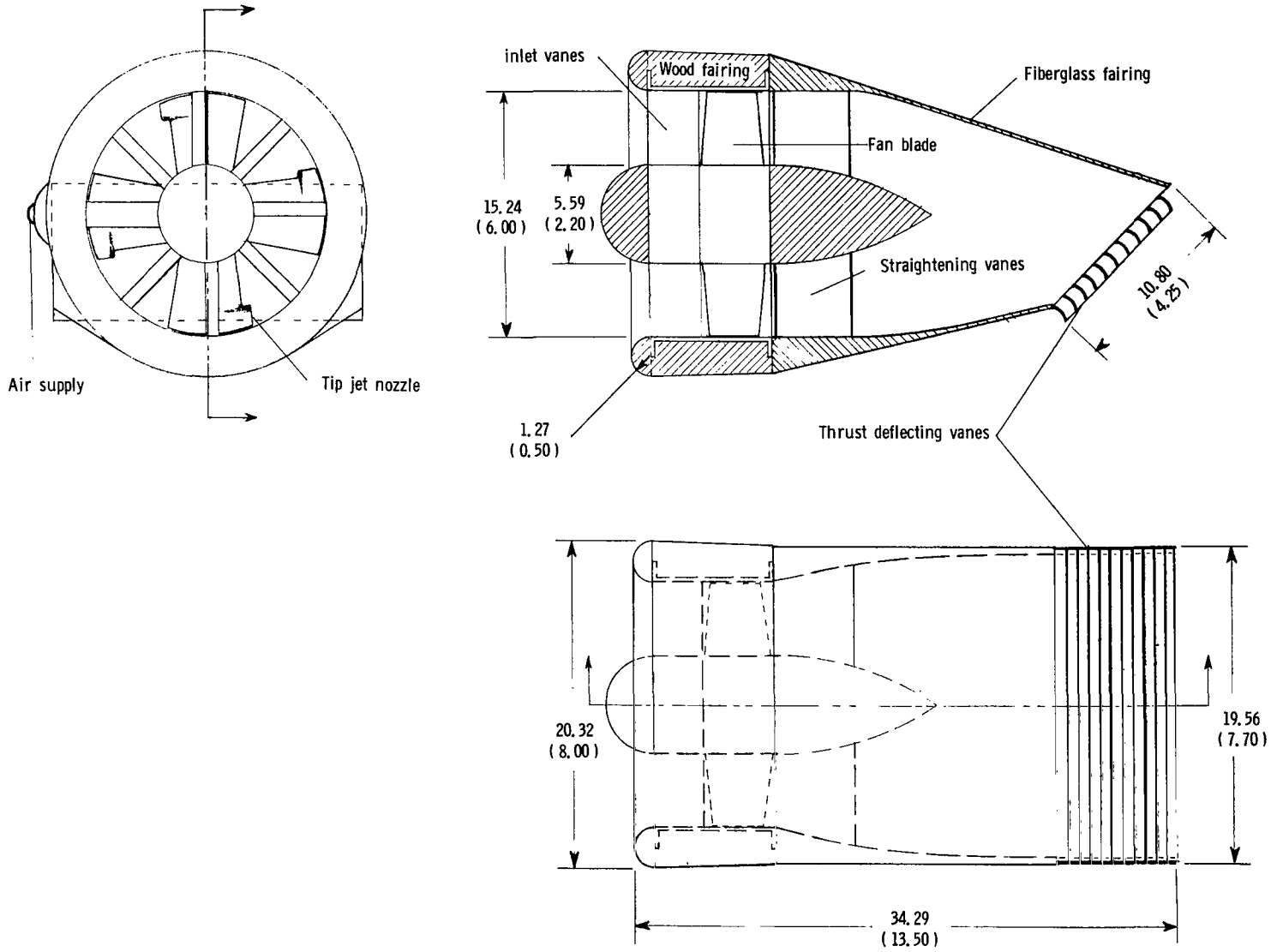

(c) Model engine nacelles.

Figure 3.- Continued.

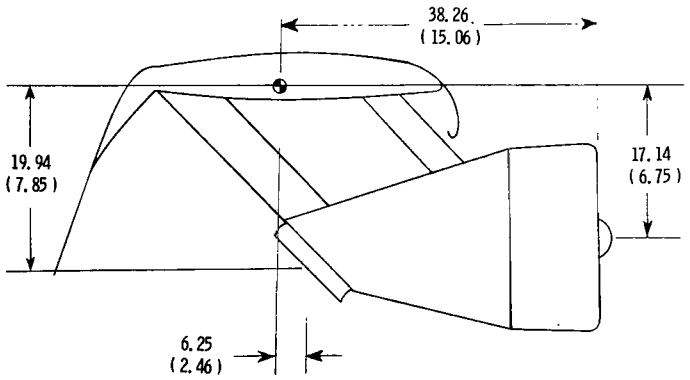

Forward

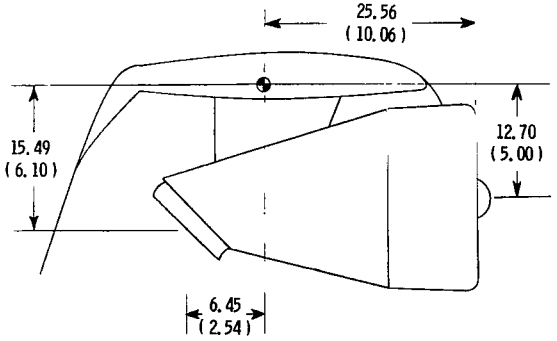

Aft

(Section A-A of figure 3(a))

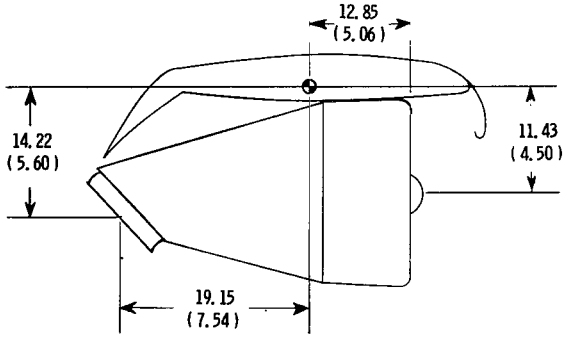

Far aft

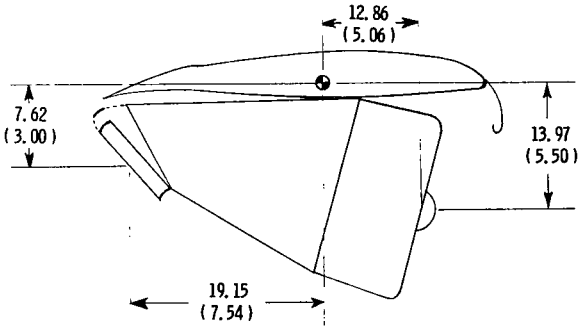

Far aft and tilted

(d) Engine positions used during the tests.

Figure 3.- Concluded.

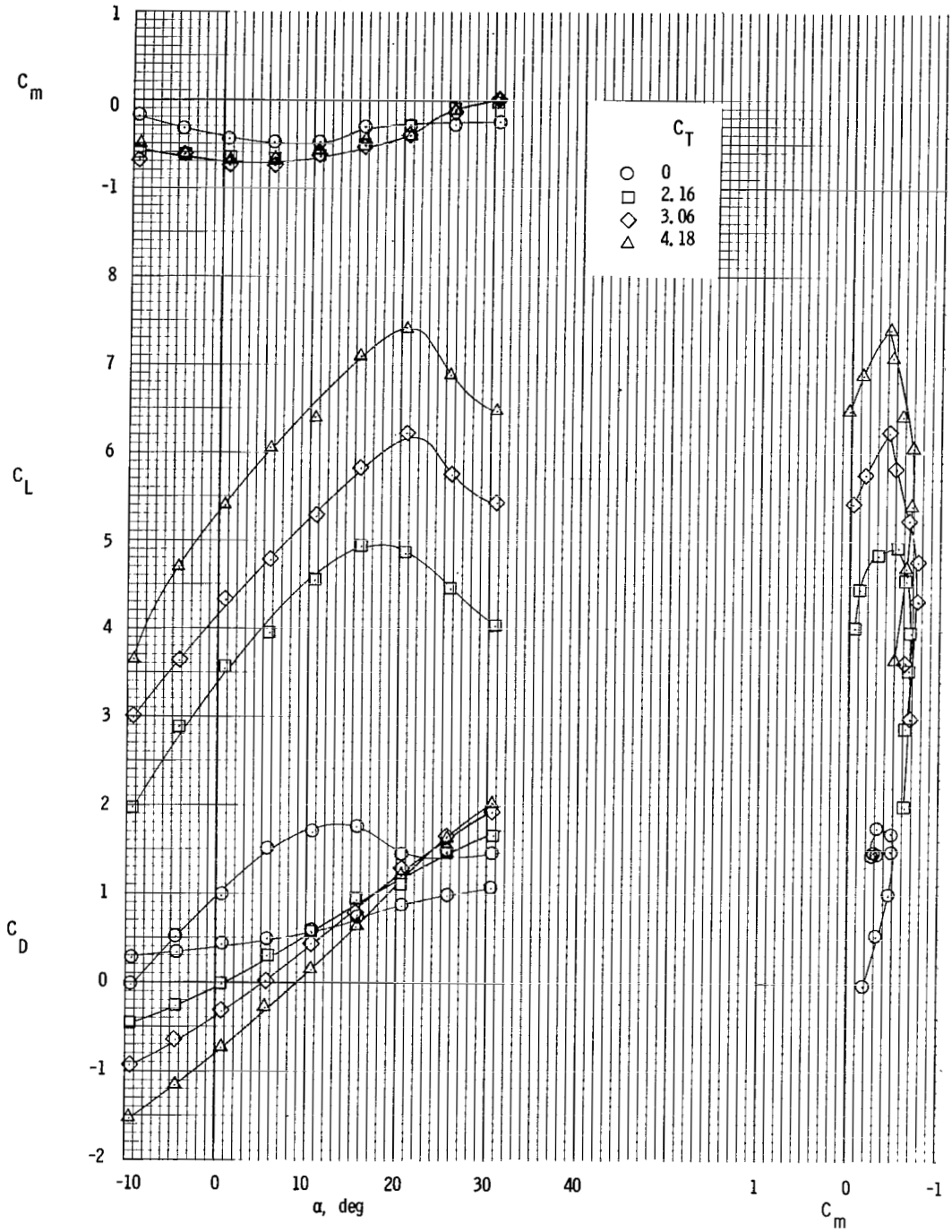

(a) $C_\mu = 0$.

Figure 4.- Longitudinal characteristics of model with aft engines. $\delta_{f,ext} = 50^o$.

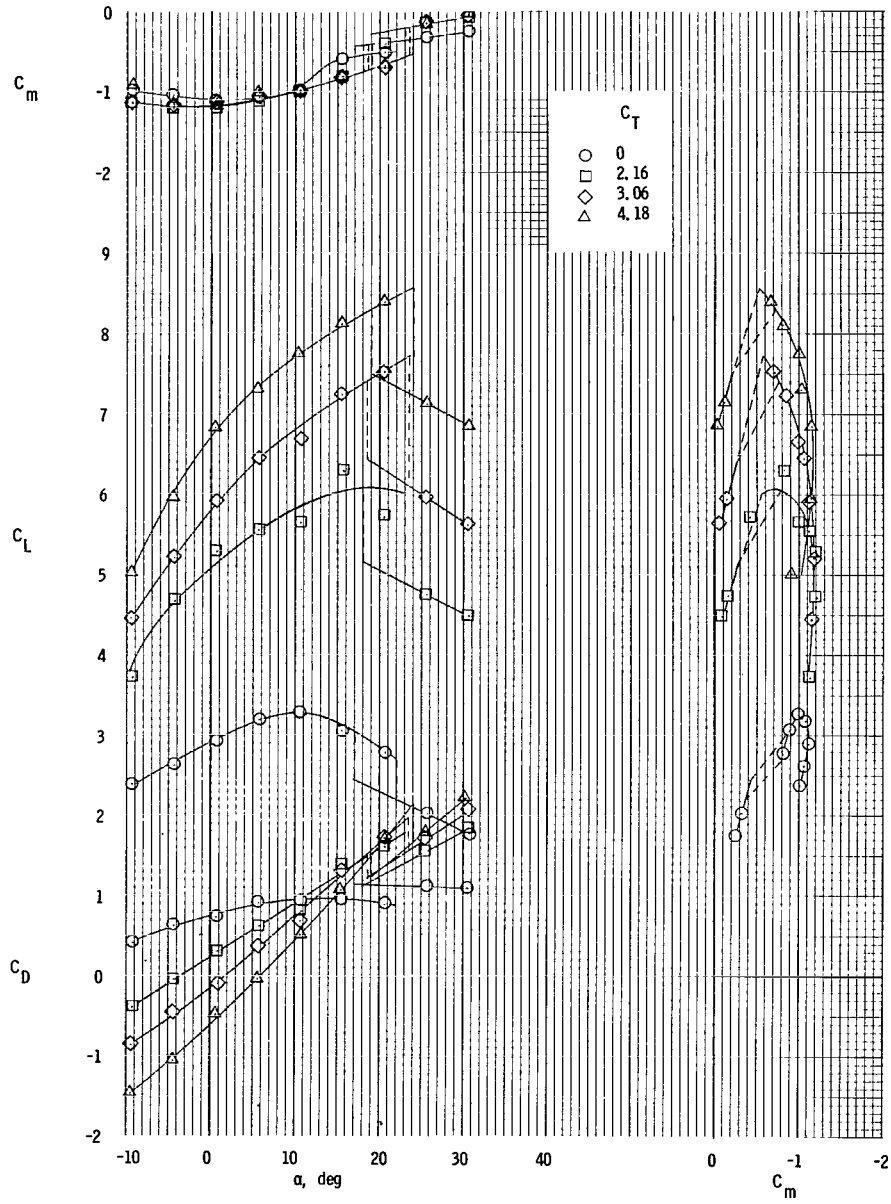

(b) $C_\mu = 0.078$.

Figure 4.- Continued.

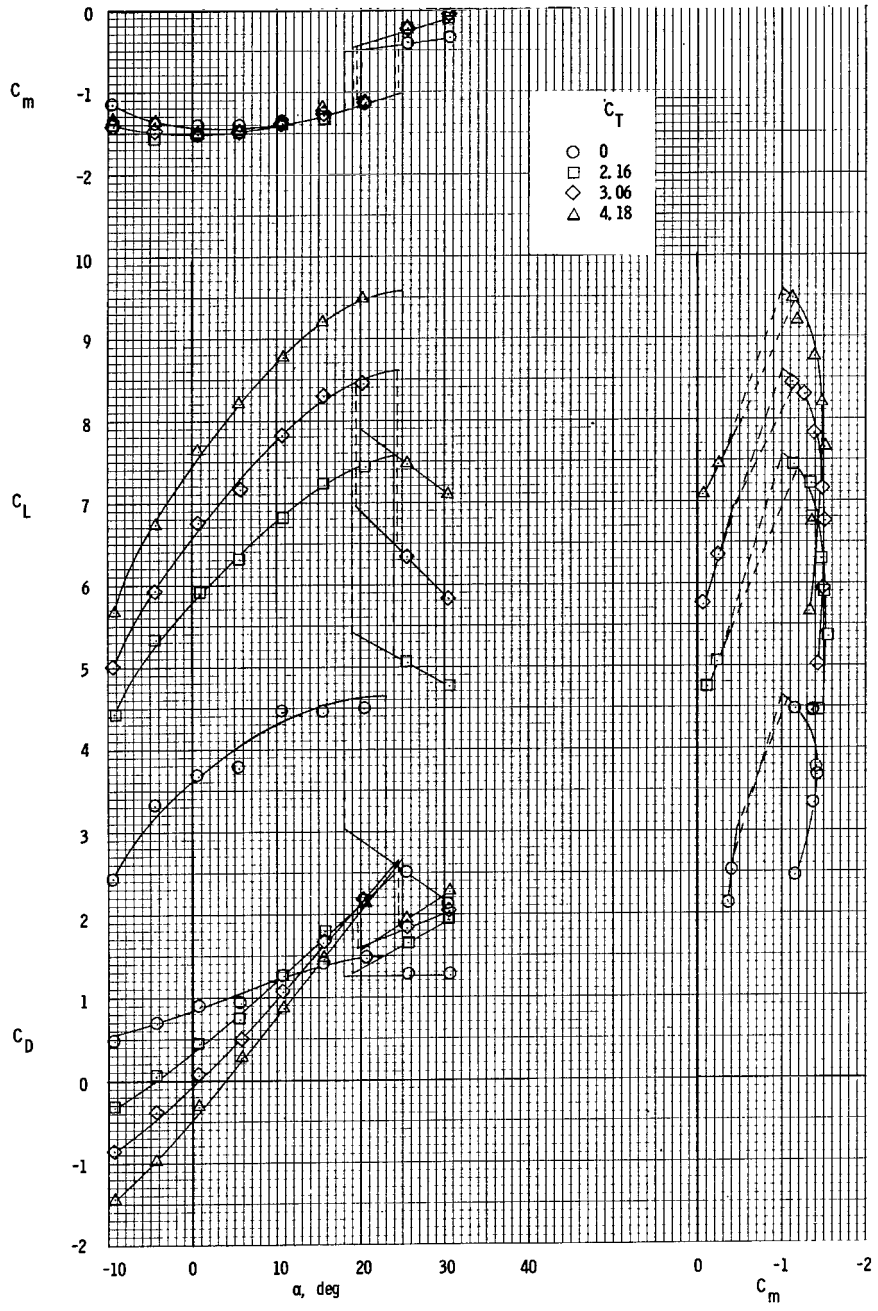

(c) $C_\mu = 0.198$.

Figure 4.- Continued.

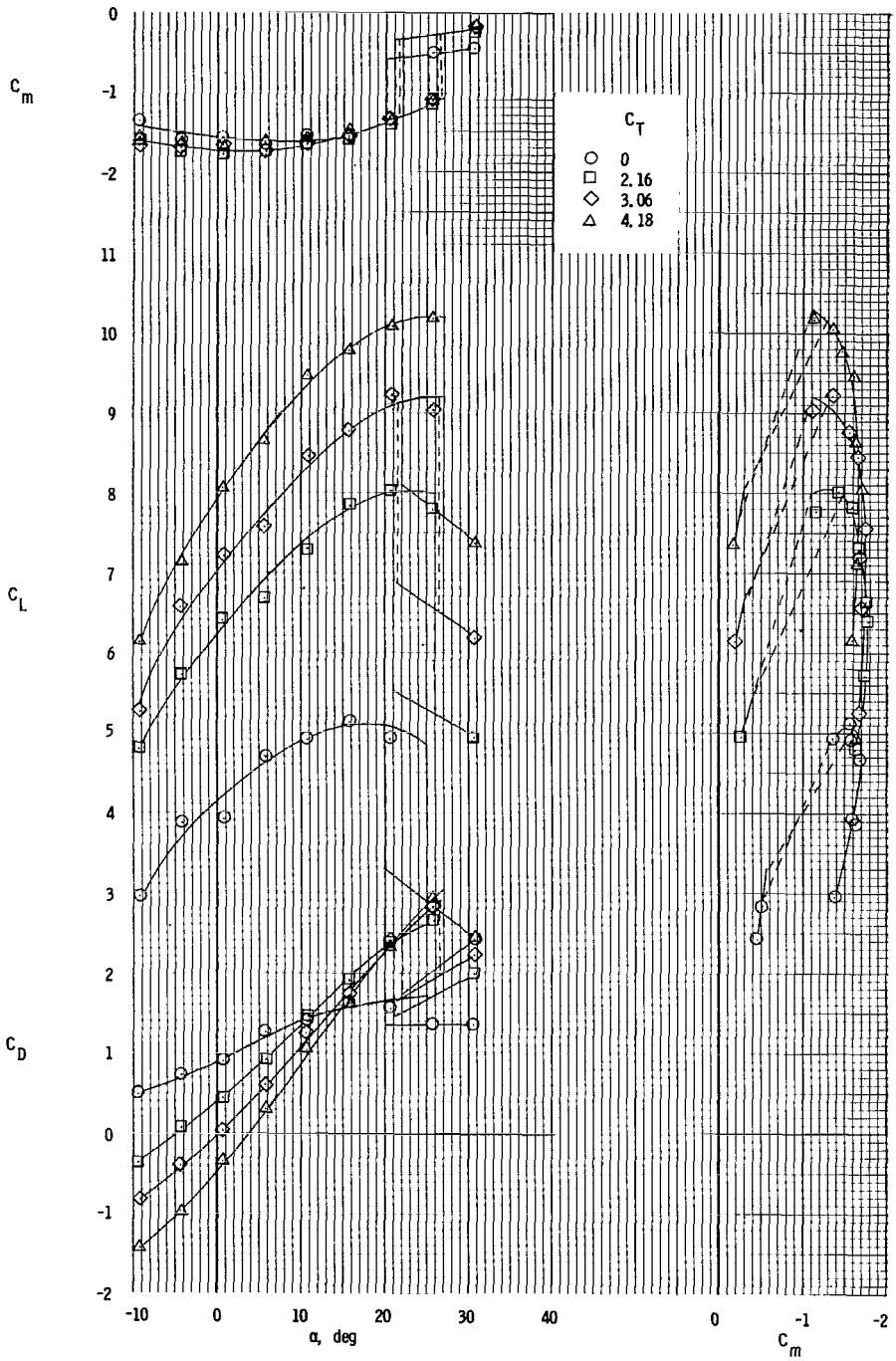

(d) $C_\mu = 0.335$.

Figure 4.- Concluded.

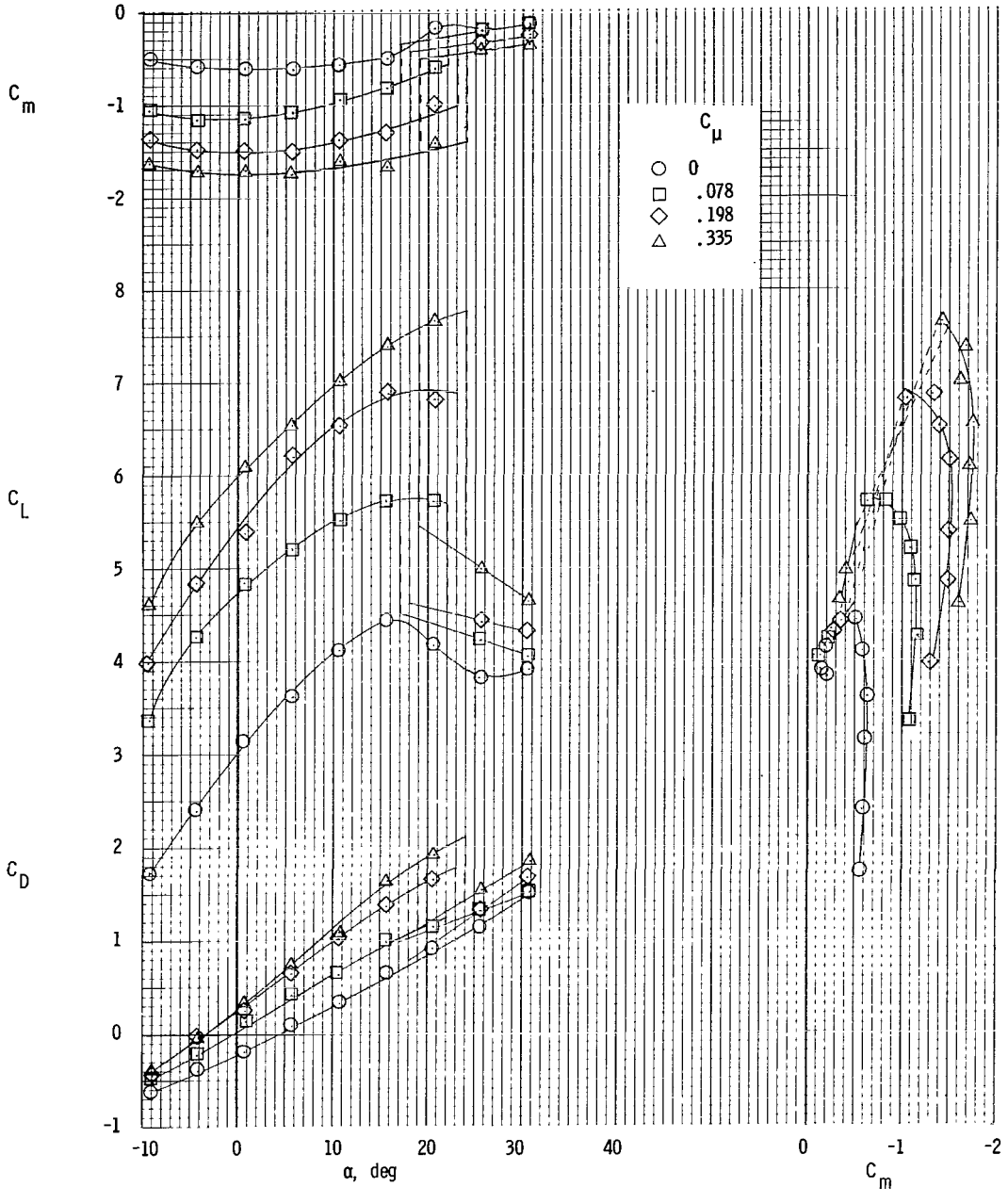

Figure 5.- Longitudinal characteristics of model with aft engines. Outboard engine inoperative. $\delta_{f,ext} = 50^o$; $C_T = 2.16$.

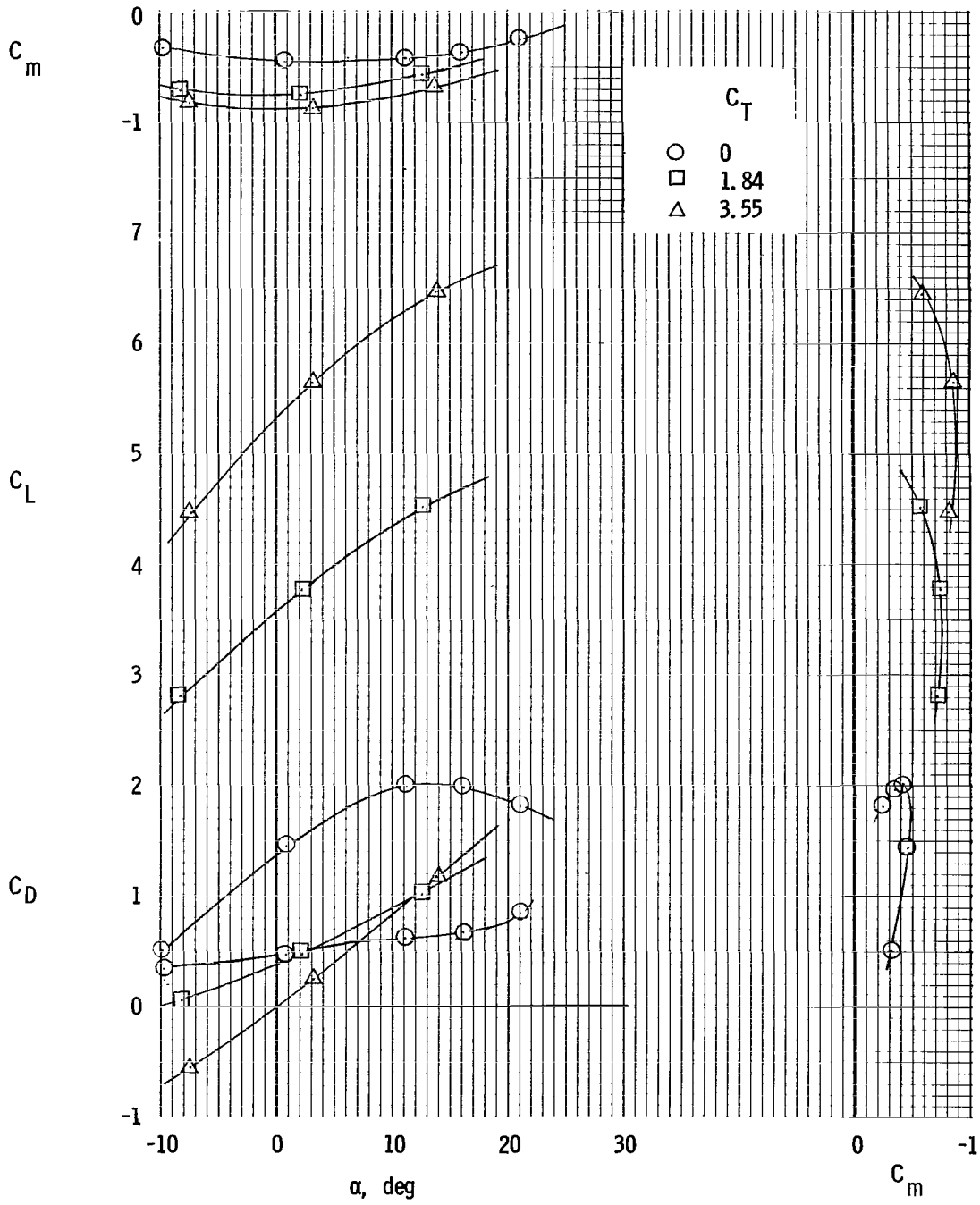

(a) $C_\mu = 0$.

Figure 6.- Longitudinal characteristics of model with aft engines. $\delta_{f,ext} = 65^o$.

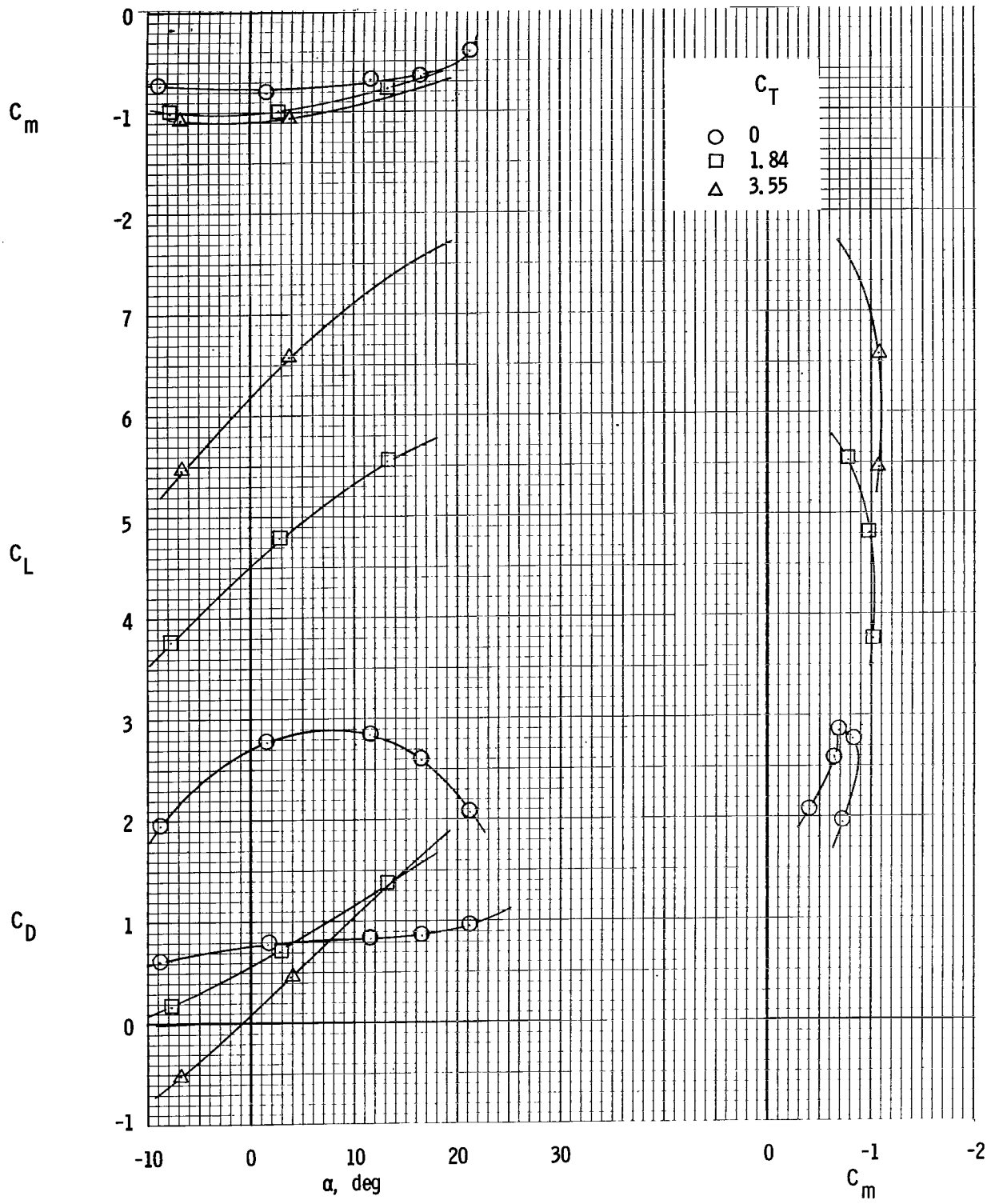

(b) $C_\mu = 0.066$.

Figure 6.- Continued.

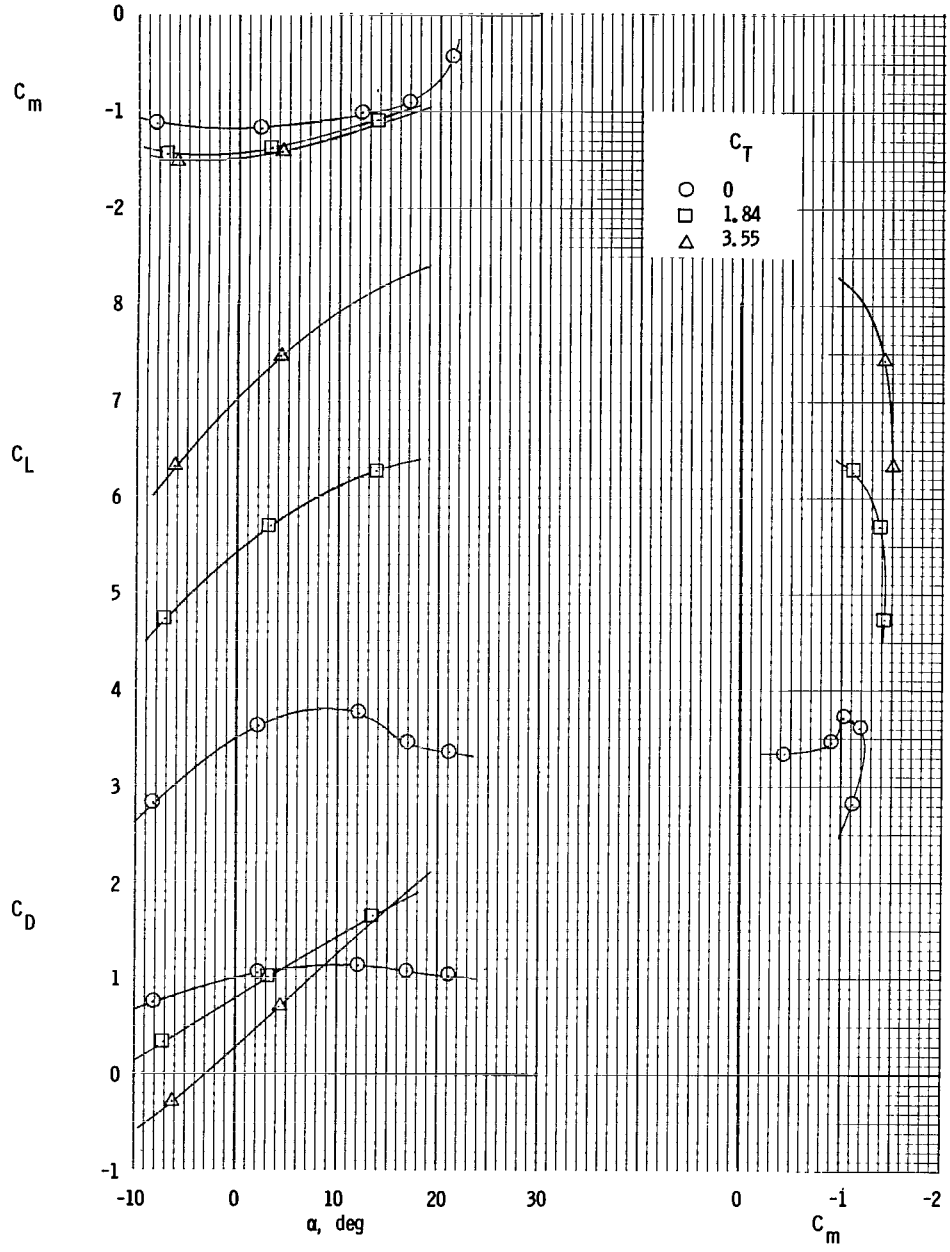

(c) $C_\mu = 0.168$.

Figure 6.- Continued.

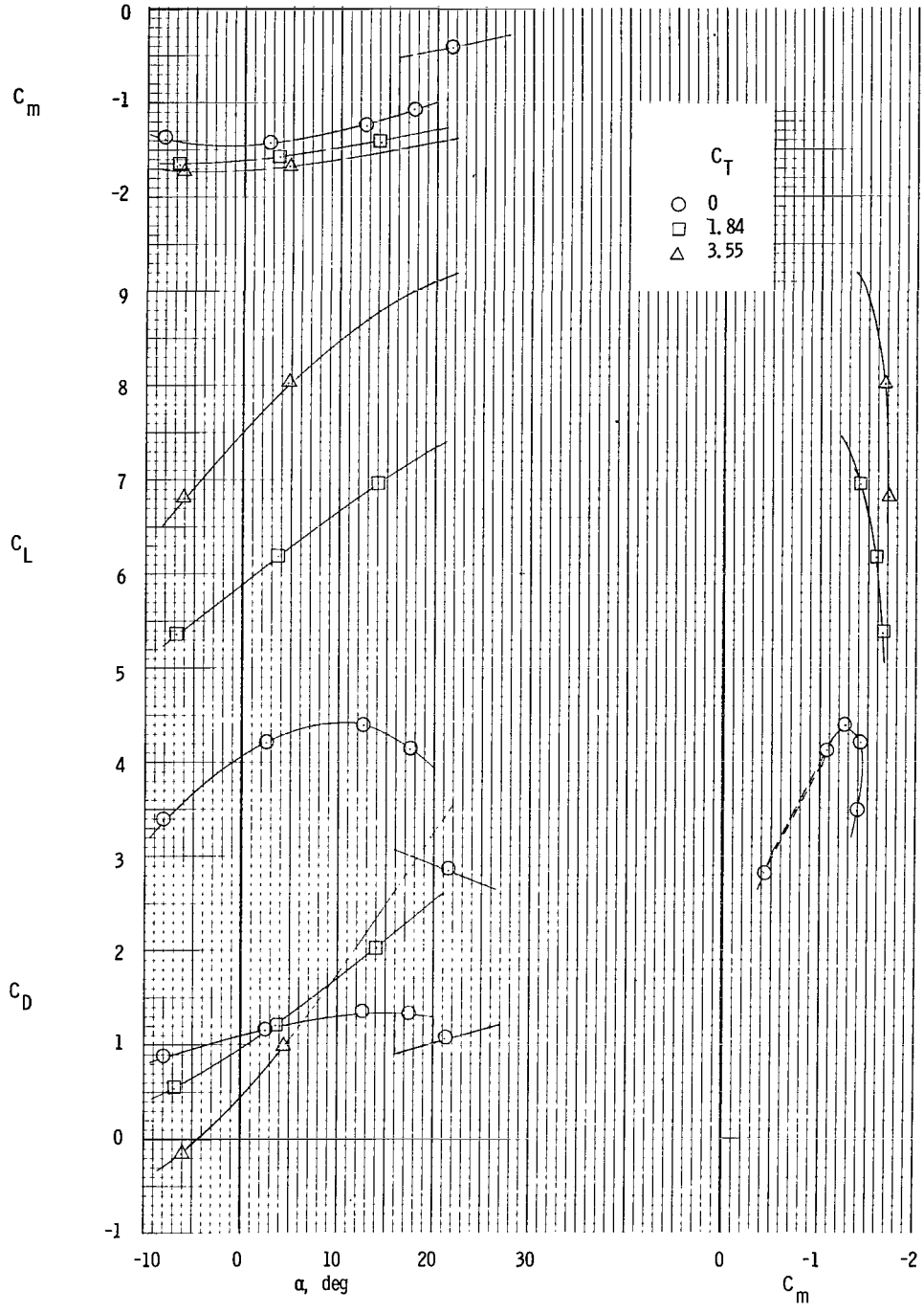

(d) $C_\mu = 0.285$.

Figure 6.- Concluded.

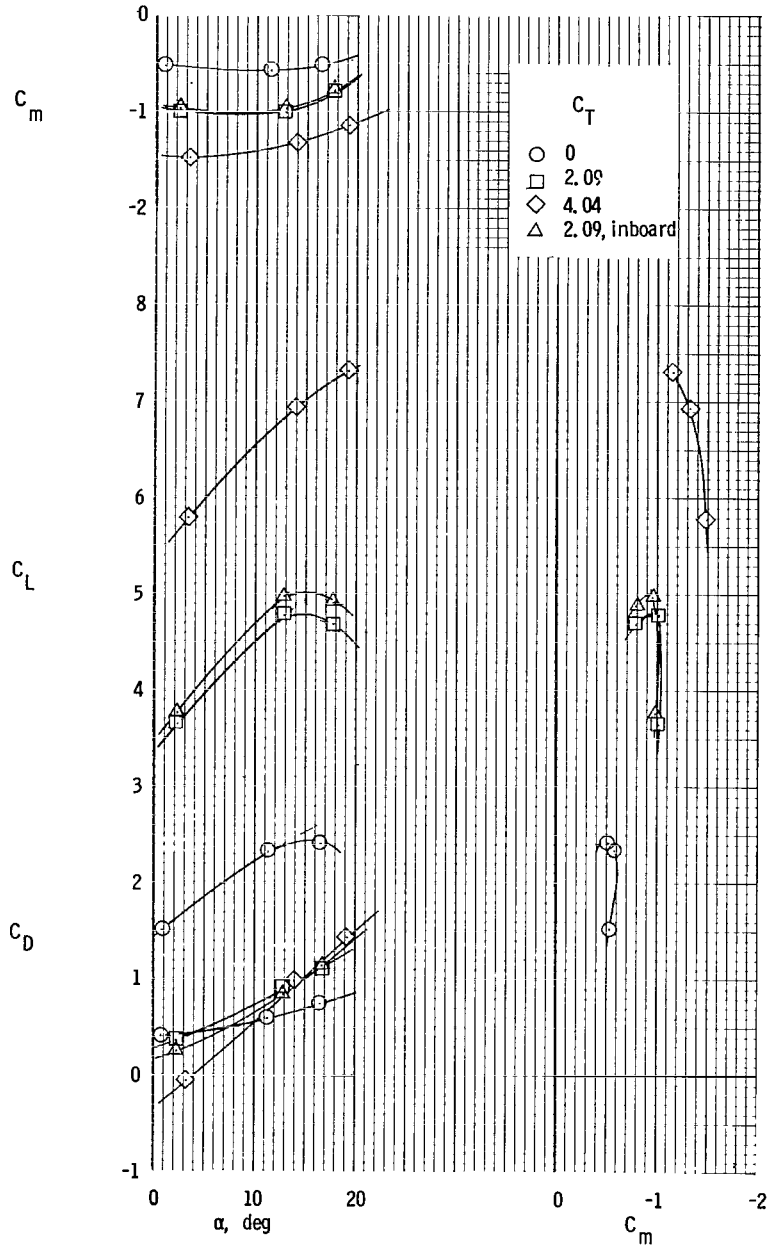

(a) $C_\mu = 0$.

Figure 7.- Longitudinal characteristics of model with thrust deflected by the flap. $\delta_{f,ext} = 50^o$; aft engine position; turning vanes removed.

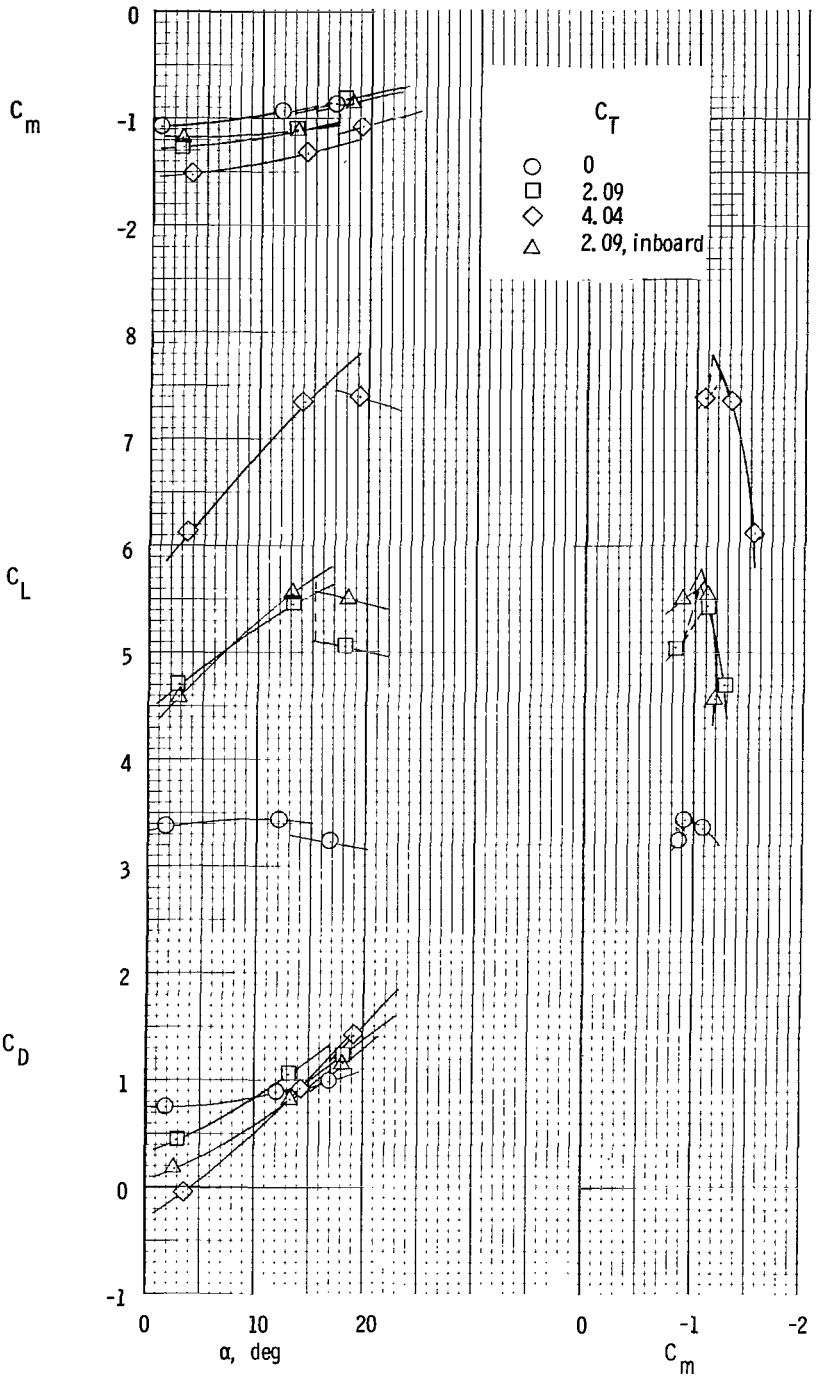

(b) $C_\mu = 0.075$.

Figure 7.- Continued.

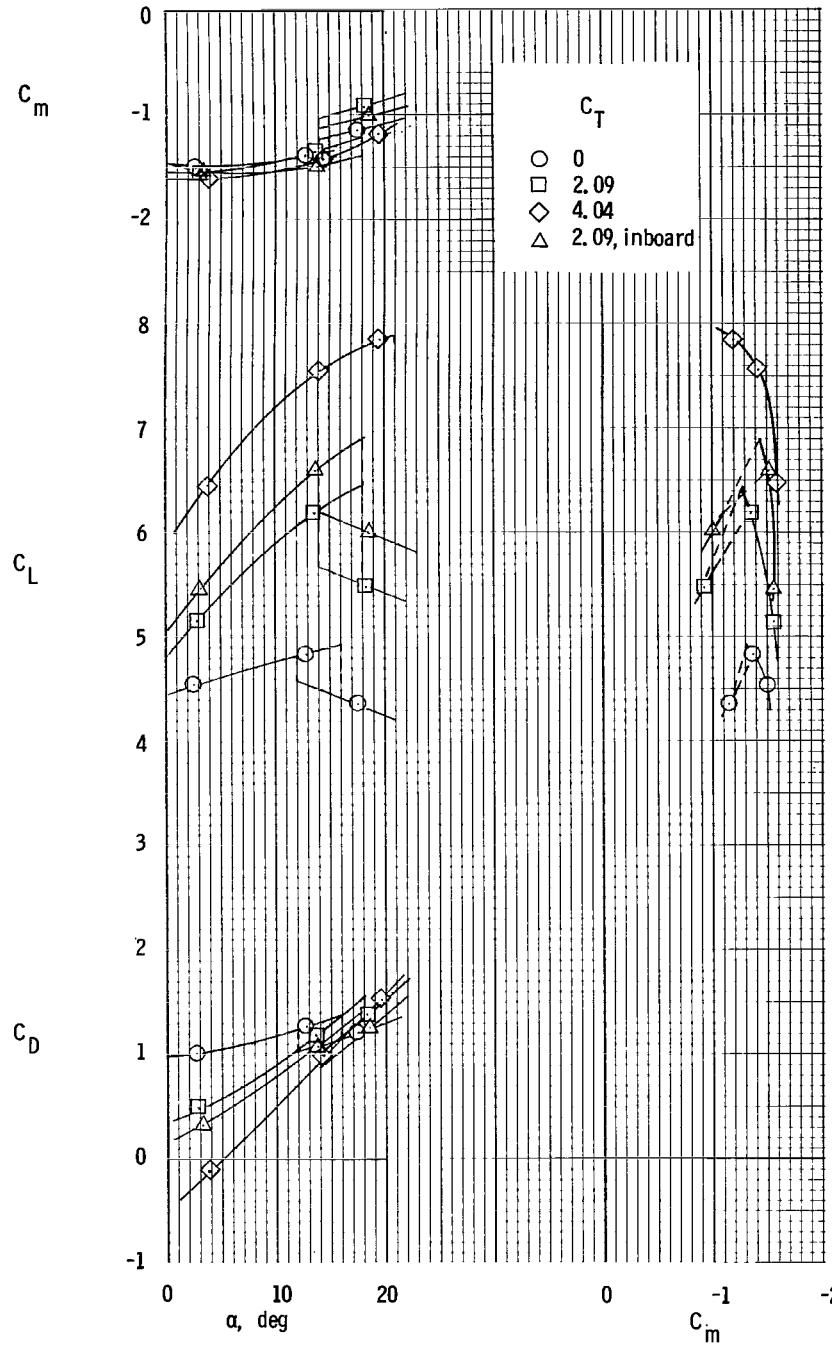

(c) C_μ = 0.191.

Figure 7.- Continued.

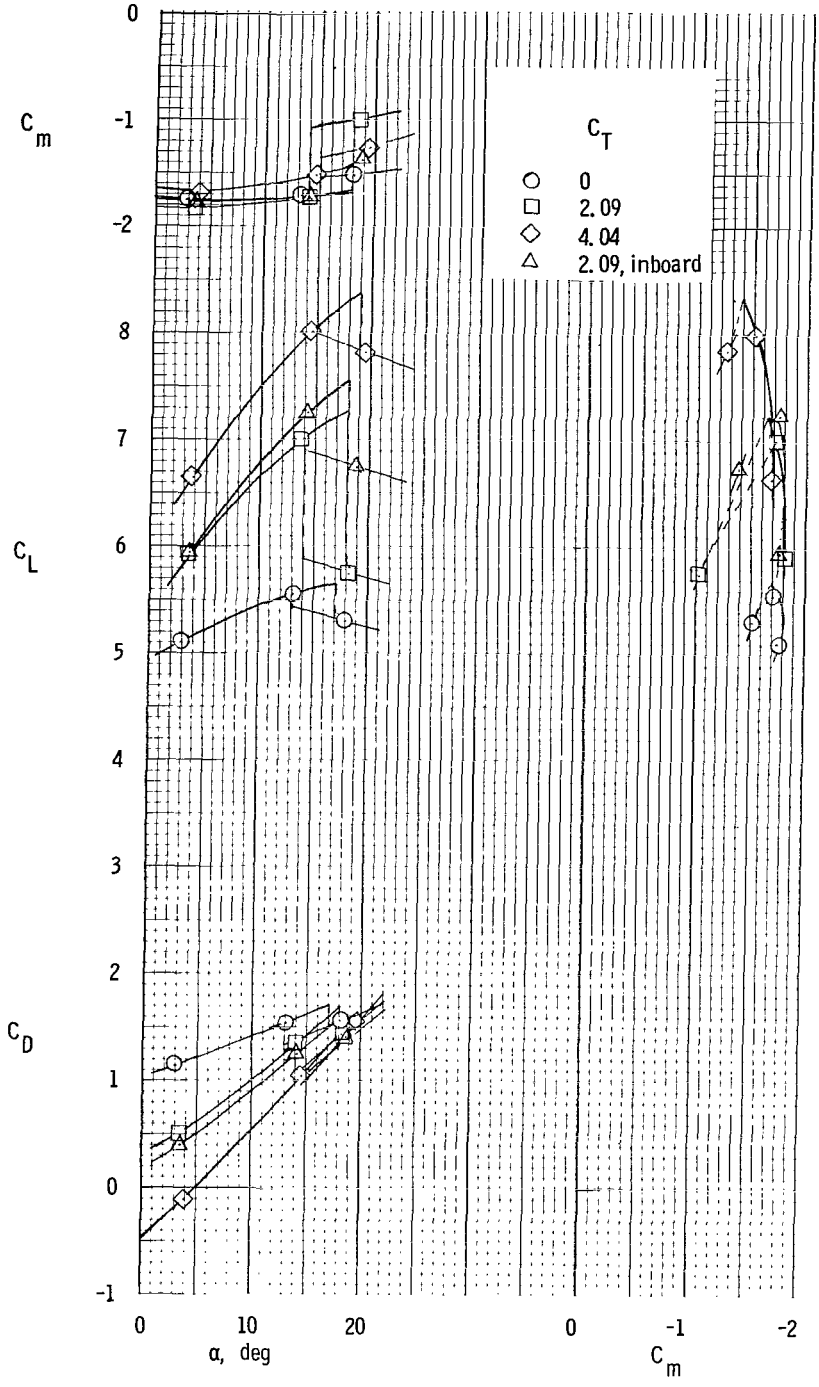

(d) $C_\mu = 0.324$.

Figure 7.- Concluded.

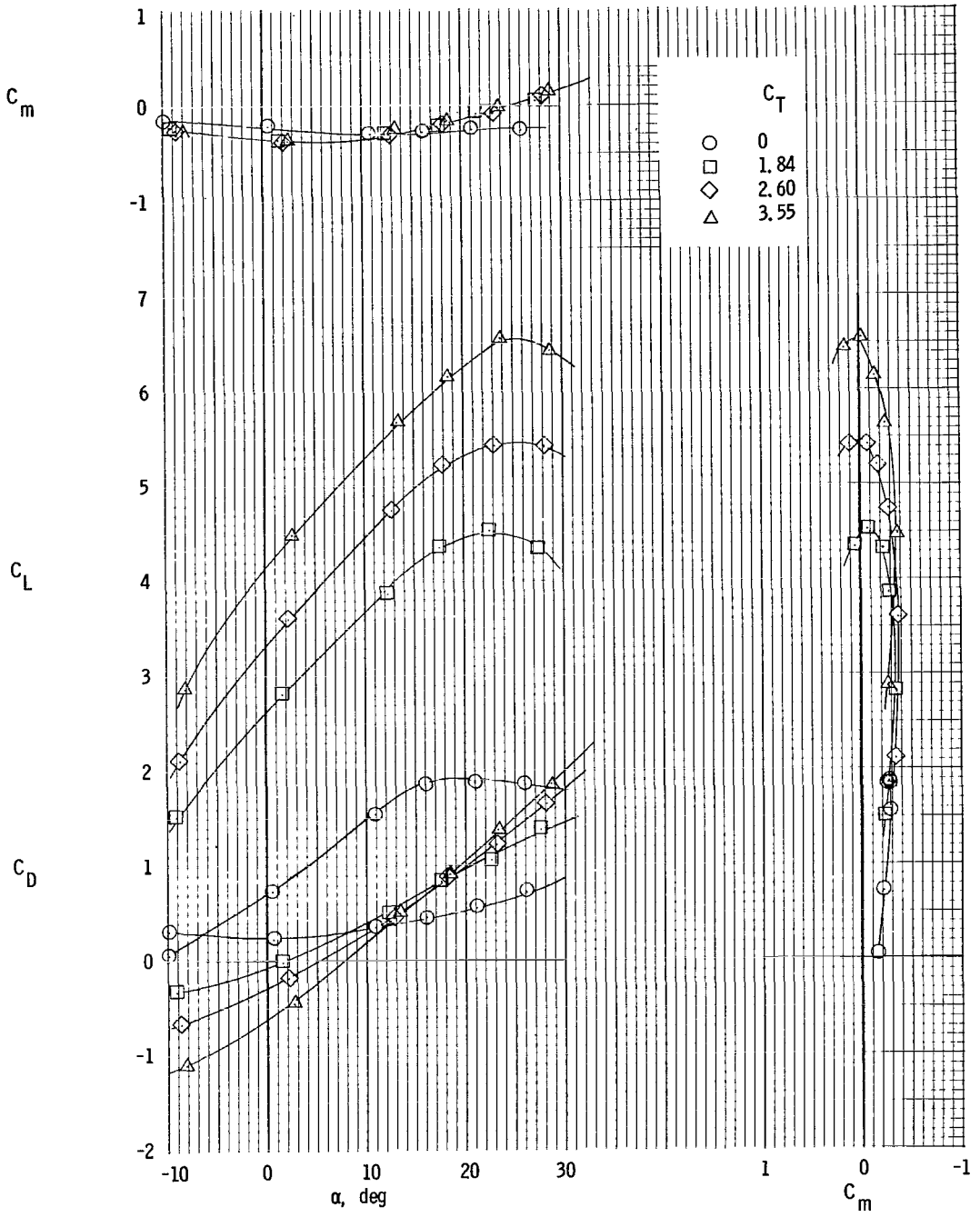

(a) $C_\mu = 0$.

Figure 8.- Longitudinal characteristics of model with aft engines and short chord. $\delta_f = 50^o$.

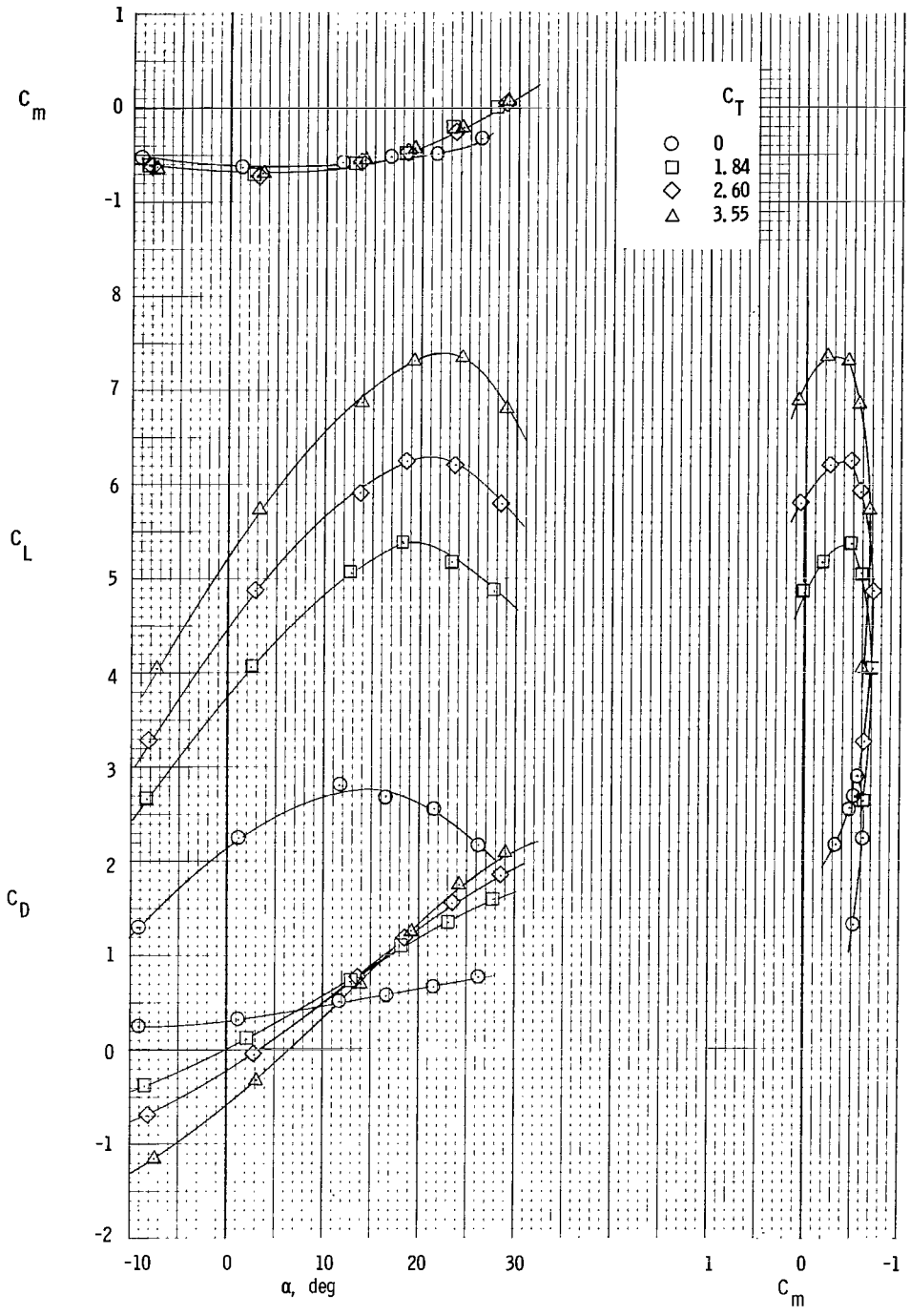

(b) $C_\mu = 0.066$.

Figure 8.- Continued.

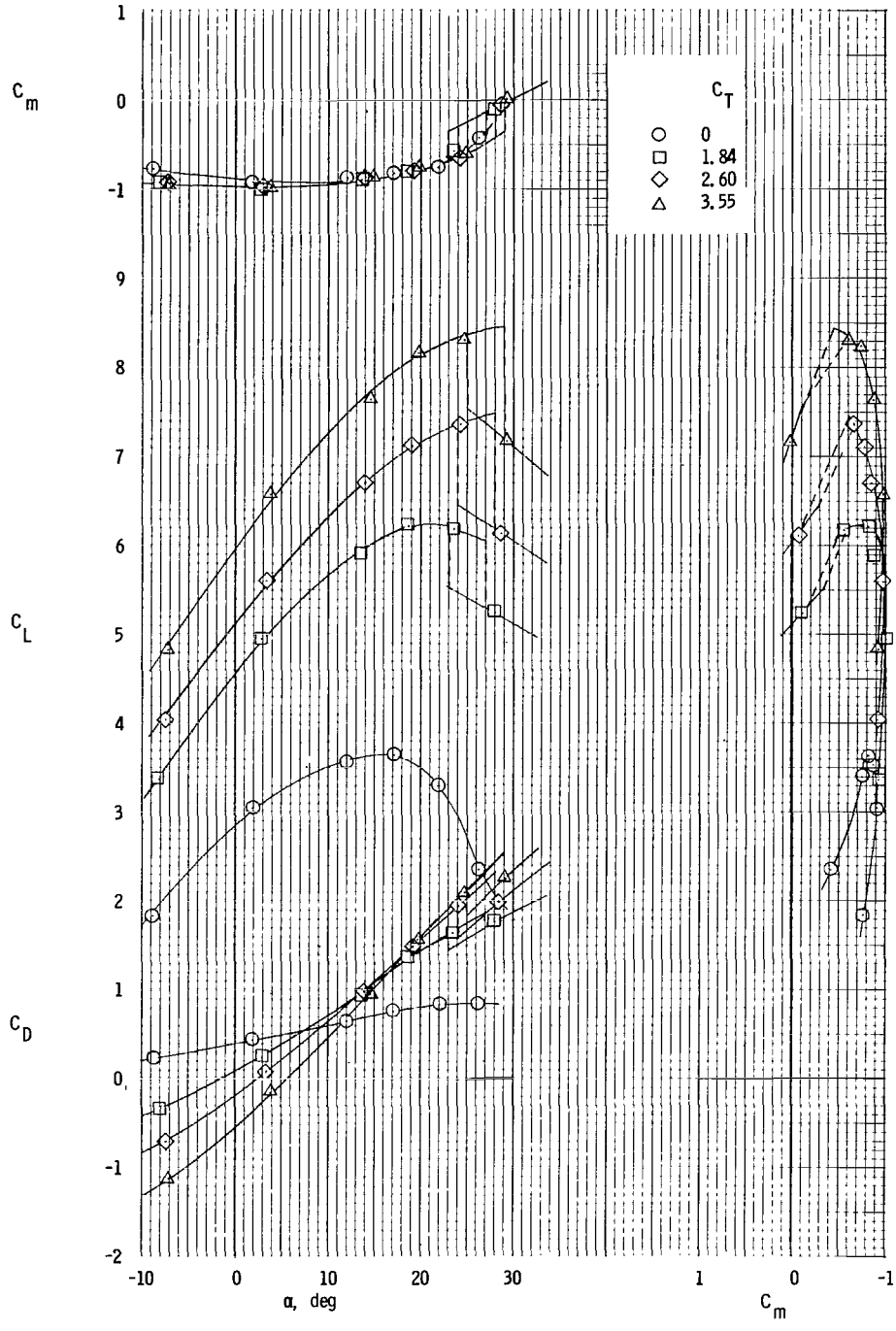

(c) $C_\mu = 0.168$.

Figure 8.- Continued.

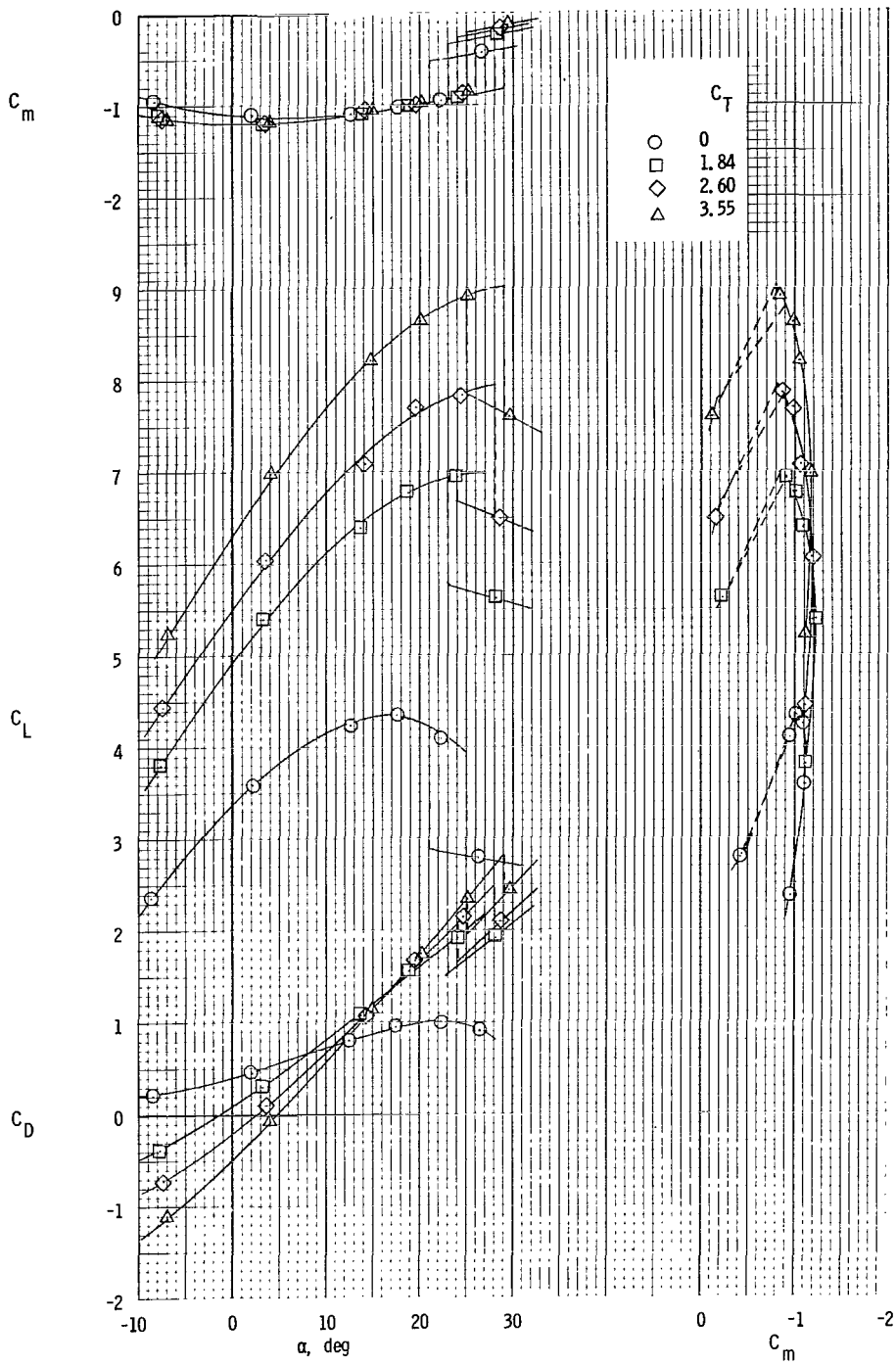

(d) $C_\mu = 0.285$.

Figure 8.- Concluded.

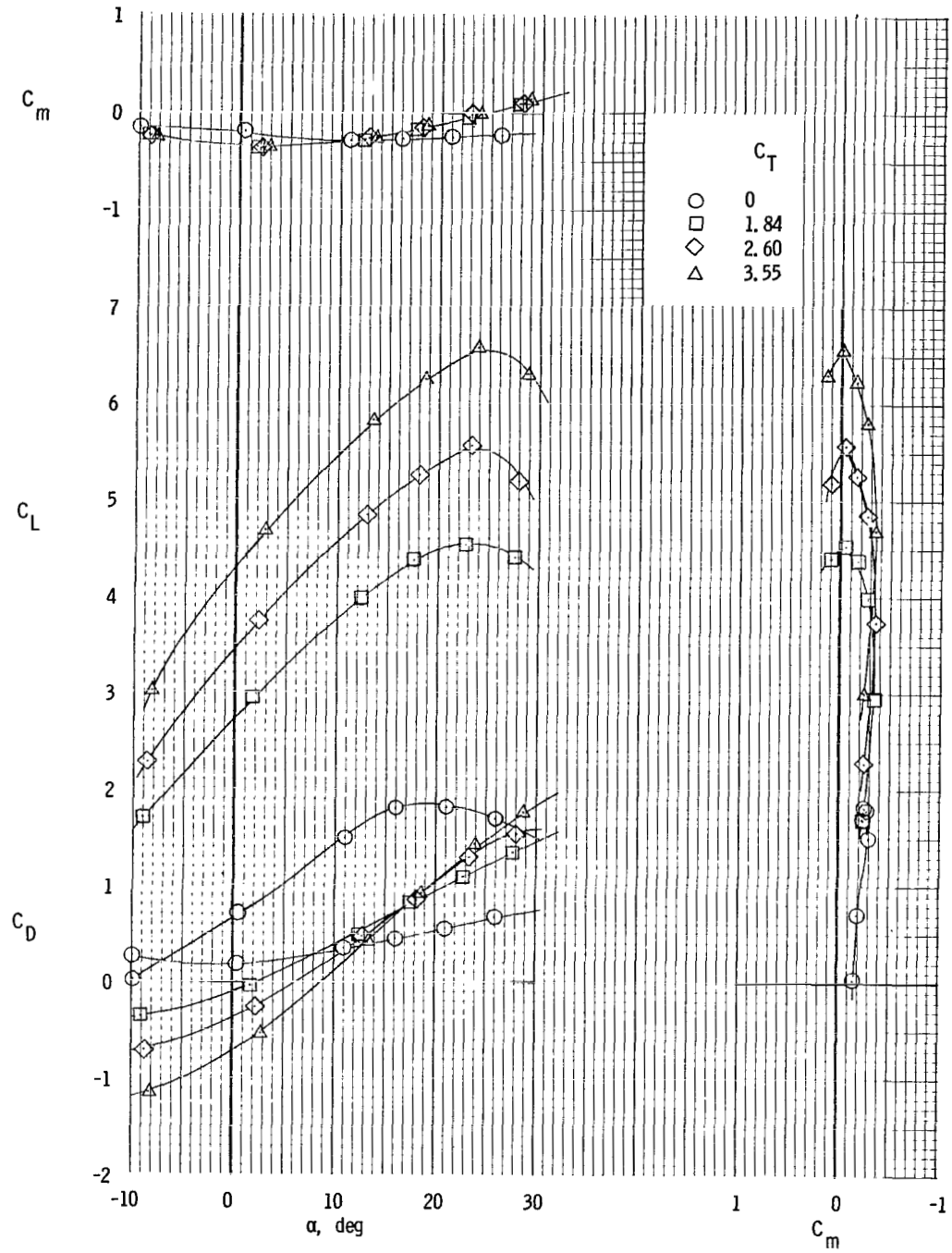

(a) $C_\mu = 0$.

Figure 9.- Longitudinal characteristics of model with aft engines and short chord. $\delta_f = 65^o$.

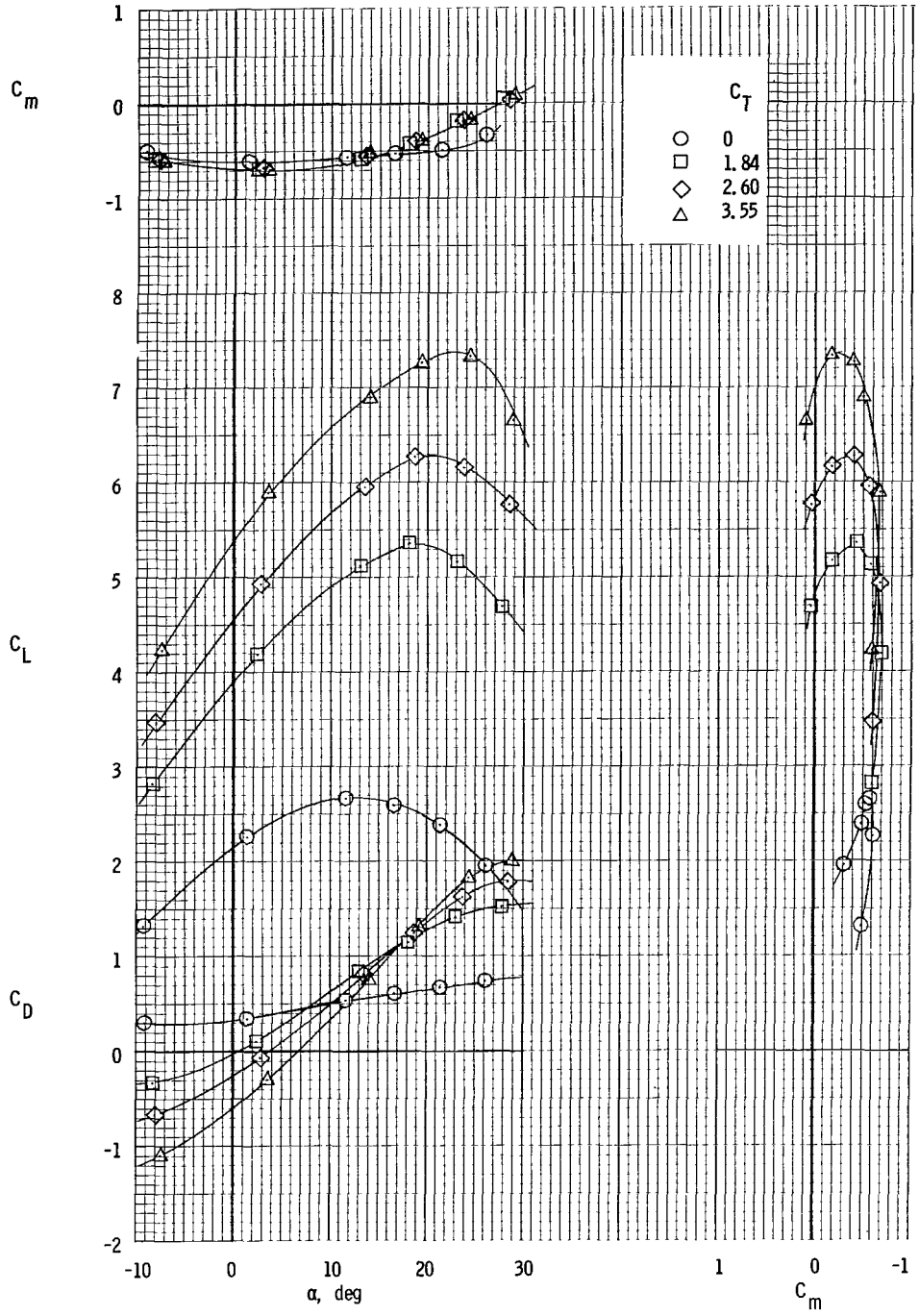

(b) $C_\mu = 0.066$.

Figure 9.- Continued.

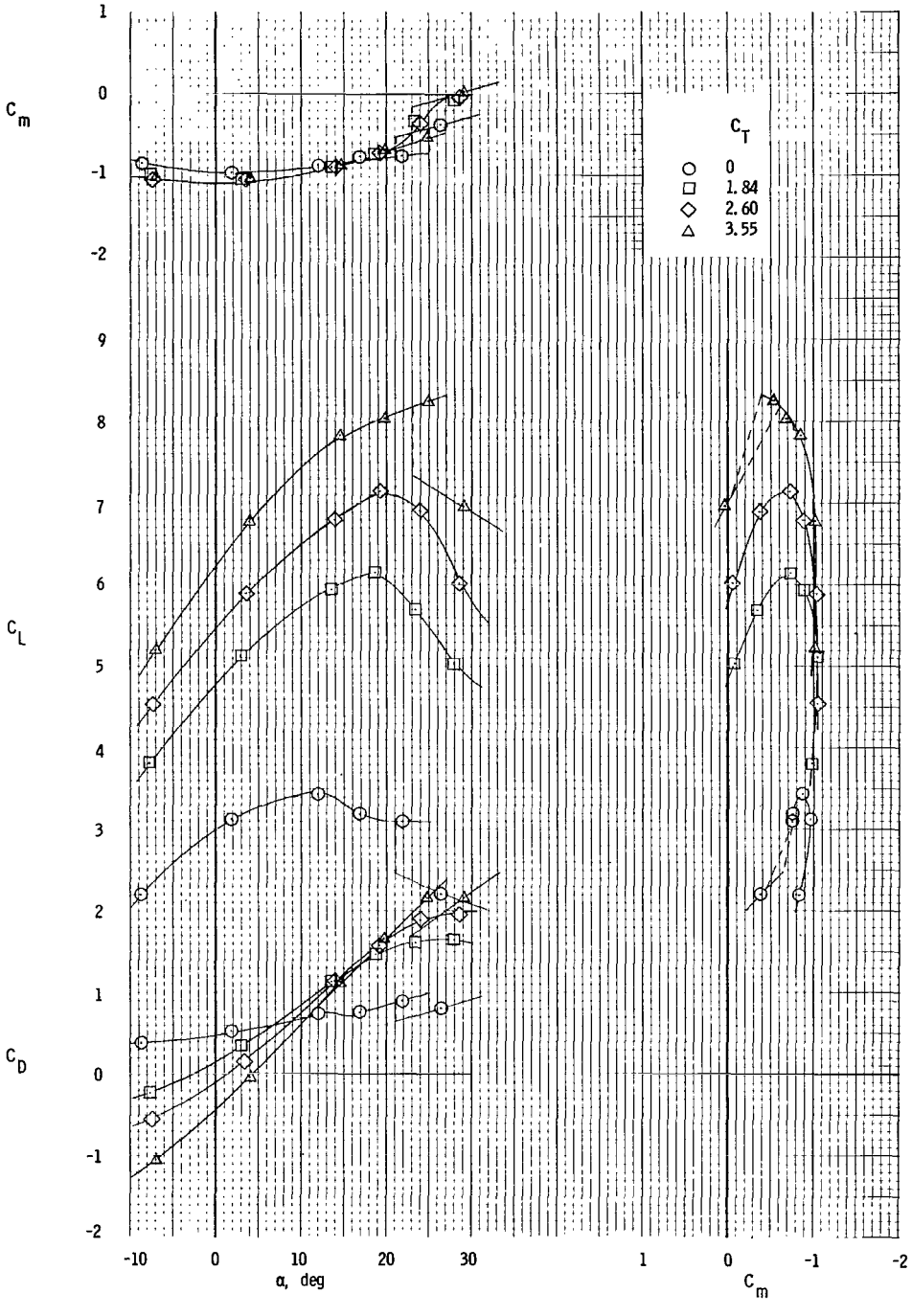

(c) $C_\mu = 0.168$.

Figure 9.- Continued.

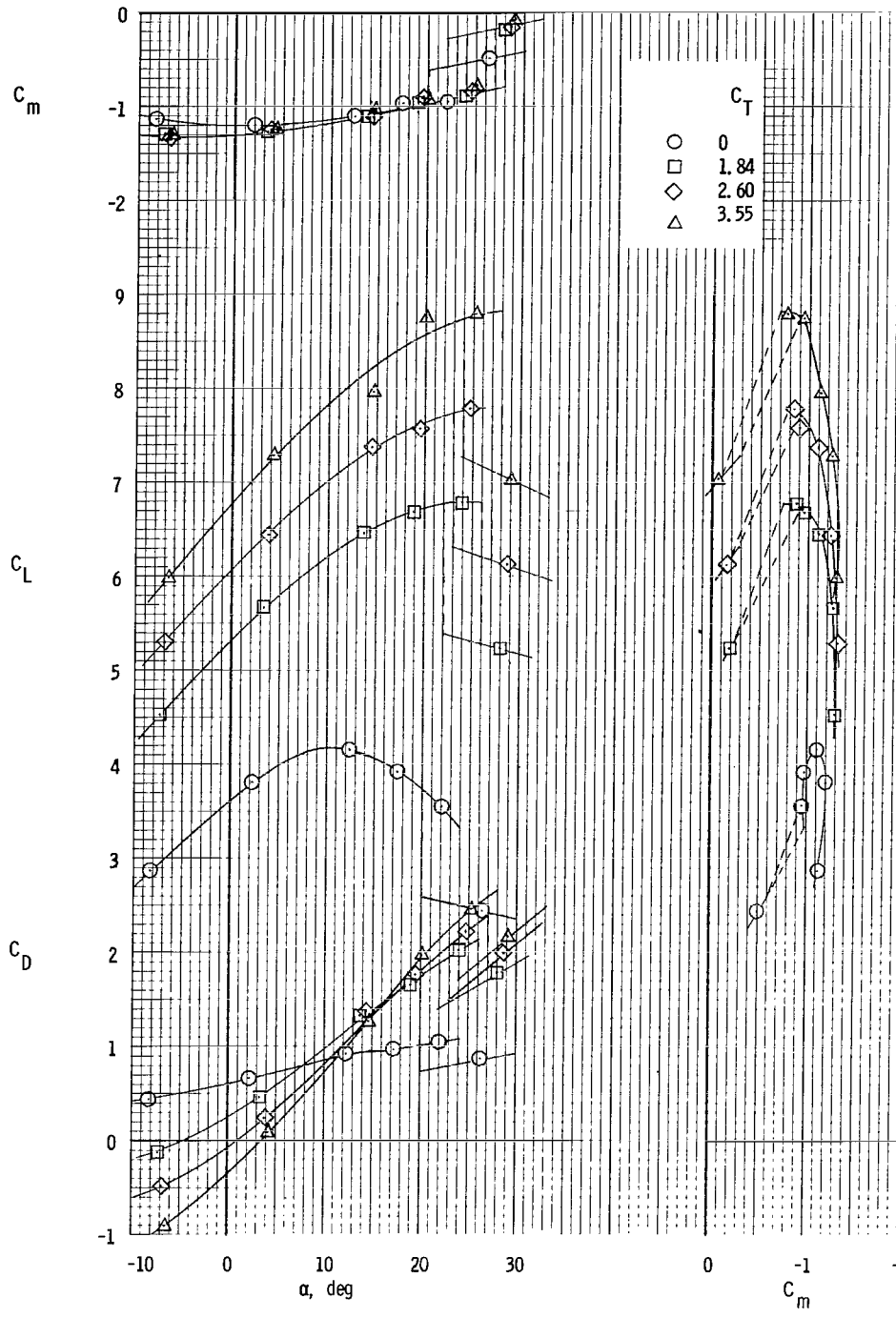

(d) C_μ = 0.285.

Figure 9.- Concluded.

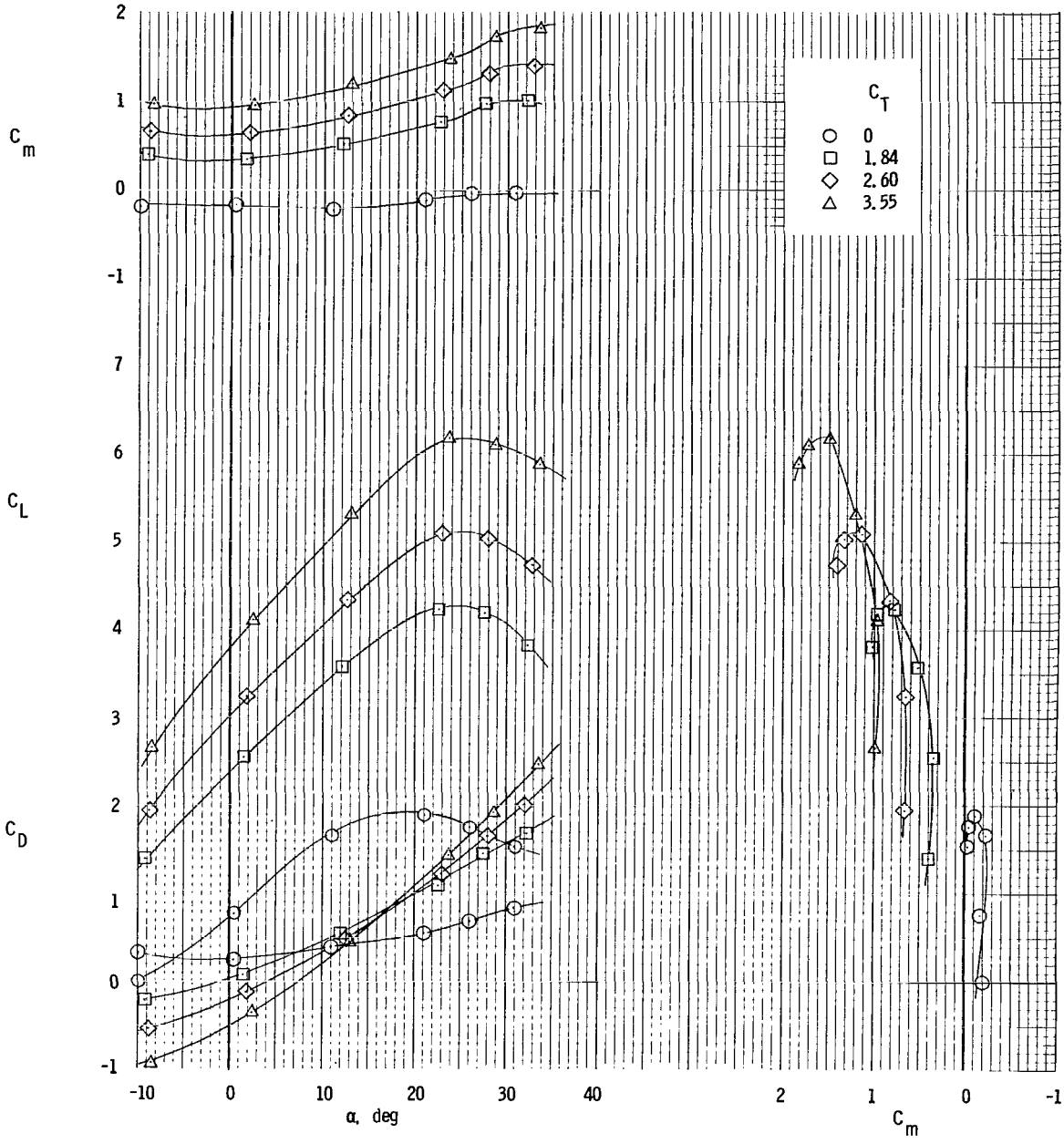

(a) $C_\mu = 0$.

Figure 10.- Longitudinal characteristics of model with short chord. $\delta_f = 50^o$; forward engine position.

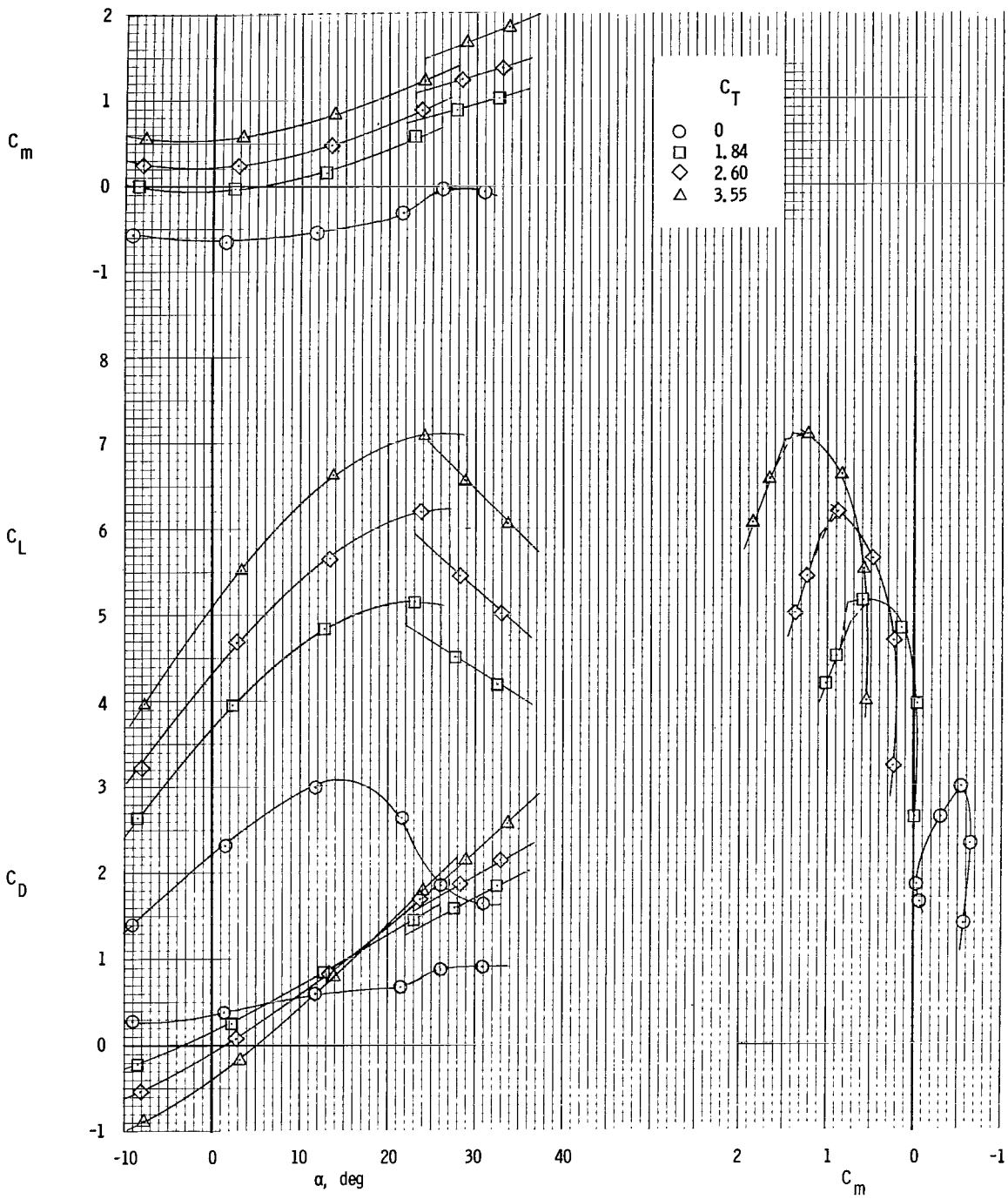

(b) $C_\mu = 0.066$.

Figure 10.- Continued.

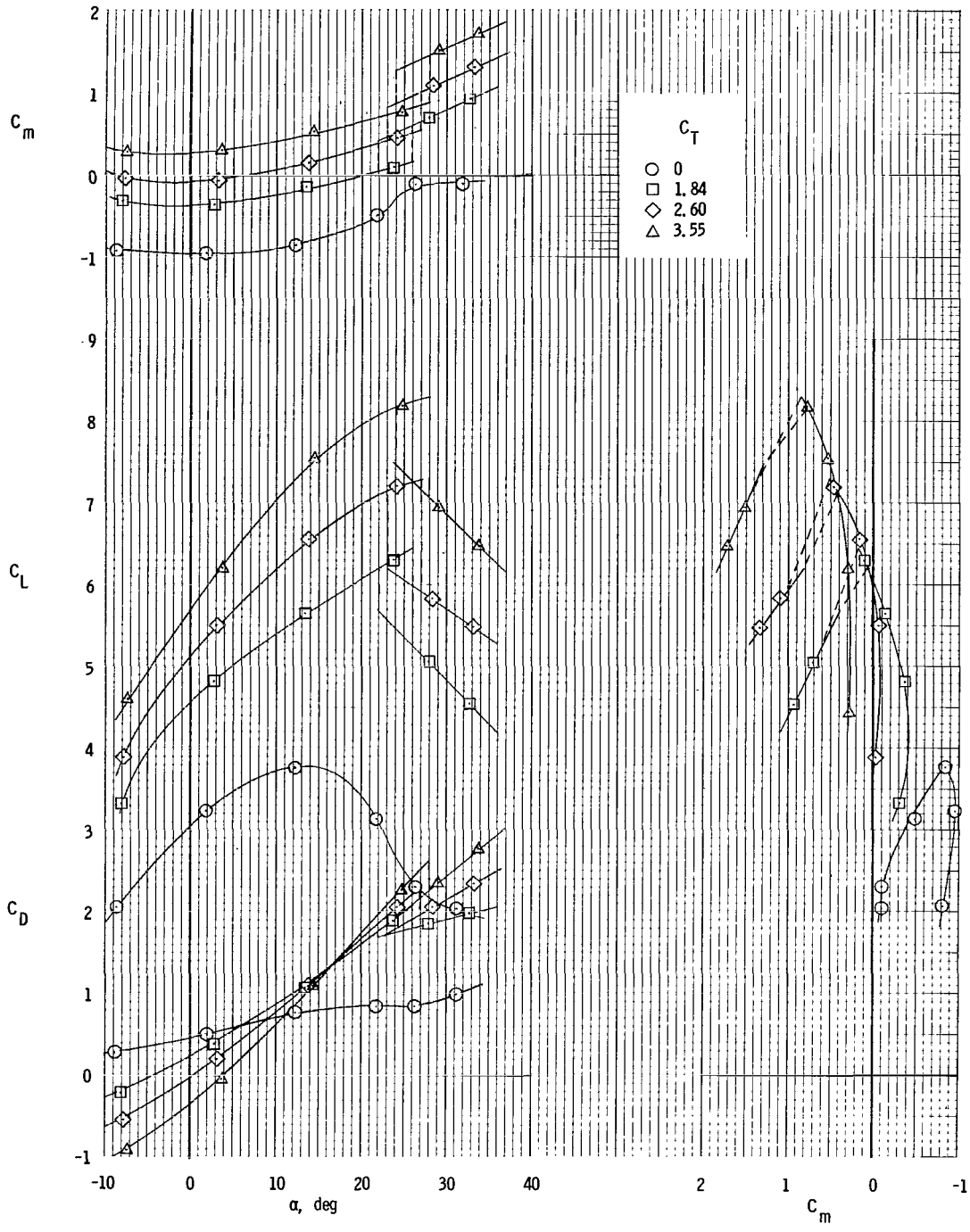

(c) $C_\mu = 0.168$.

Figure 10.- Continued.

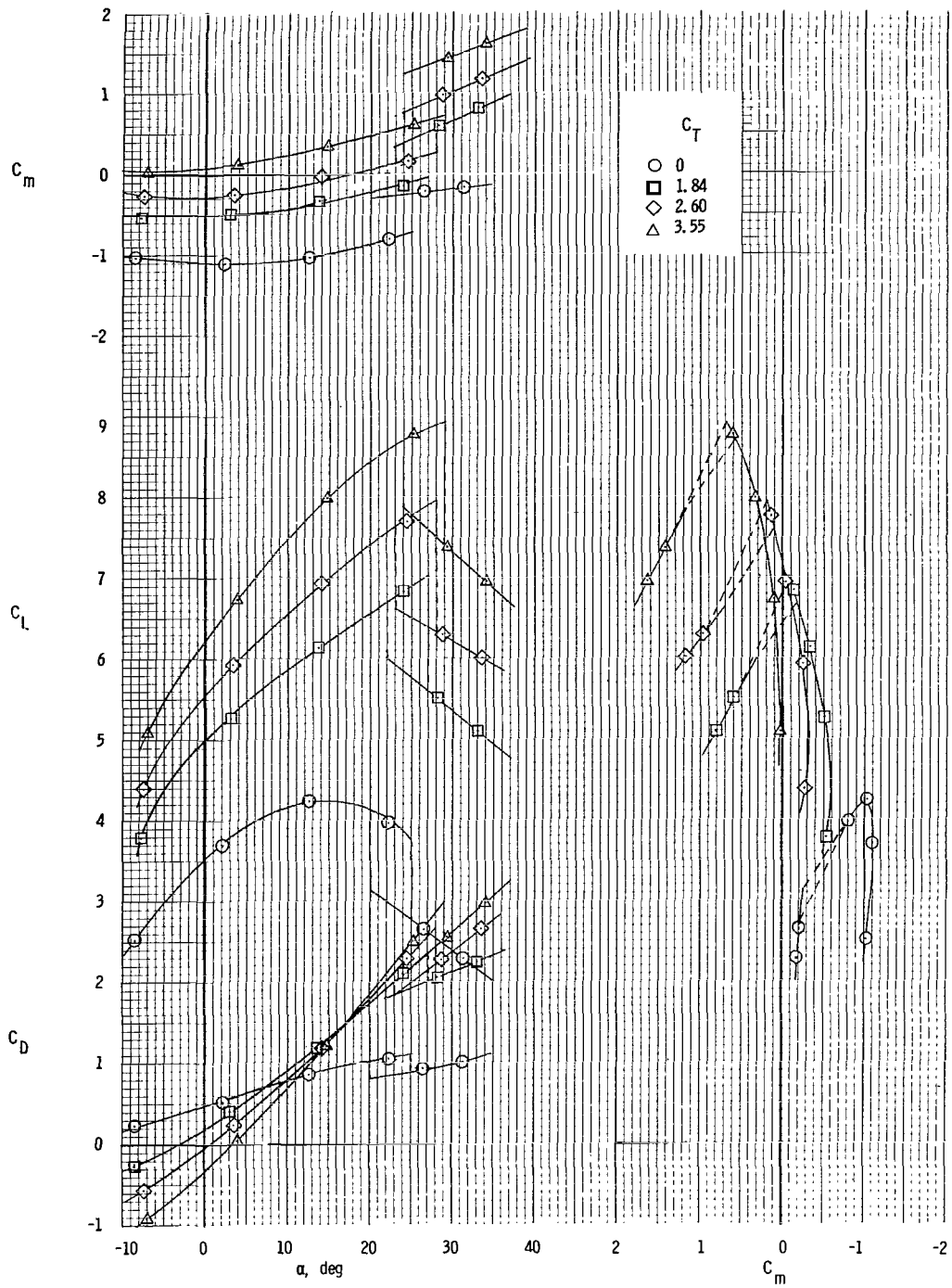

(d) $C_\mu = 0.285$.

Figure 10.- Concluded.

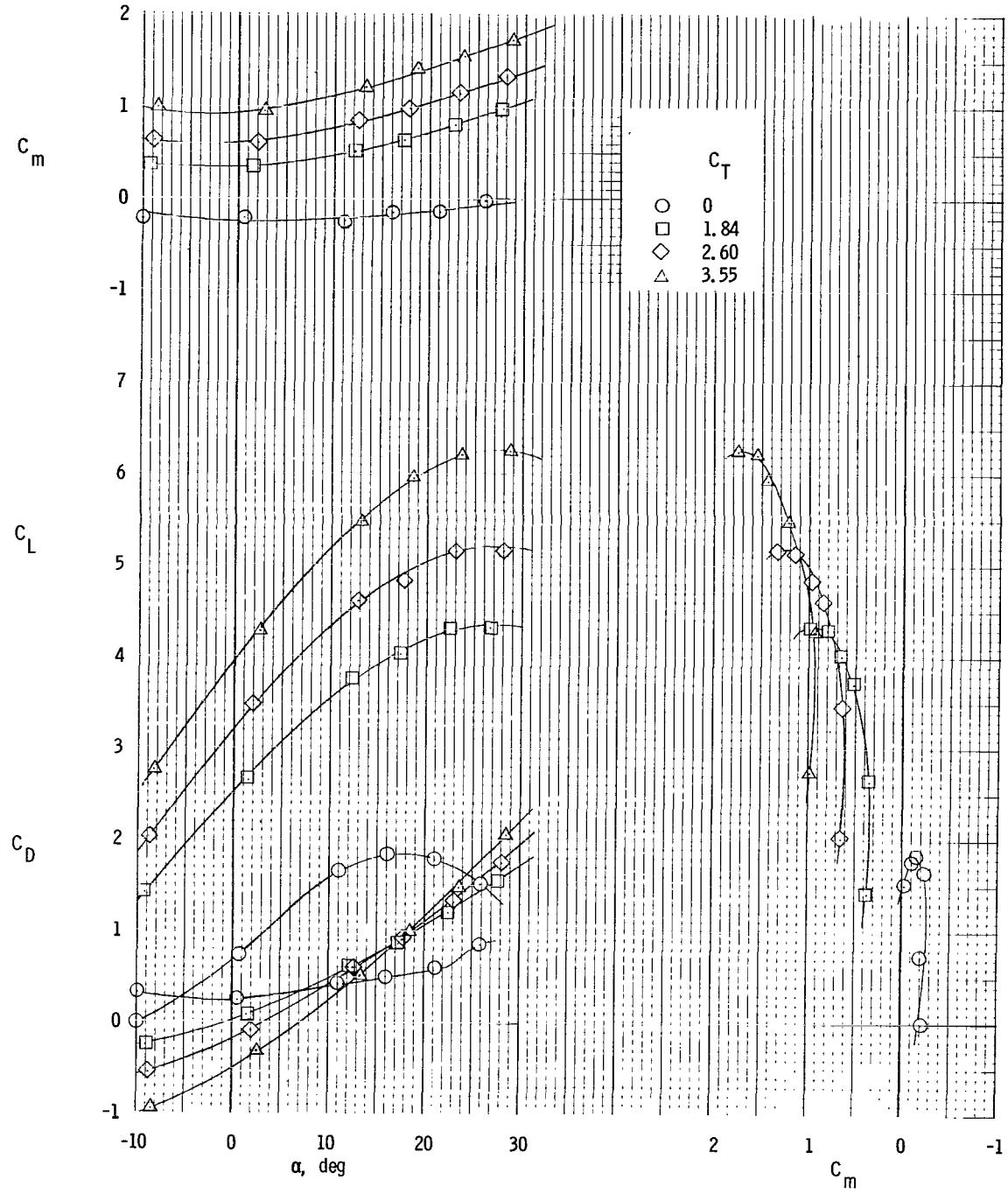

(a) $C_\mu = 0$.

Figure 11.- Longitudinal characteristics of model with short chord. $\delta_f = 65^o$; forward engine position.

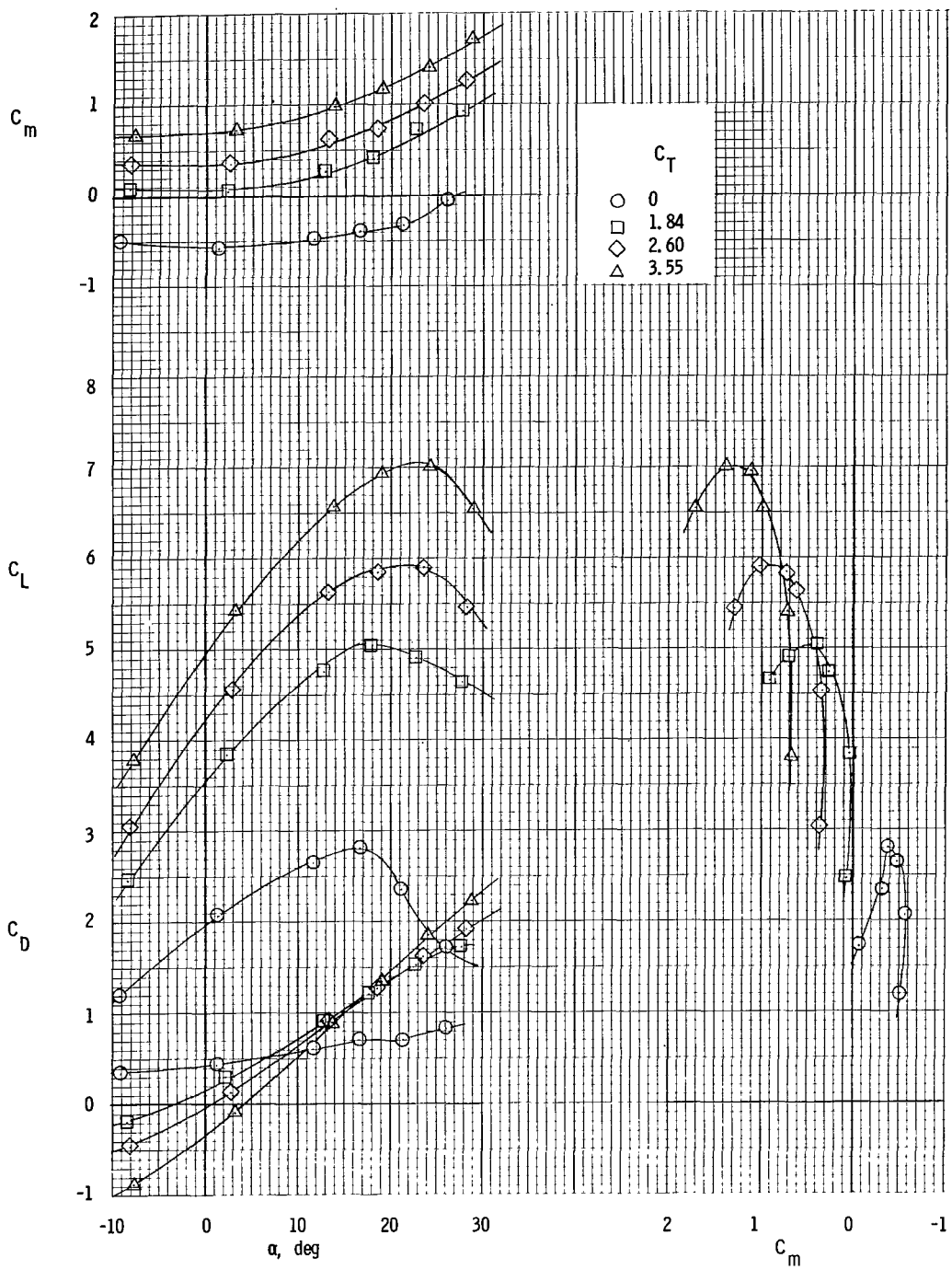

(b) C_μ = 0.066.

Figure 11.- Continued.

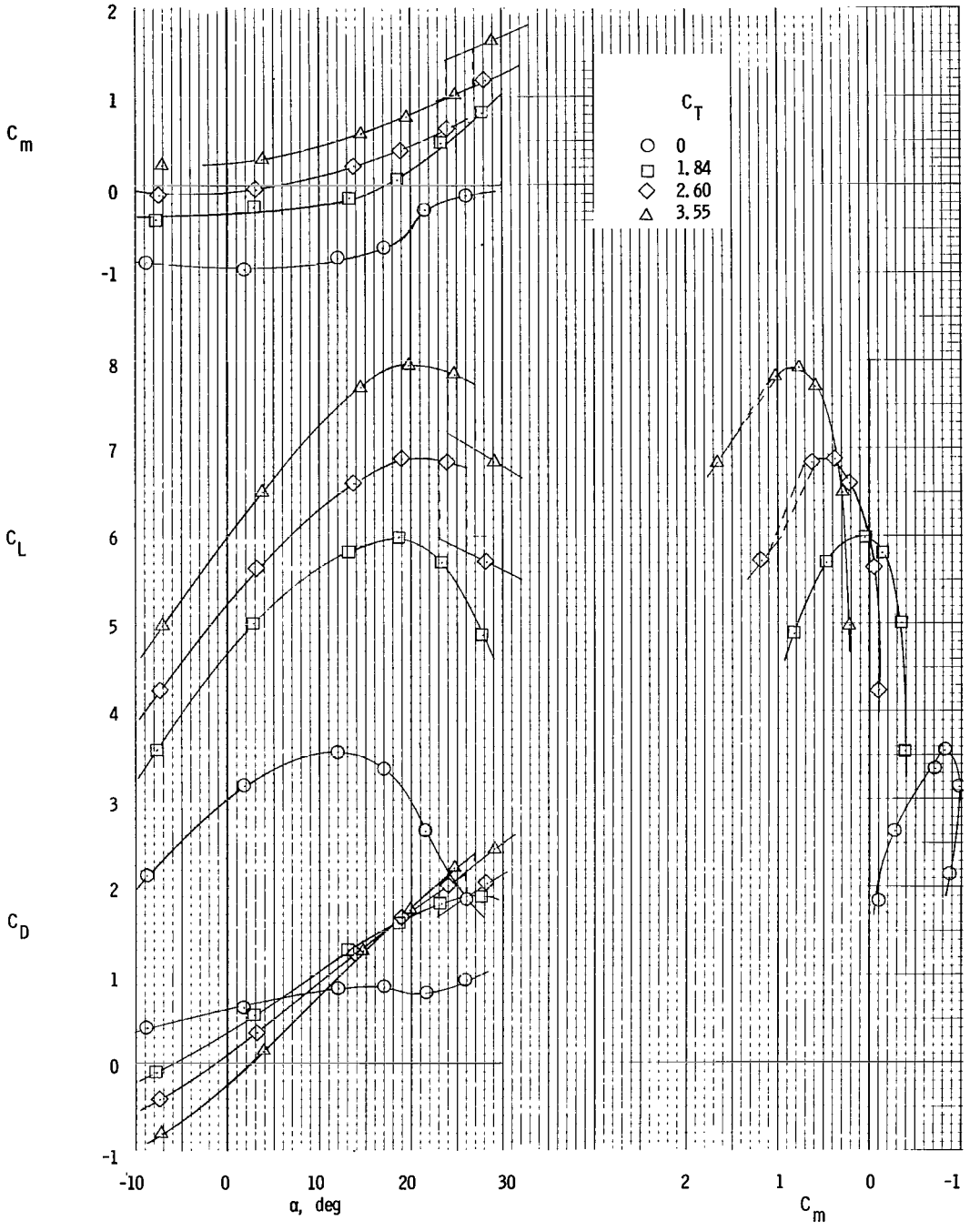

(c) $C_\mu = 0.168$.

Figure 11.- Continued.

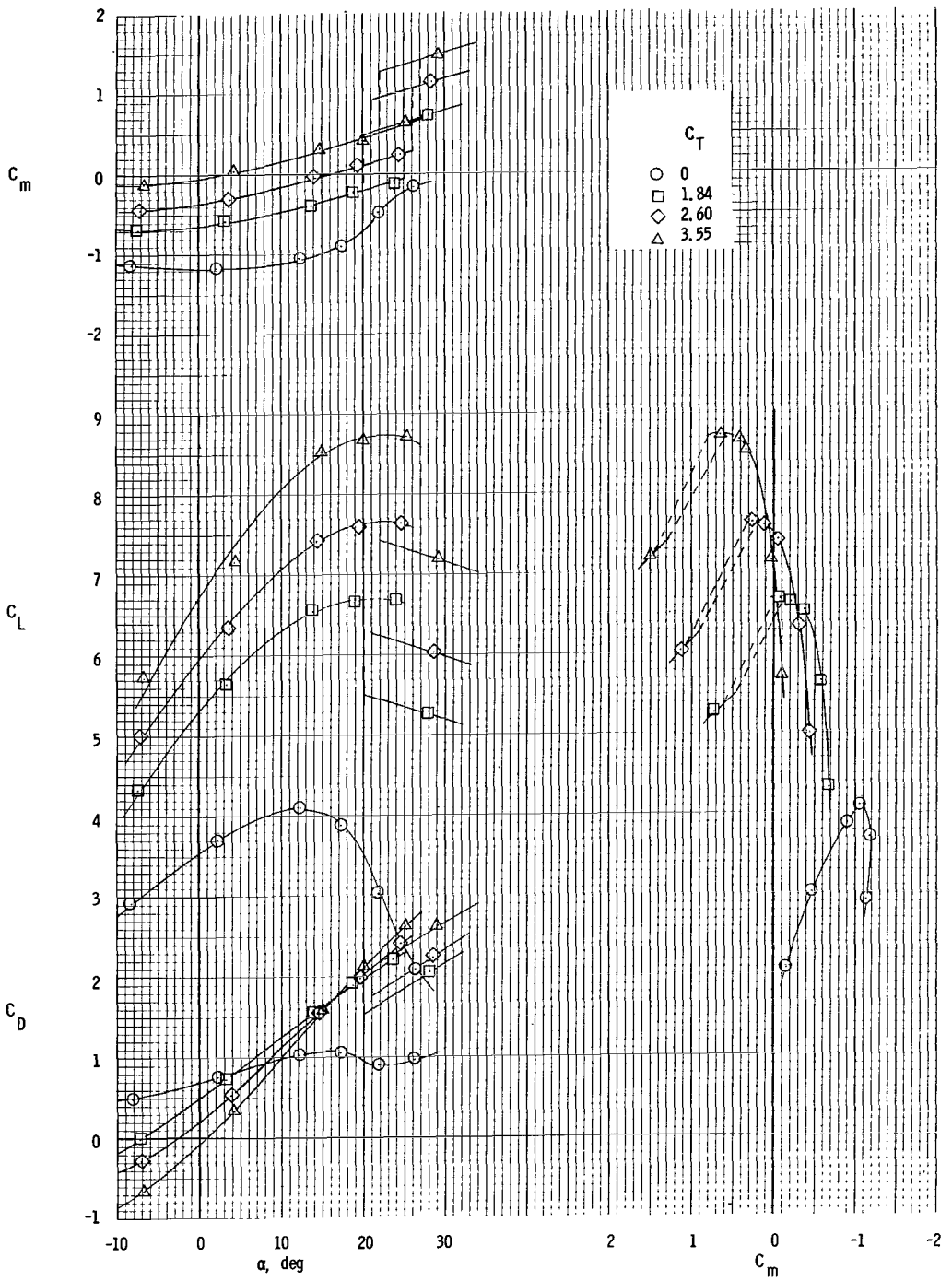

(d) $C_\mu = 0.285$.

Figure 11.- Concluded.

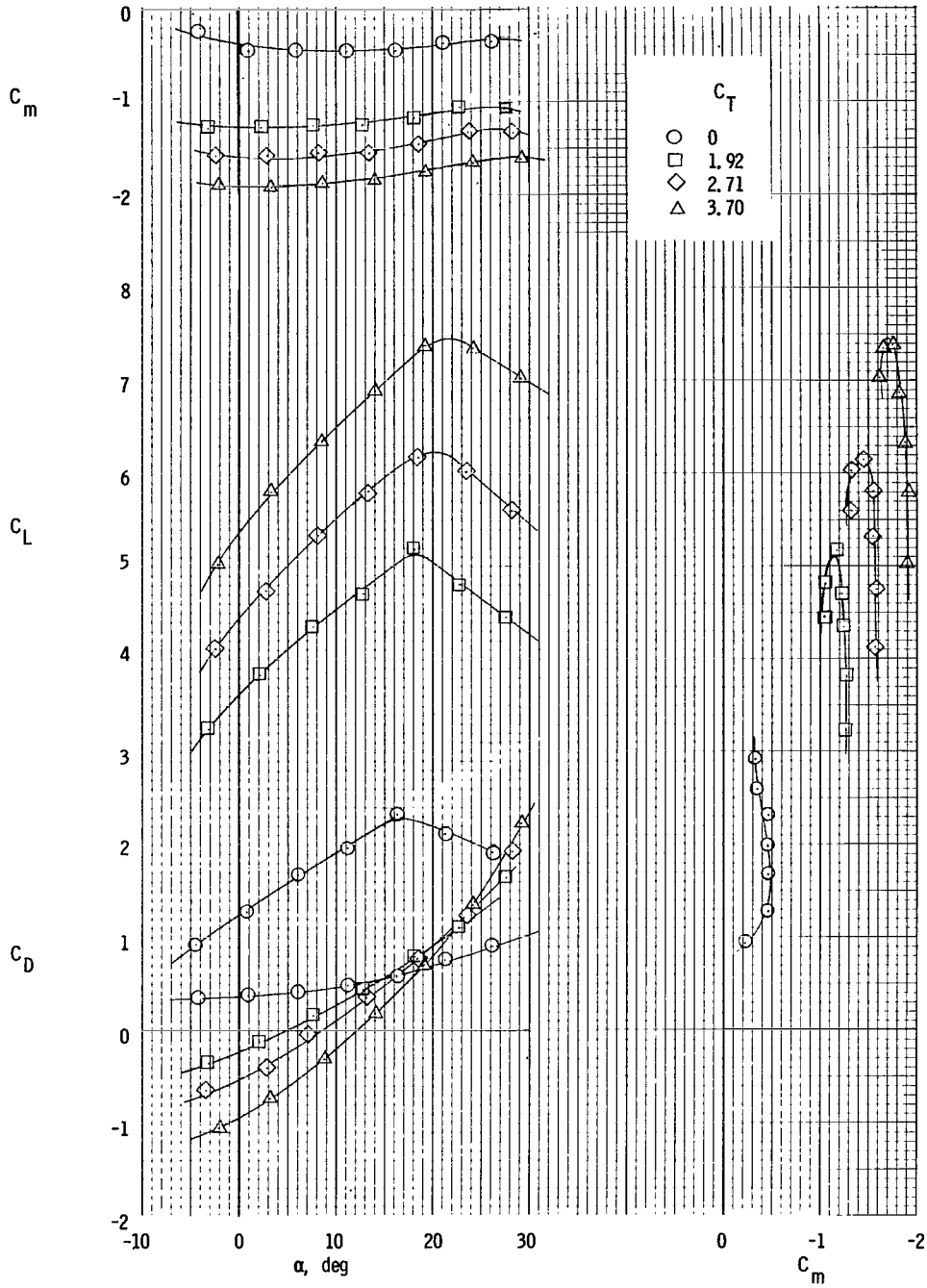

(a) $C_\mu = 0$.

Figure 12.- Longitudinal characteristics of model with engines far aft, with inboard flap segment shortened. $\delta_{f,ext} = 65^o$.

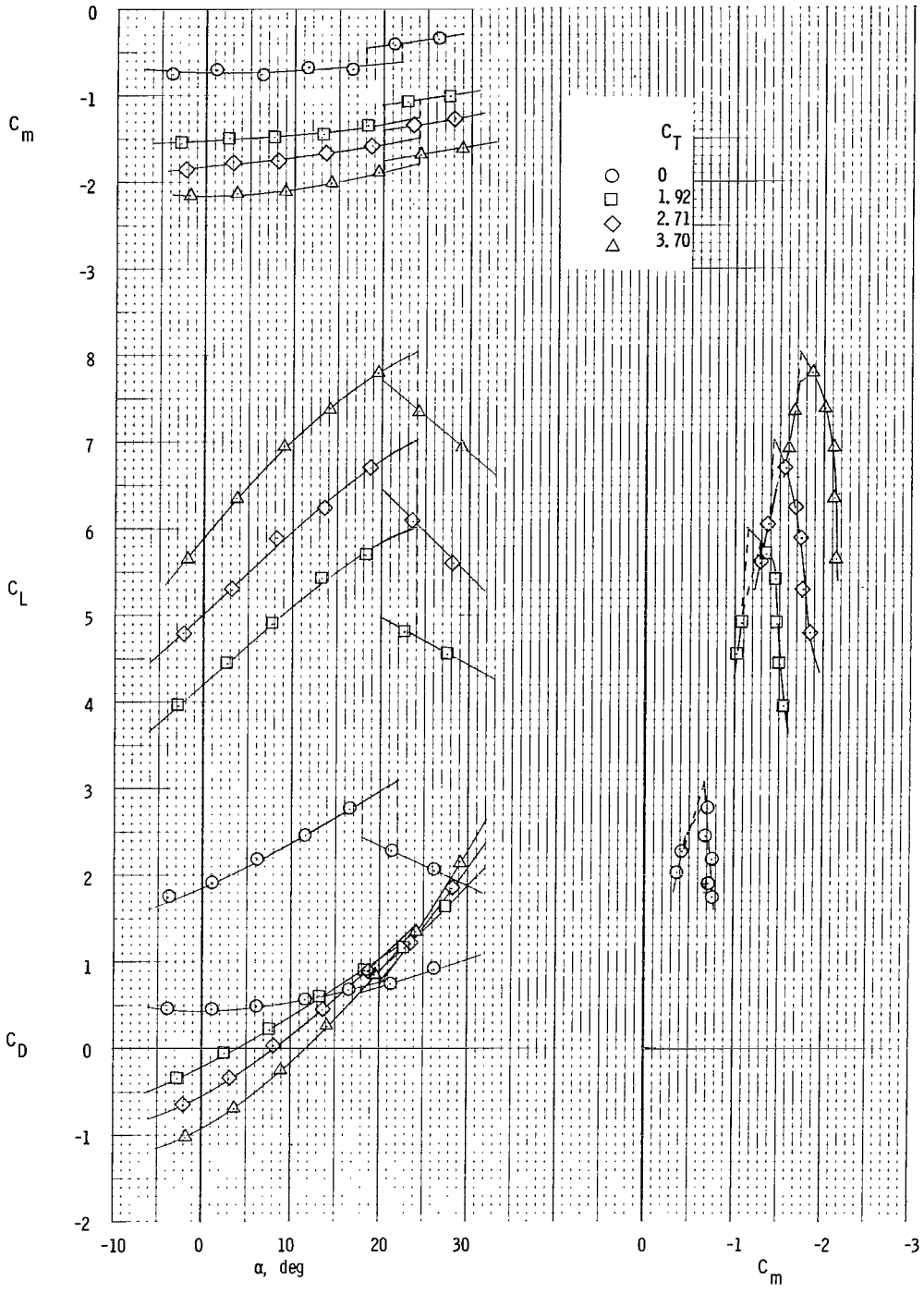

(b) $C_\mu = 0.075$.

Figure 12.- Continued.

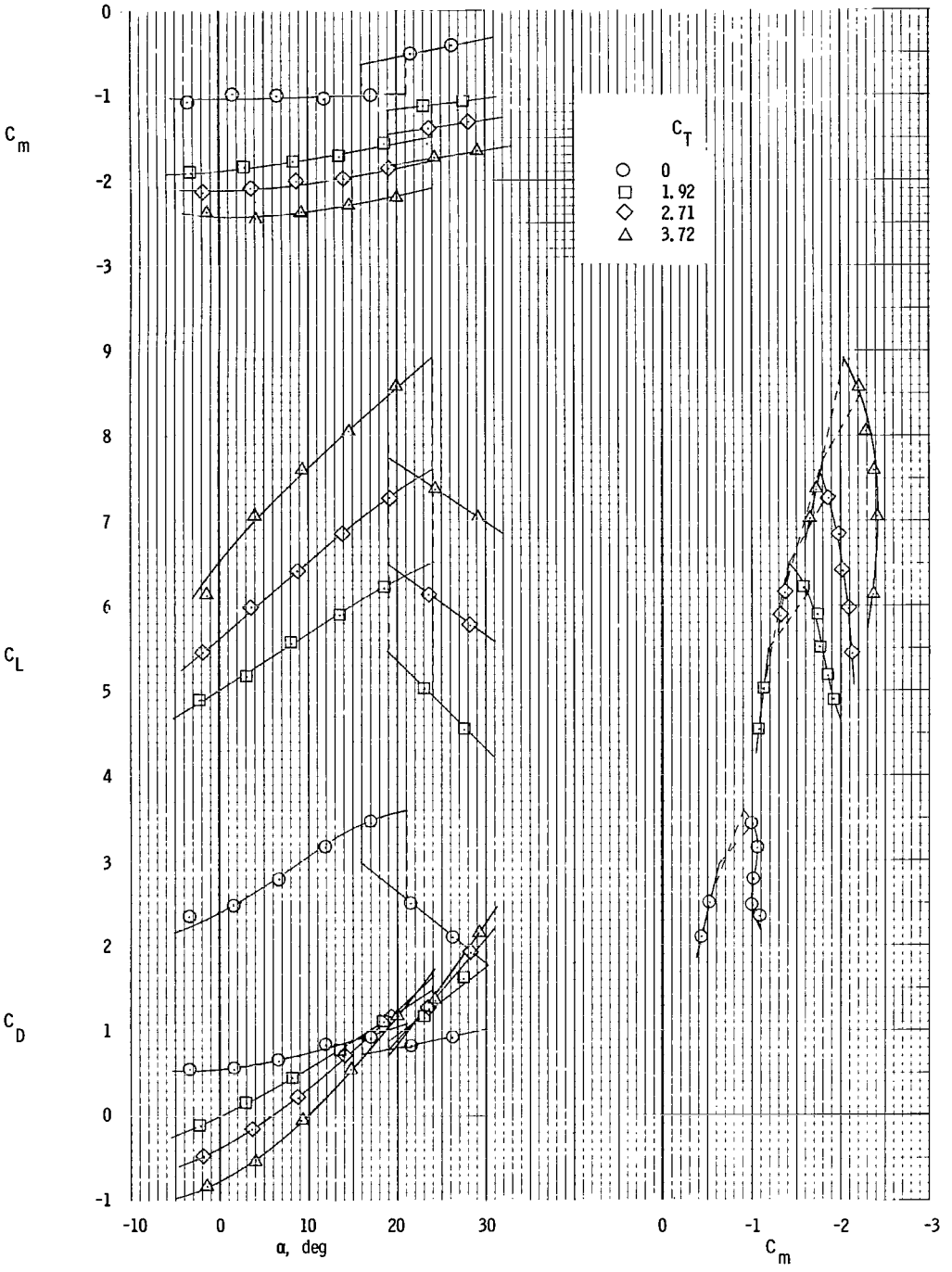

(c) $C_\mu = 0.191$.

Figure 12.- Continued.

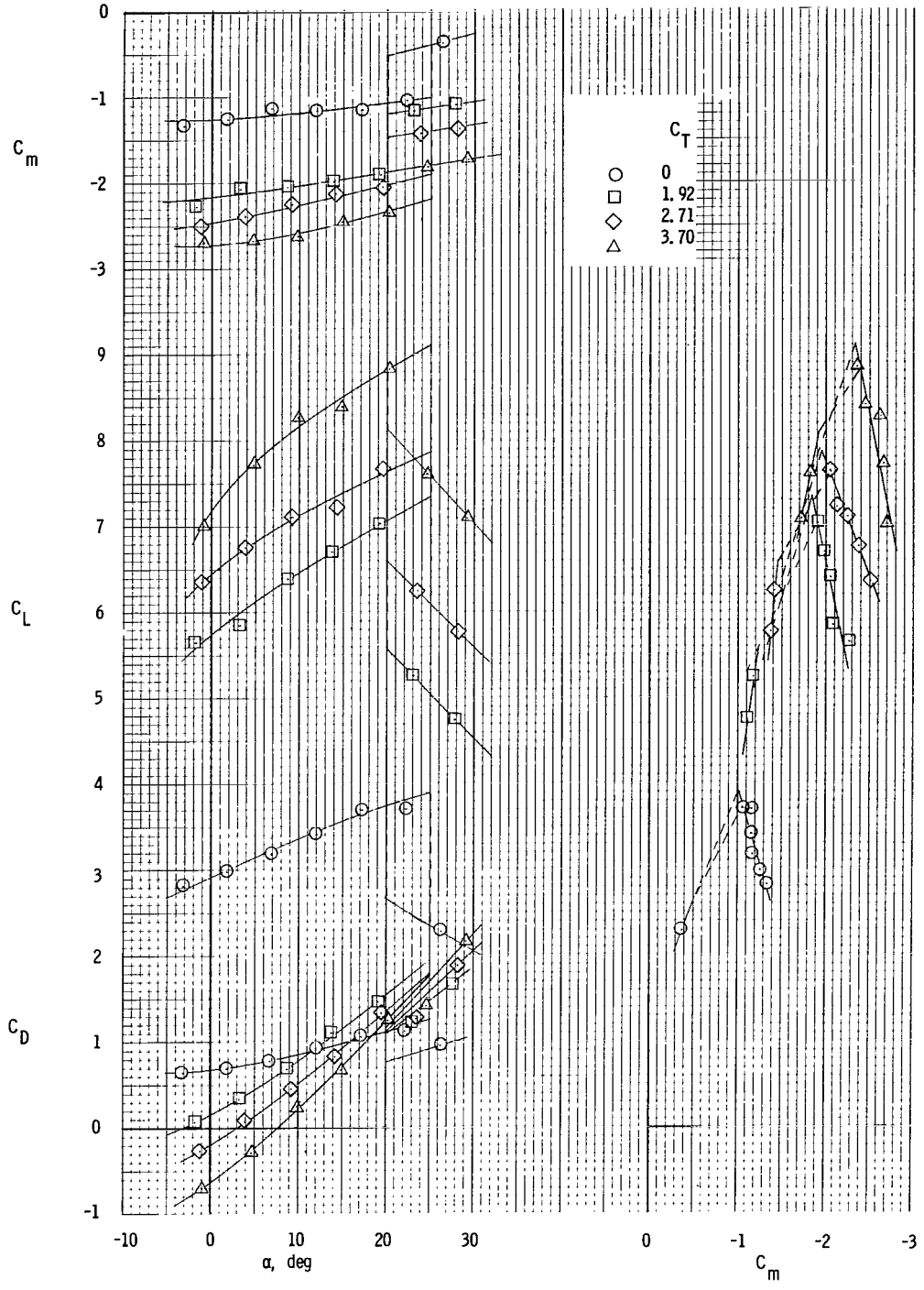

(d) $C_\mu = 0.324$.

Figure 12.- Concluded.

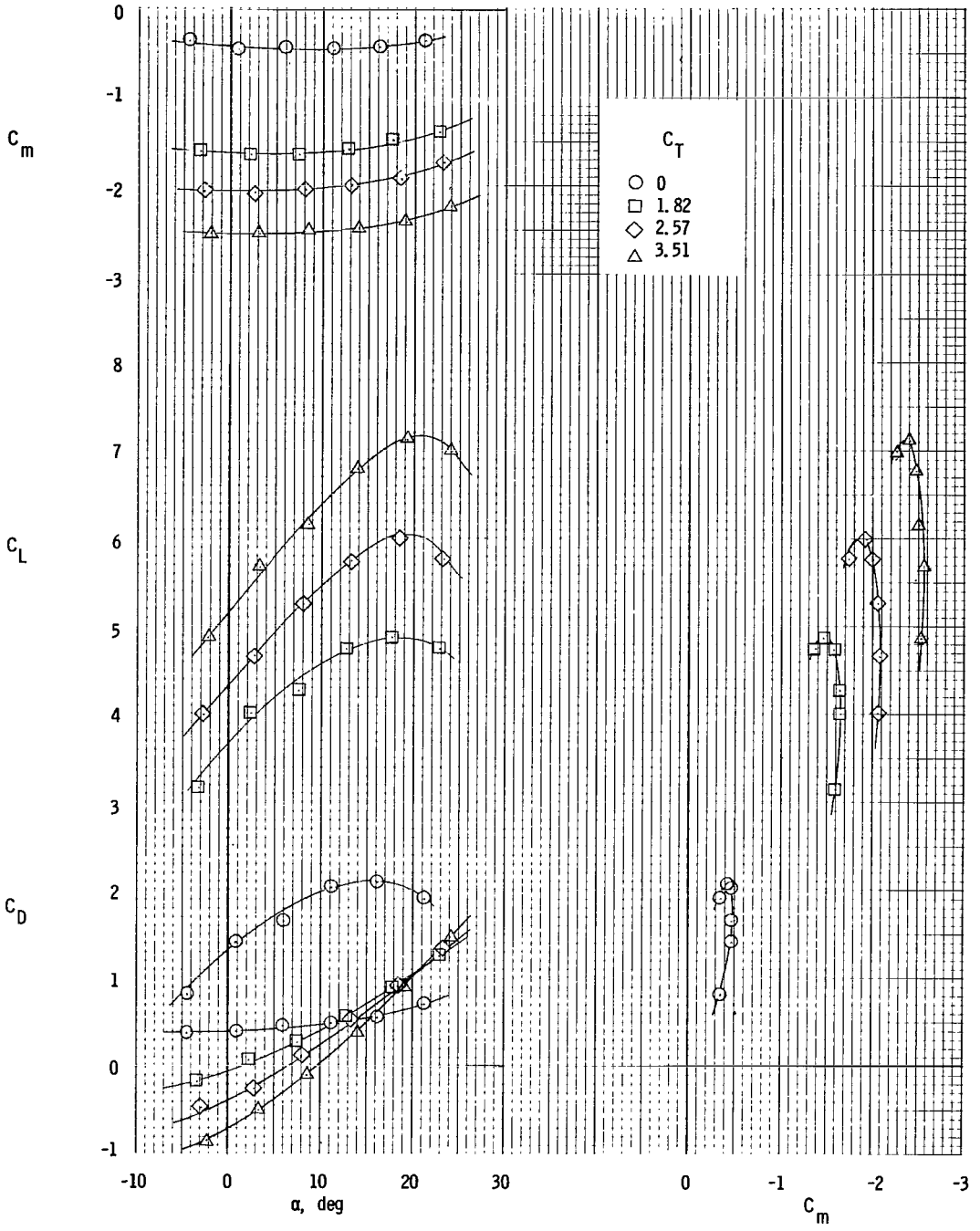

(a) $C_\mu = 0$.

Figure 13.- Longitudinal characteristics of model with engines far aft and tilted, with inboard flap segment shortened. $\delta_{f,ext} = 65^o$.

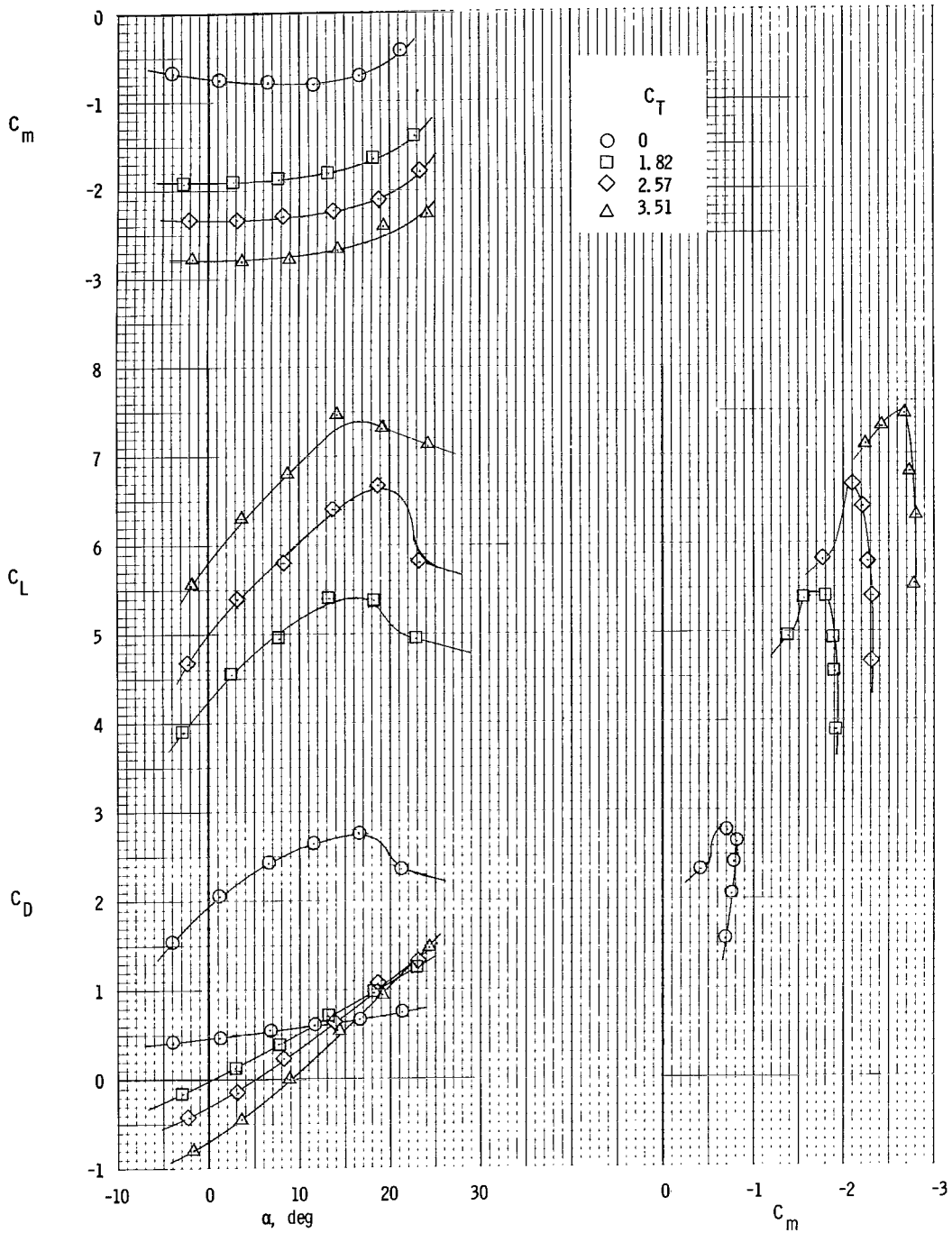

(b) $C_\mu = 0.075$.

Figure 13.- Continued.

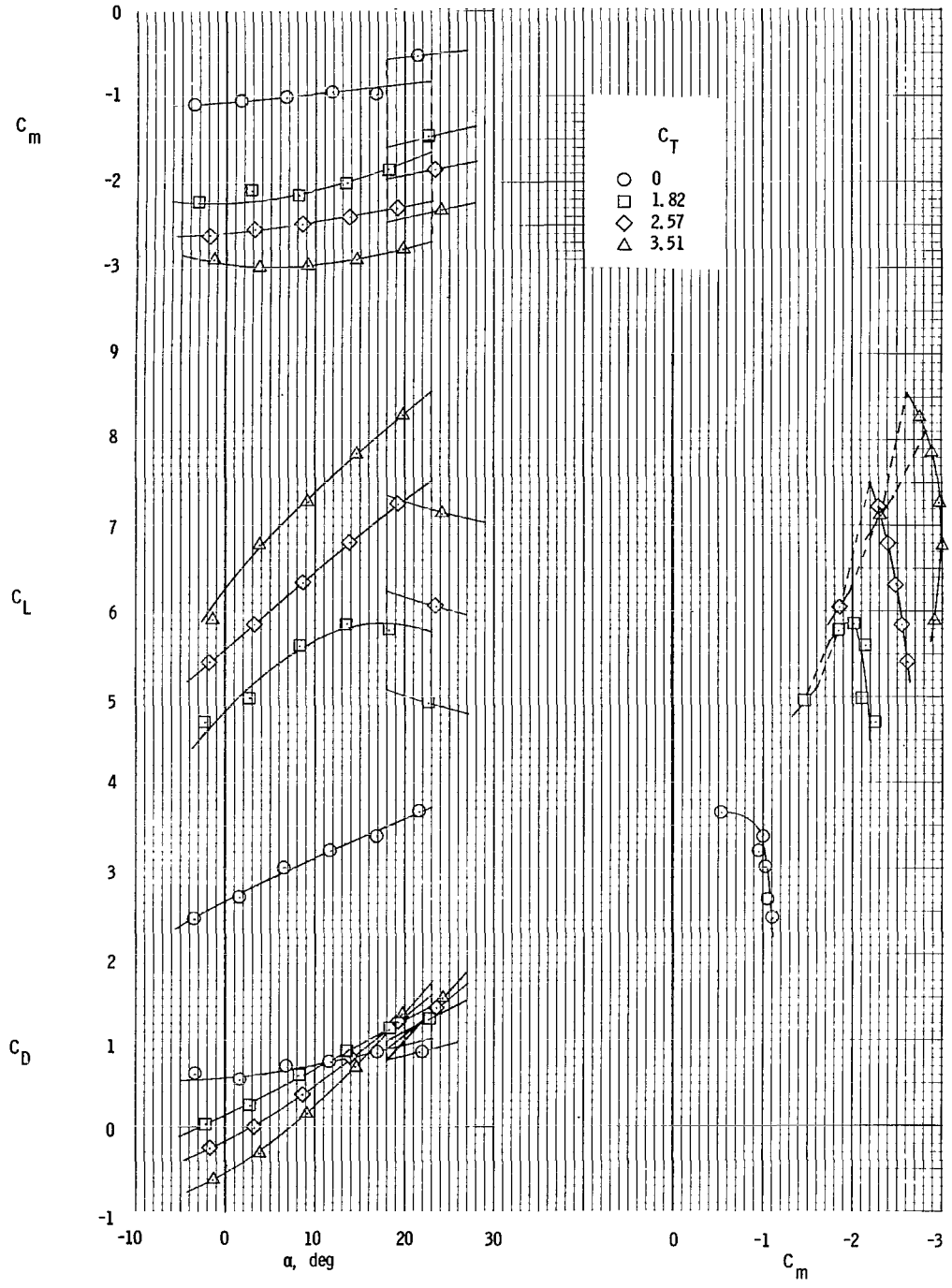

(c) $C_\mu = 0.191$.

Figure 13.- Continued.

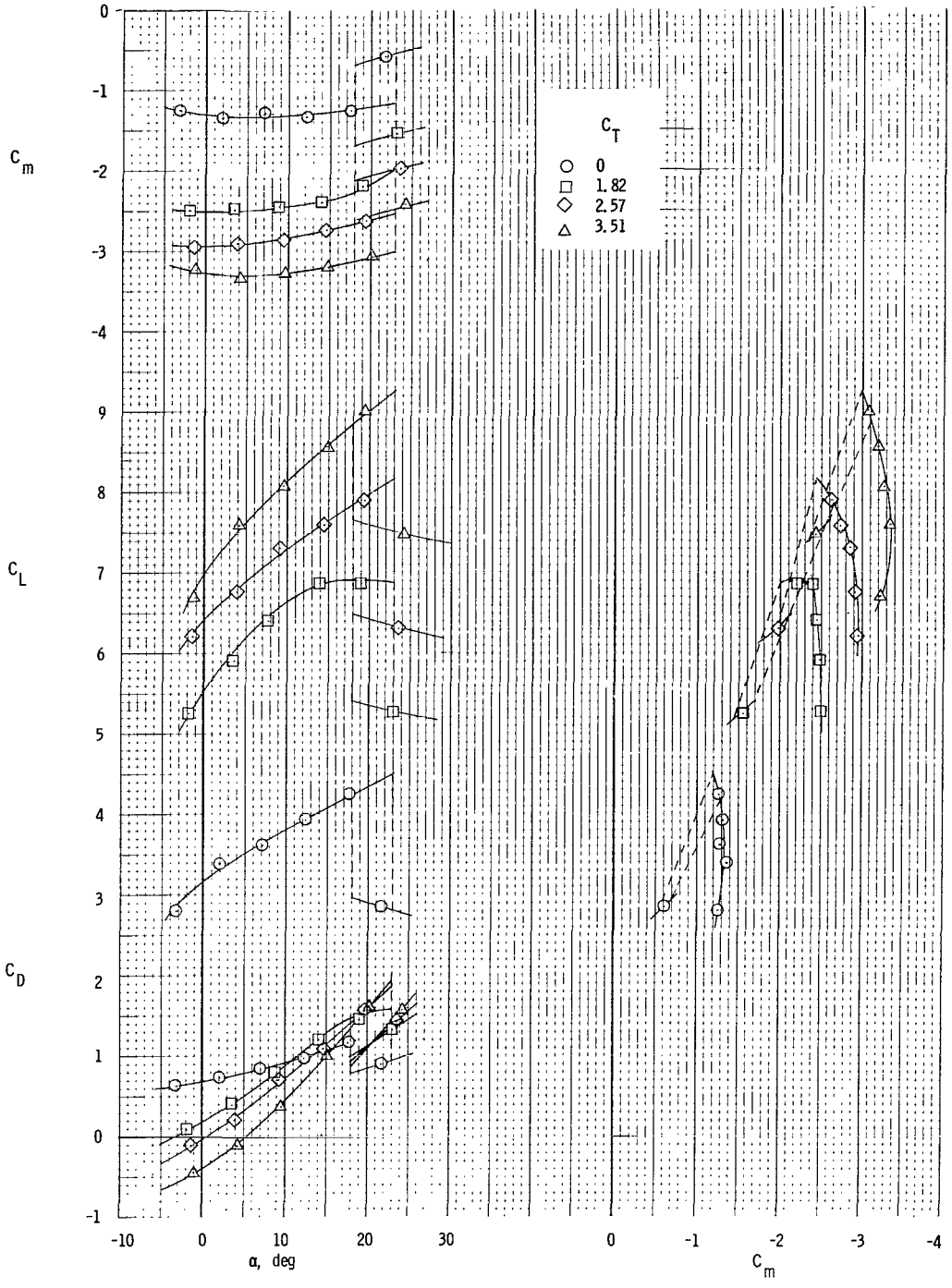

(d) $C_\mu = 0.324$.

Figure 13.- Concluded.

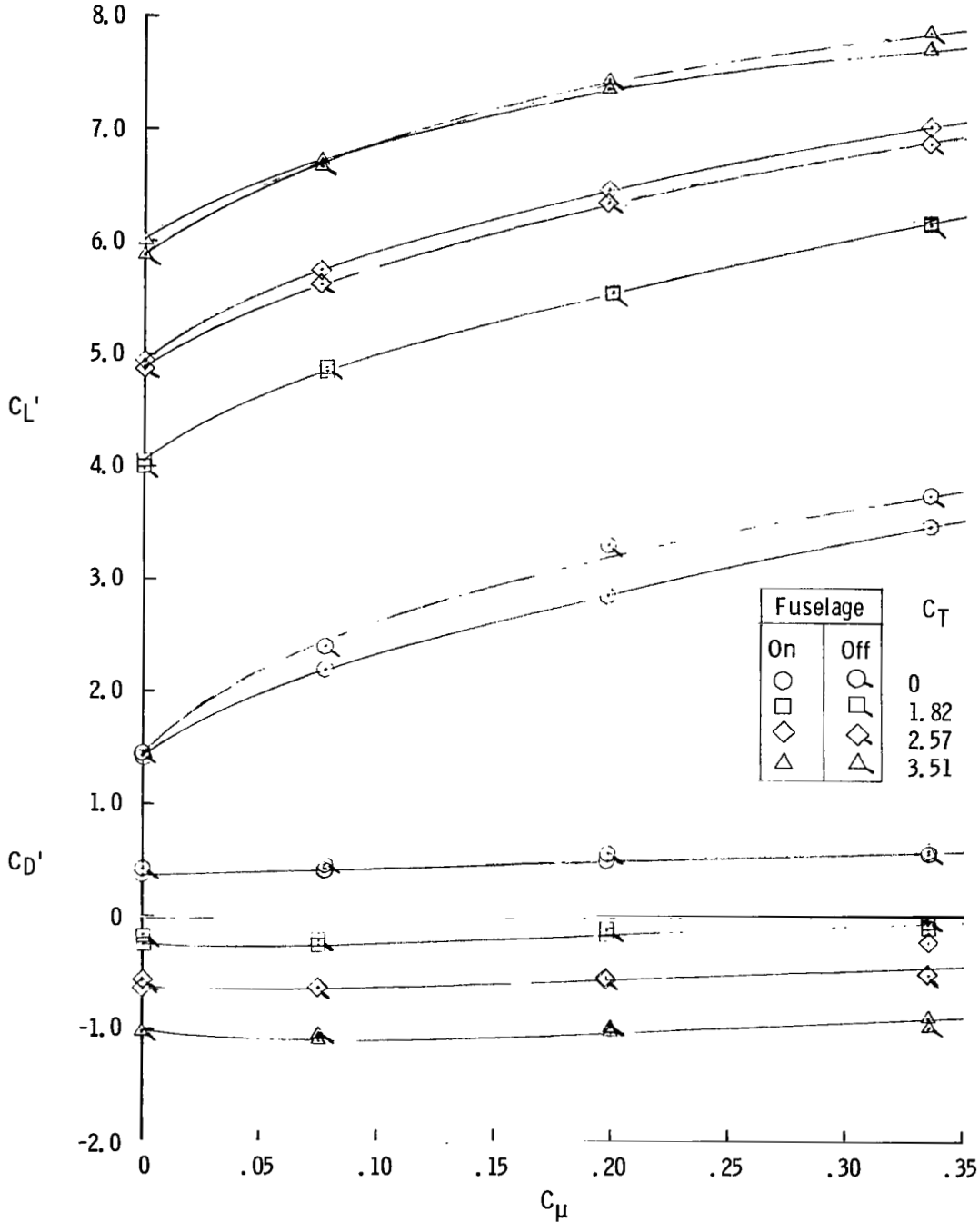

Figure 14.- The effects of the presence of a fuselage on lift and drag at $\alpha' = 0^o$.

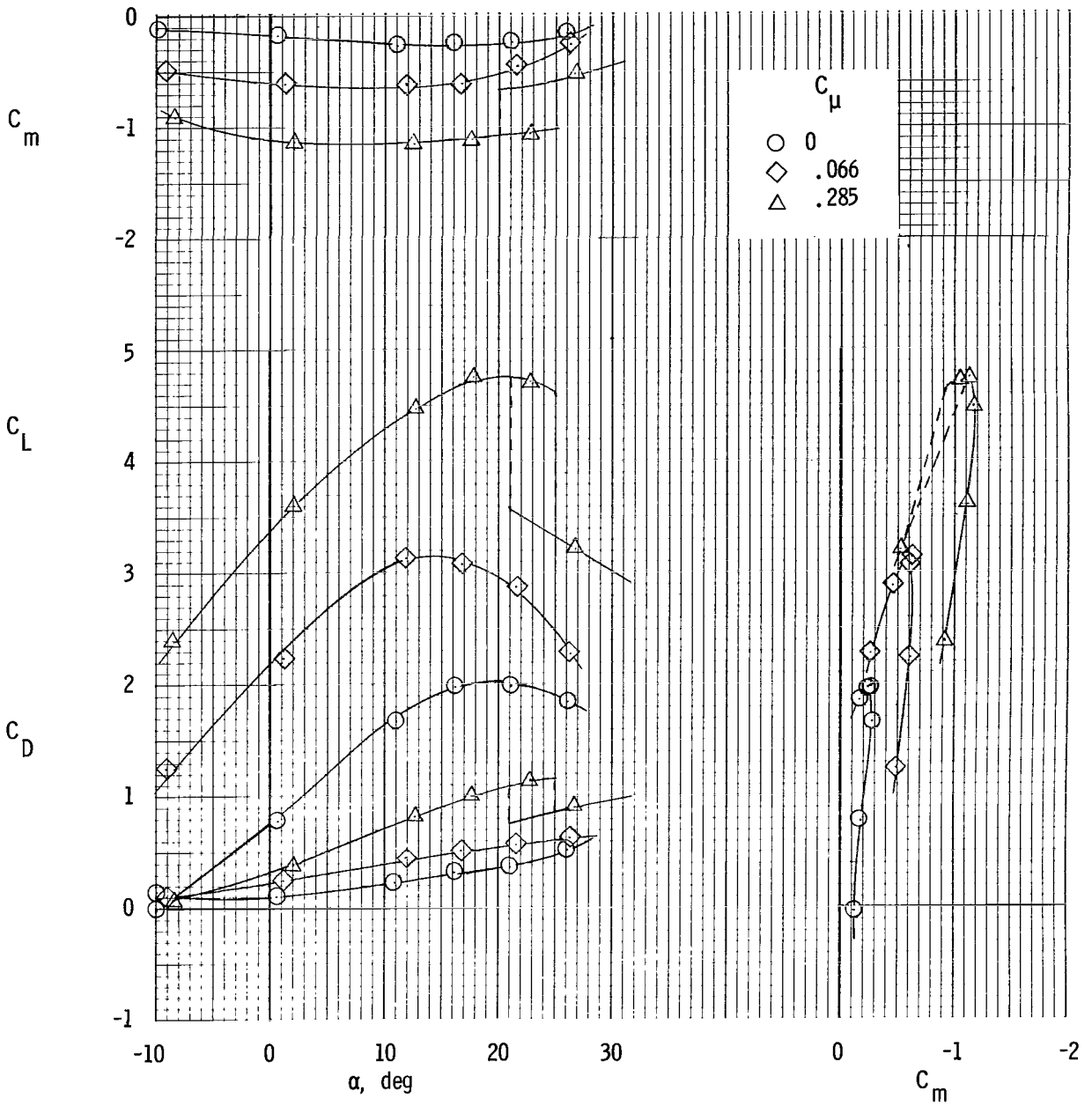

Figure 15.- Longitudinal characteristics of model with short chord flap. Engines removed; $\delta_f = 50^o$.

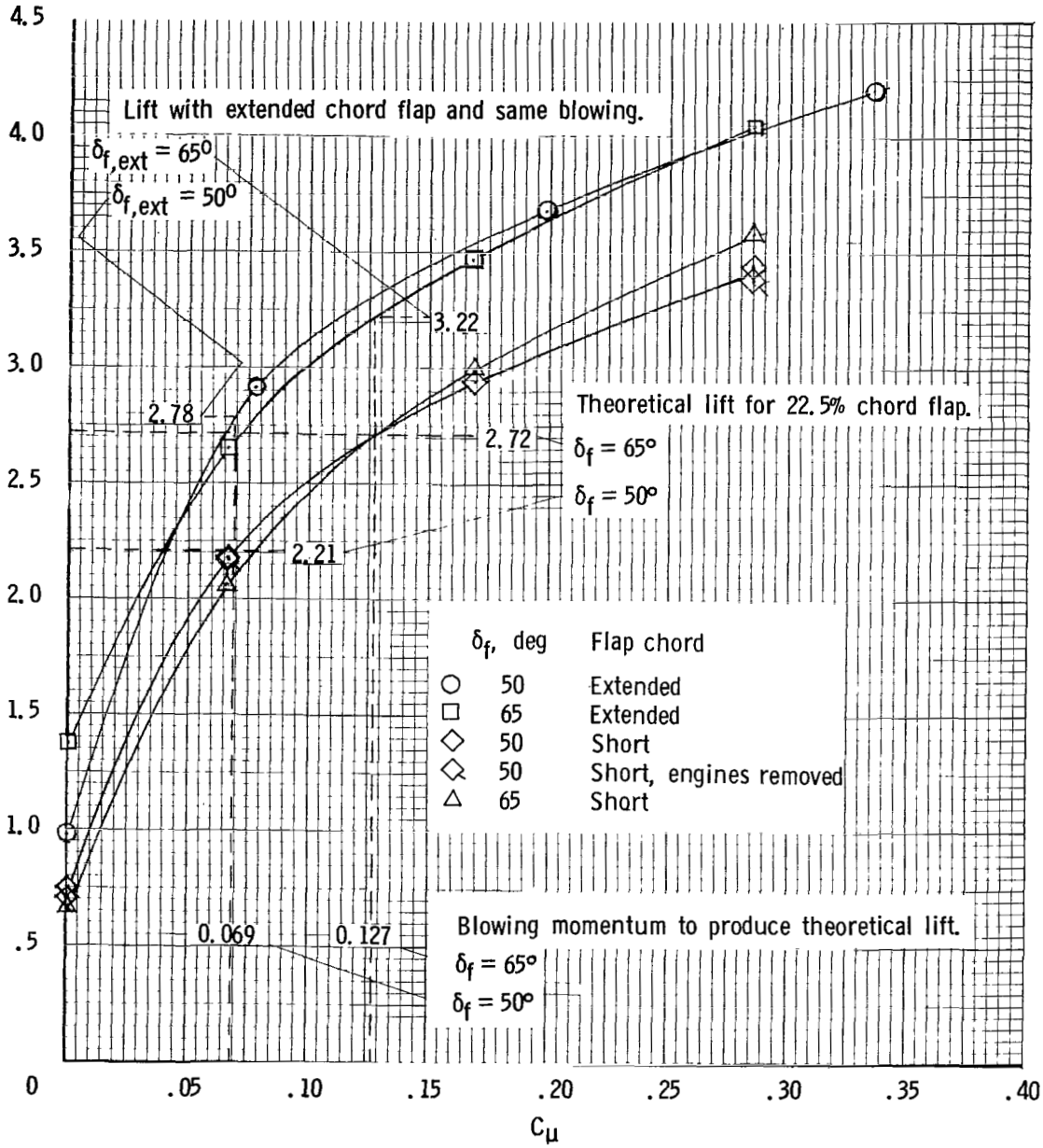

Figure 16.- Lift coefficient as a function of blowing momentum coefficient at $\alpha' = 0^o$, $C_T = 0$, with the effects of flap deflection and flap chord extension.

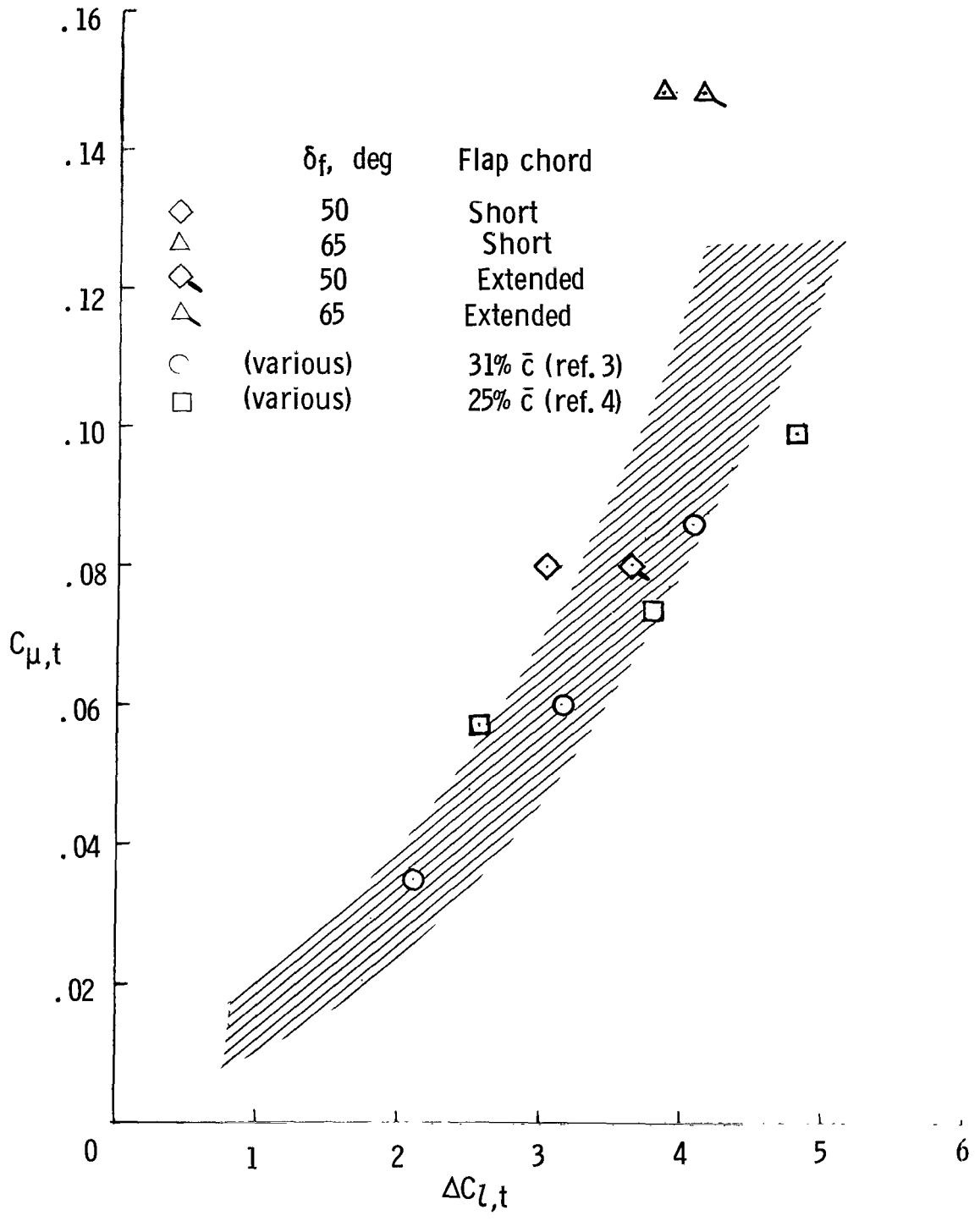

Figure 17.- Blowing momentum coefficient required to produce theoretical lift as a function of theoretical lift increment due to flap deflection.

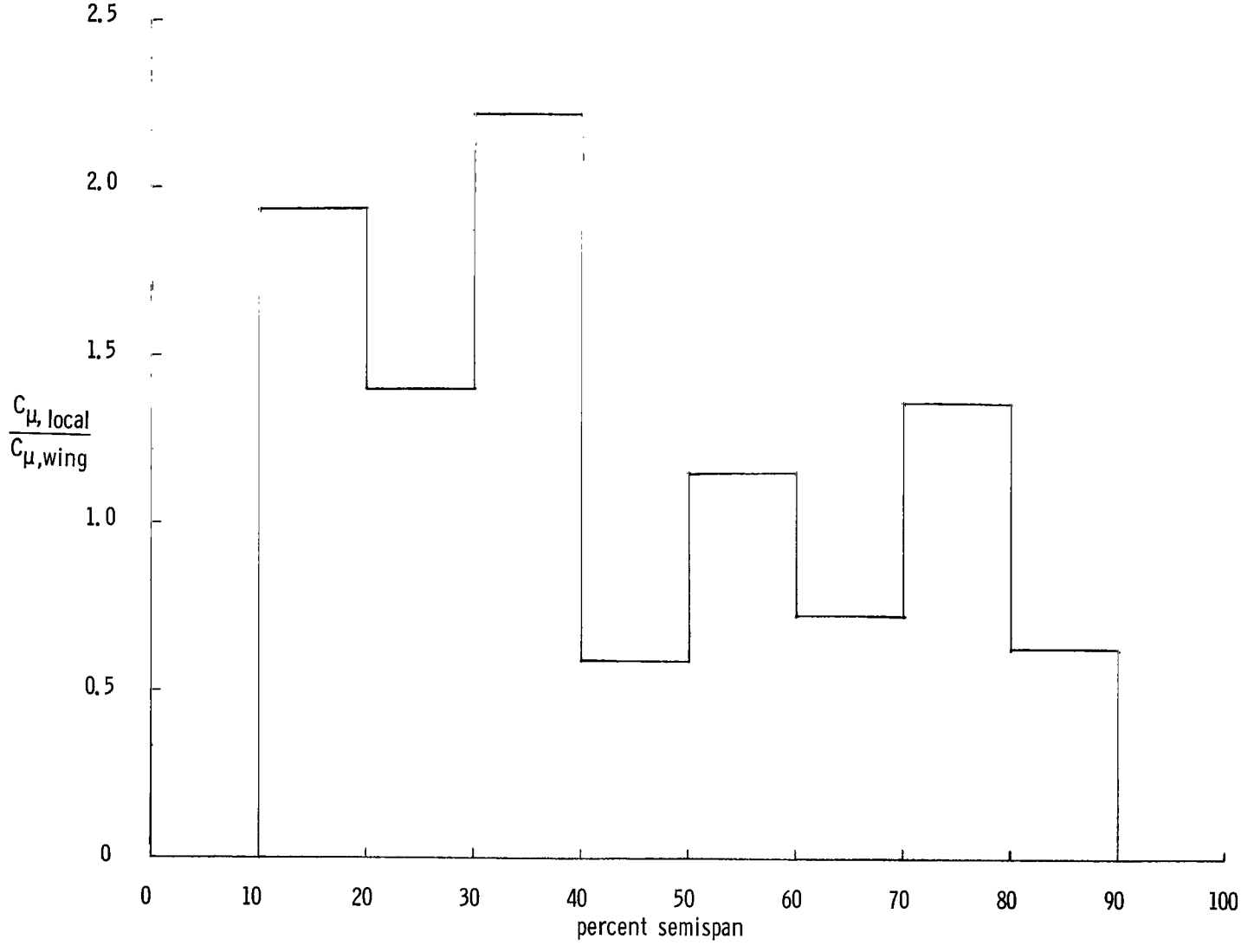

Figure 18.- The spanwise blowing momentum distribution (averaged over each 10 percent of the semispan).

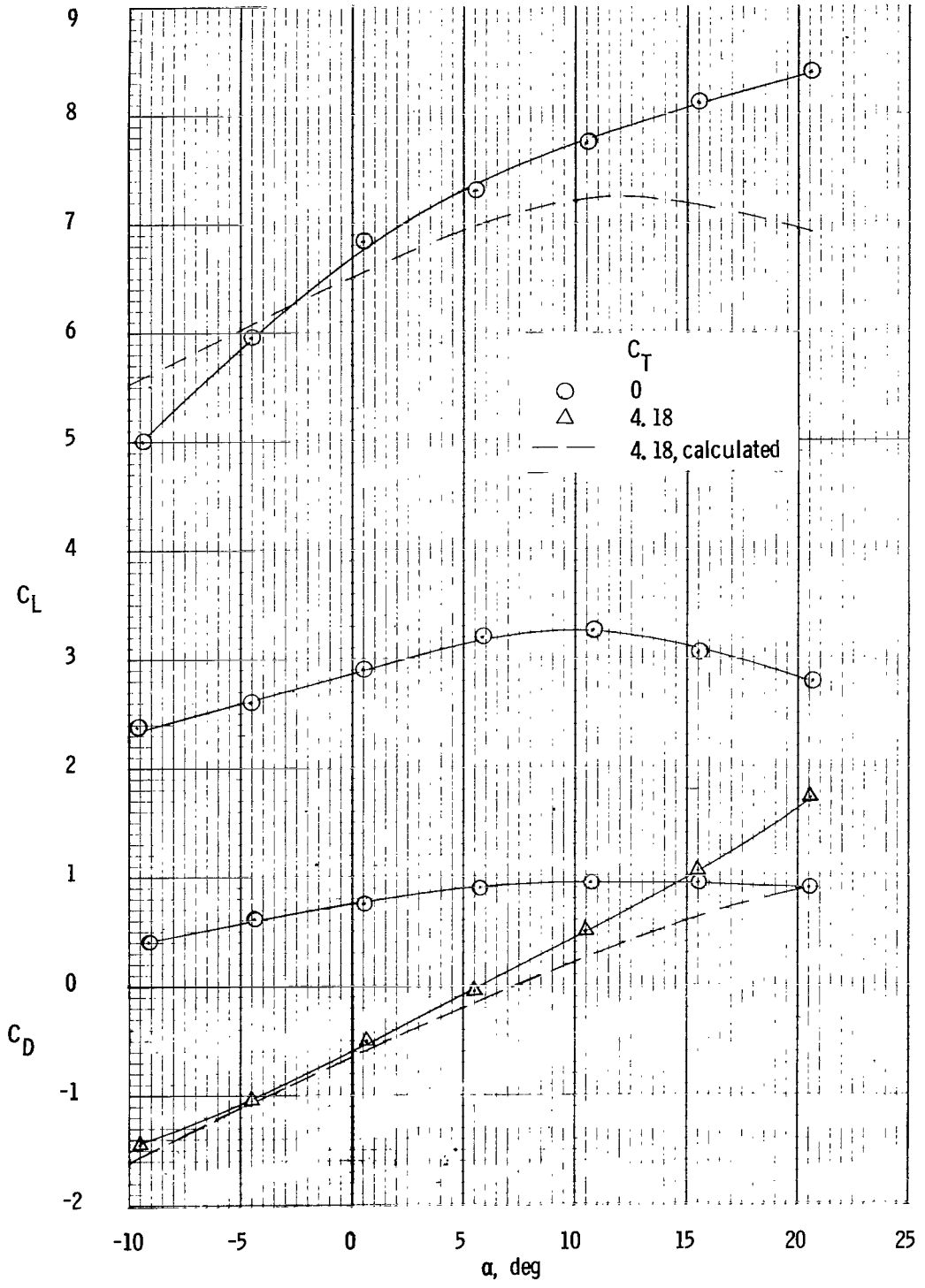

(a) Aft engine position. $C_\mu = 0.078$.

Figure 19.- Effects of engine operation on the lift and drag of the model.

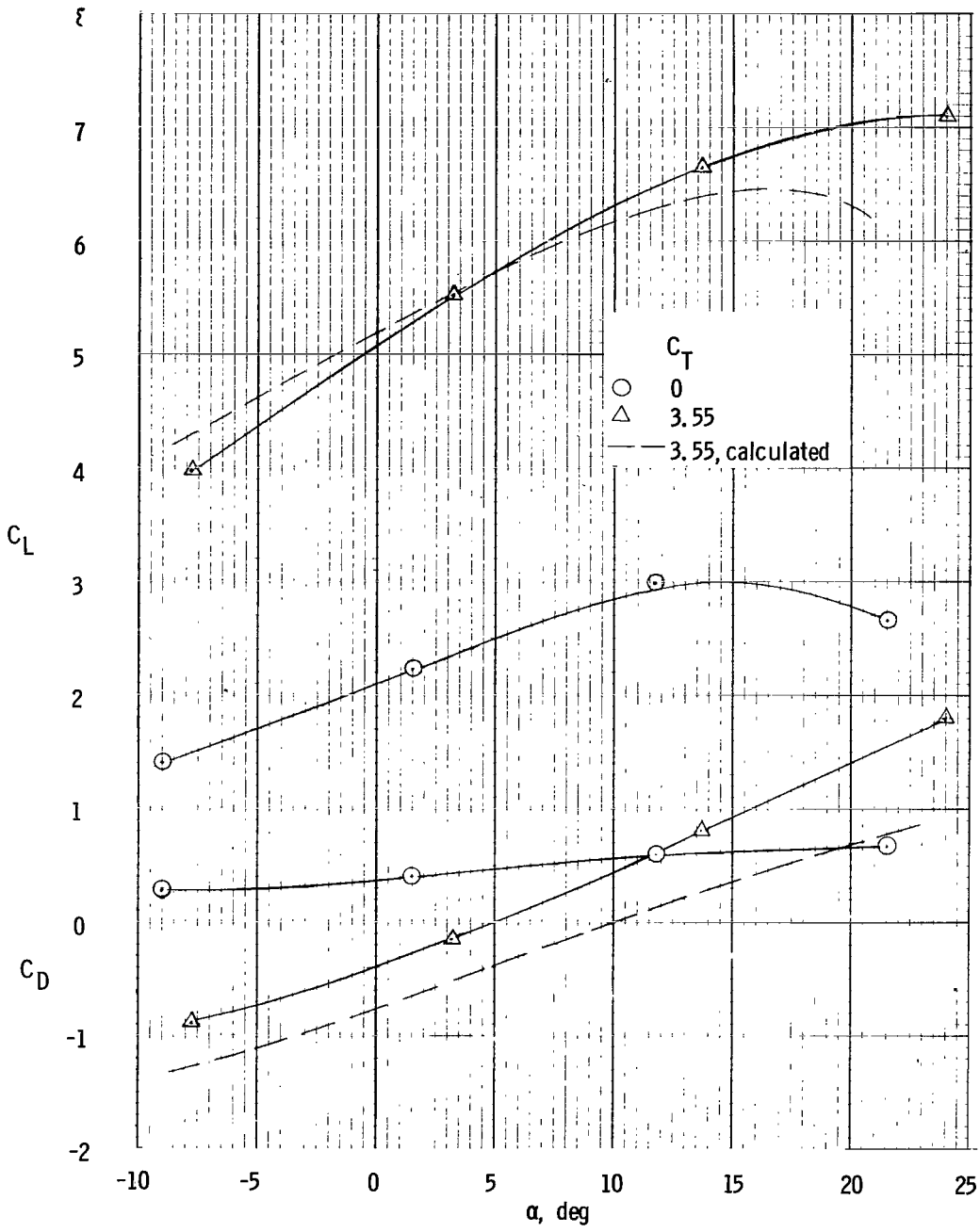

(b) Forward engine position. C_μ = 0.066.

Figure 19.- Continued.

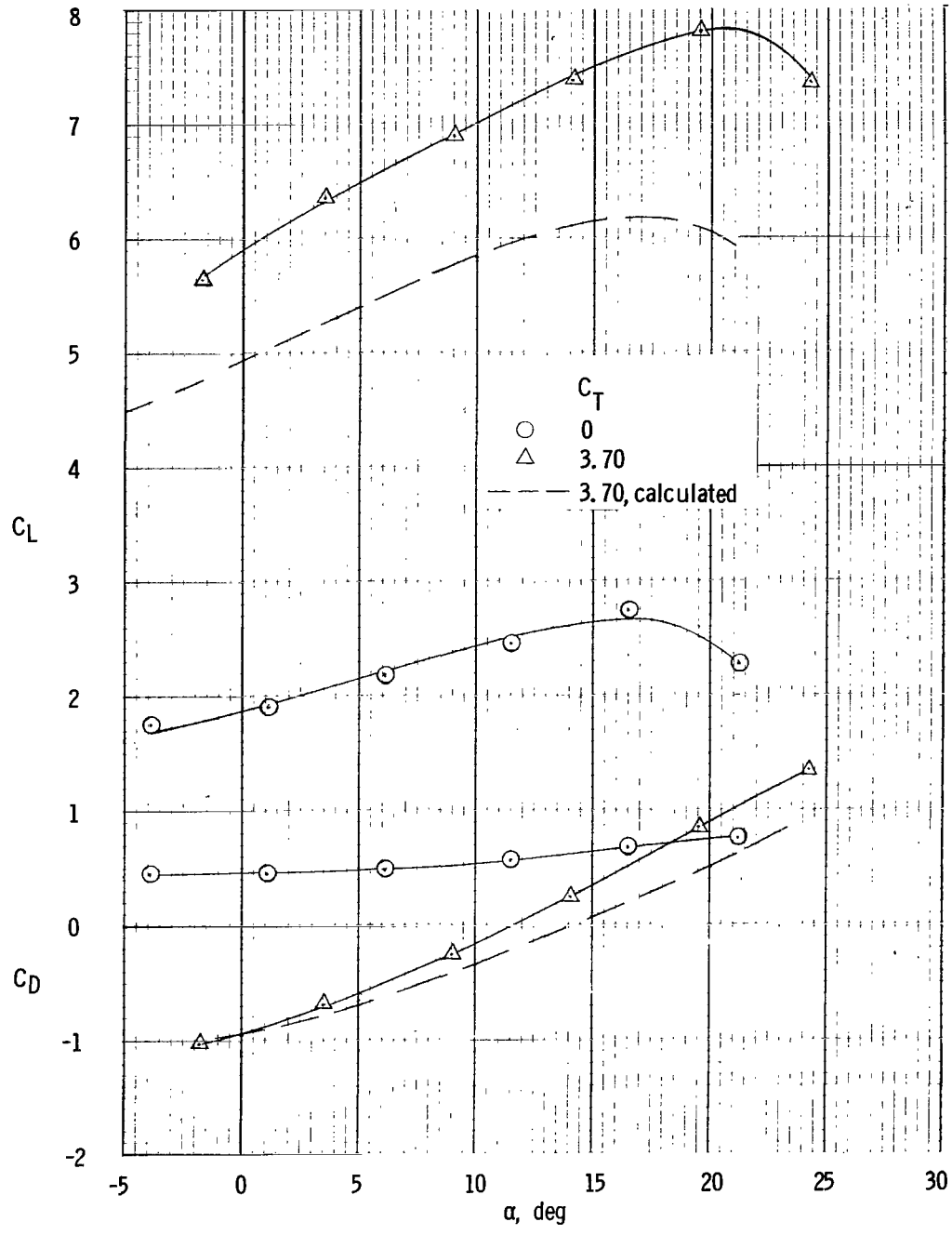

(c) Far aft engine position. $C_\mu = 0.075$.

Figure 19.- Continued.

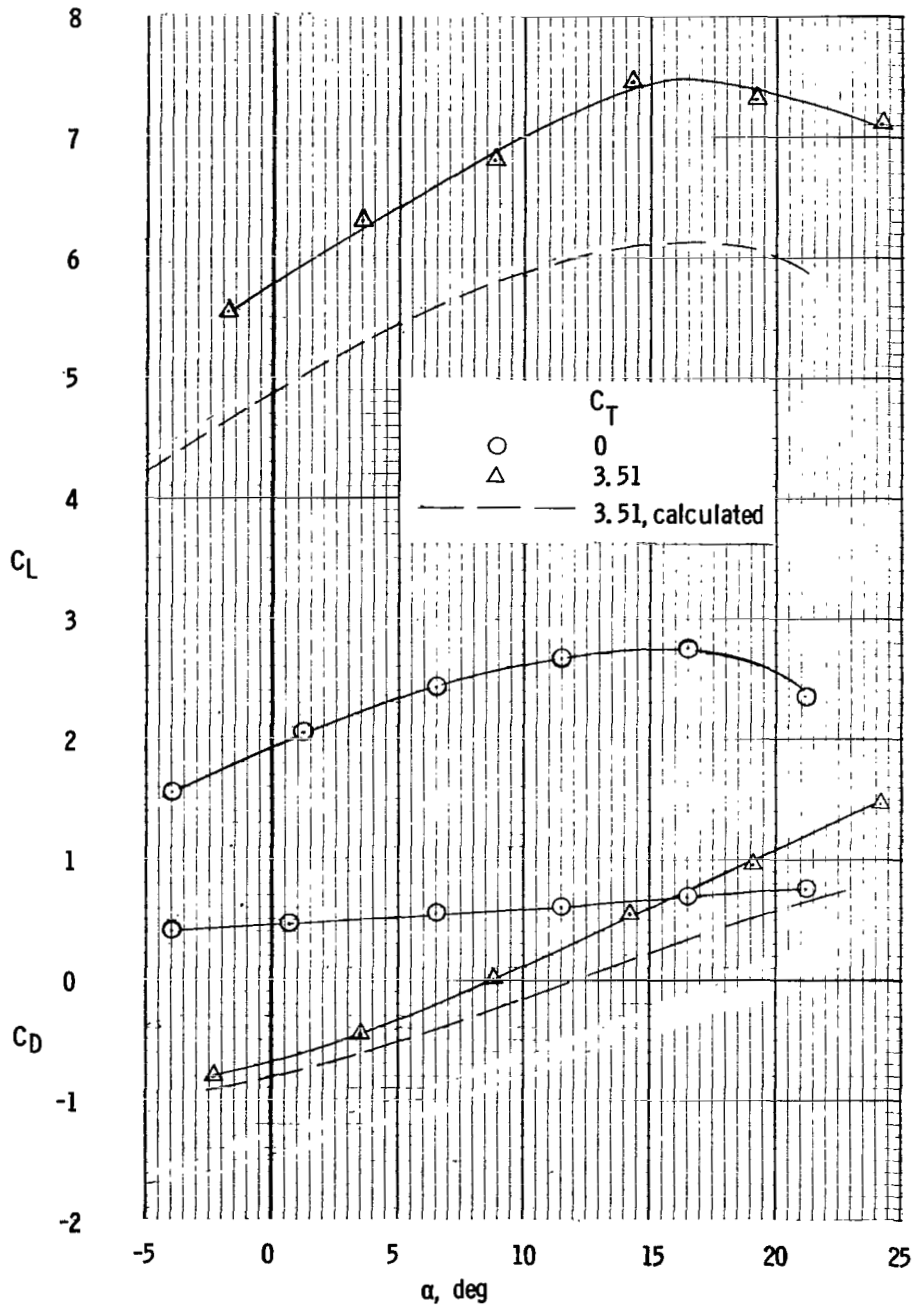

(d) Far aft and tilted engine position. C_μ = 0.075.

Figure 19.- Concluded.

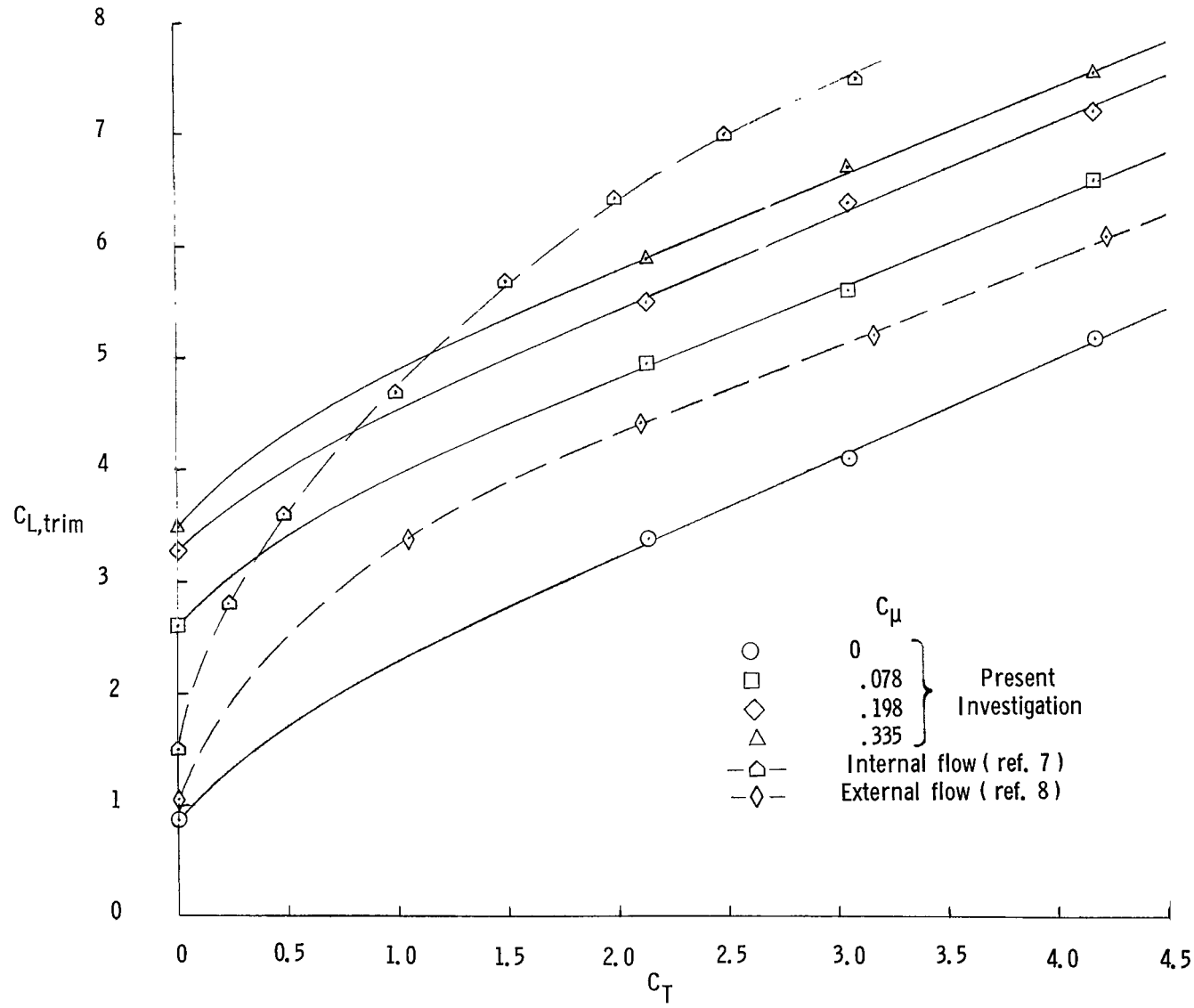

Figure 20.- Trimmed lift coefficient as a function of thrust coefficient for three high-lift models.

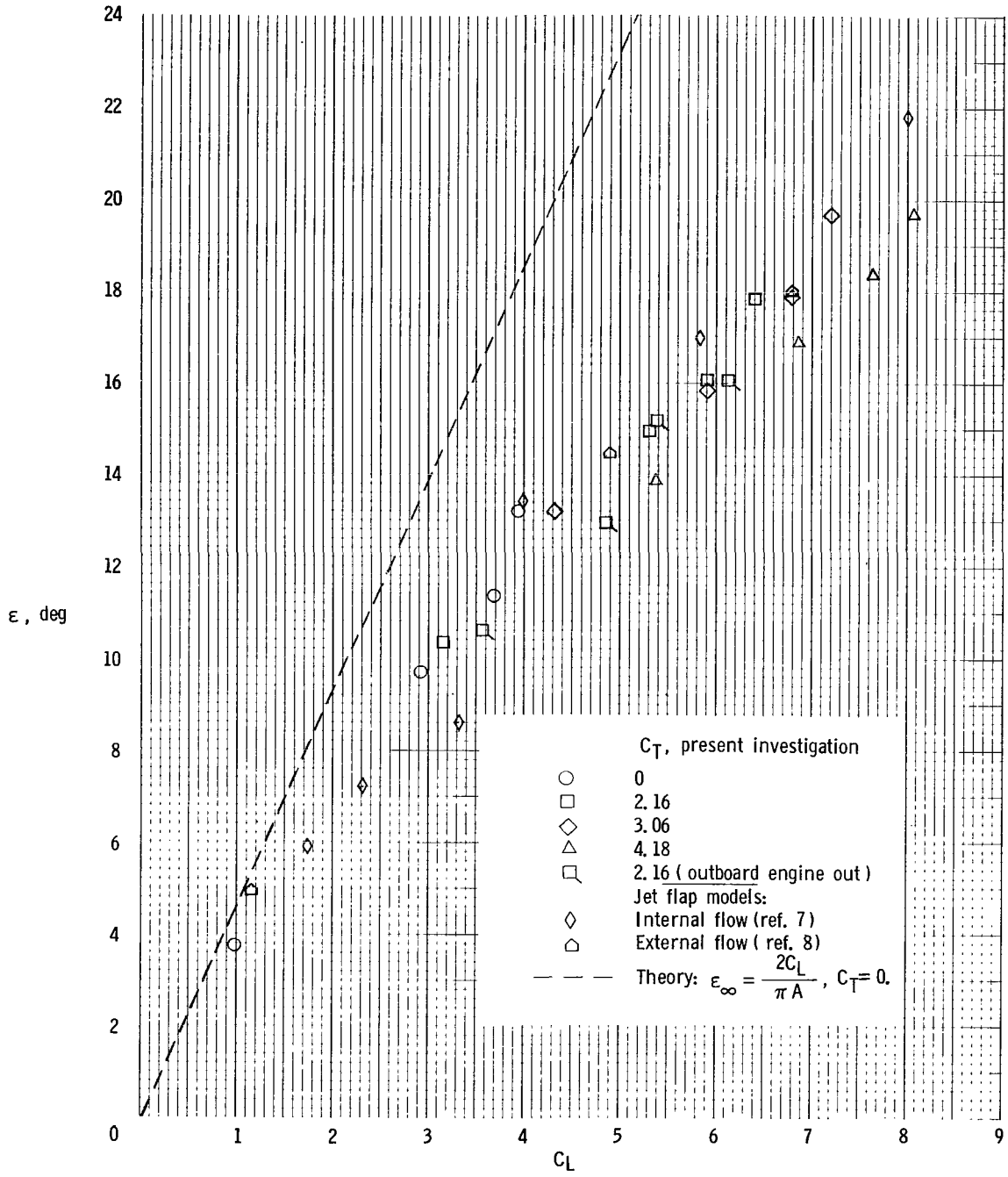

Figure 21.- Downwash measured in the region of a horizontal tail as a function of model lift coefficient at $\alpha' = 0^o$.

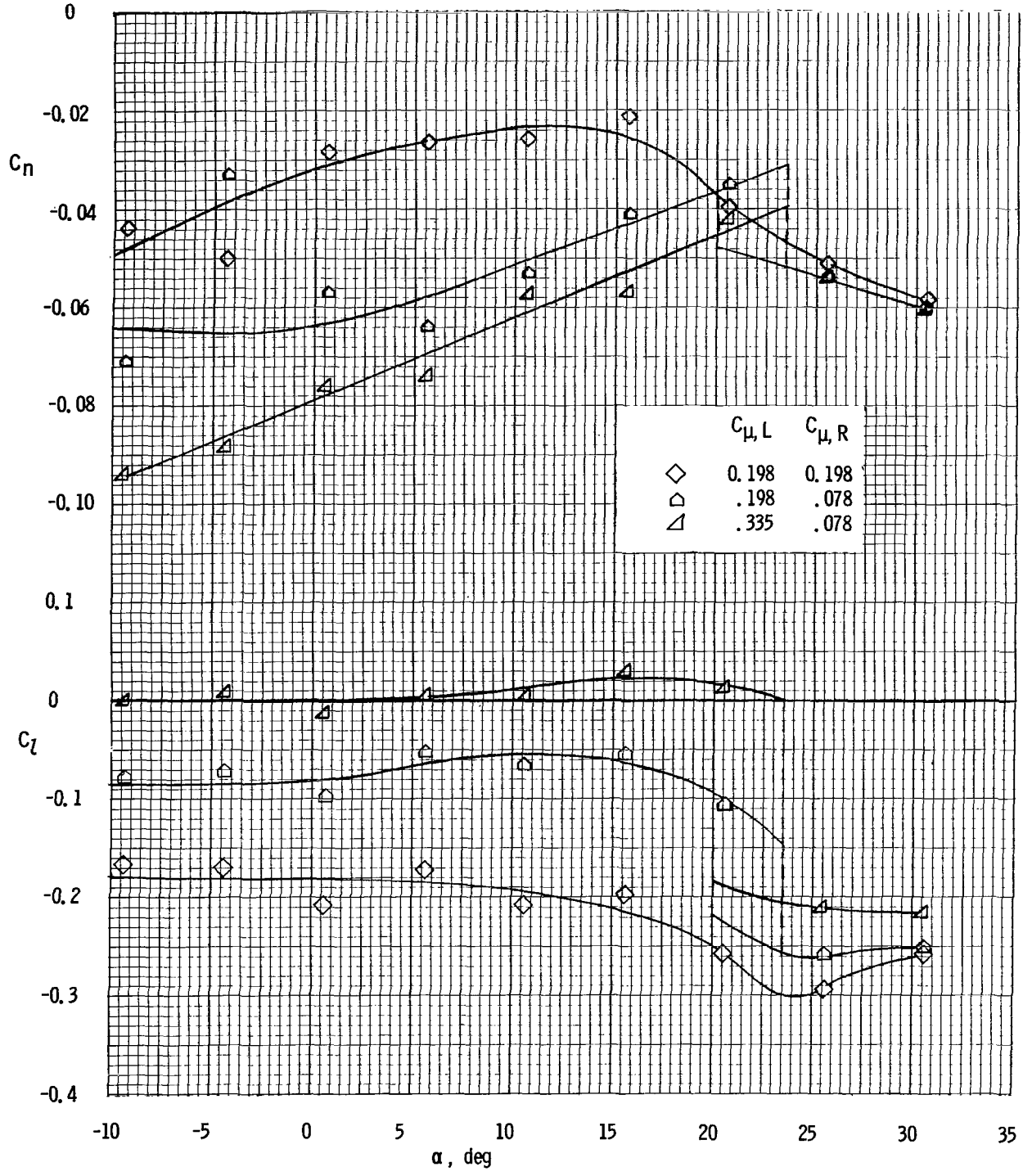

(a) Lateral characteristics.

Figure 22.- Average lateral and longitudinal characteristics of model with aft engines, with the "left" outboard engine inoperative. $C_T = 3.17$; $\delta_{f,ext} = 50^o$.

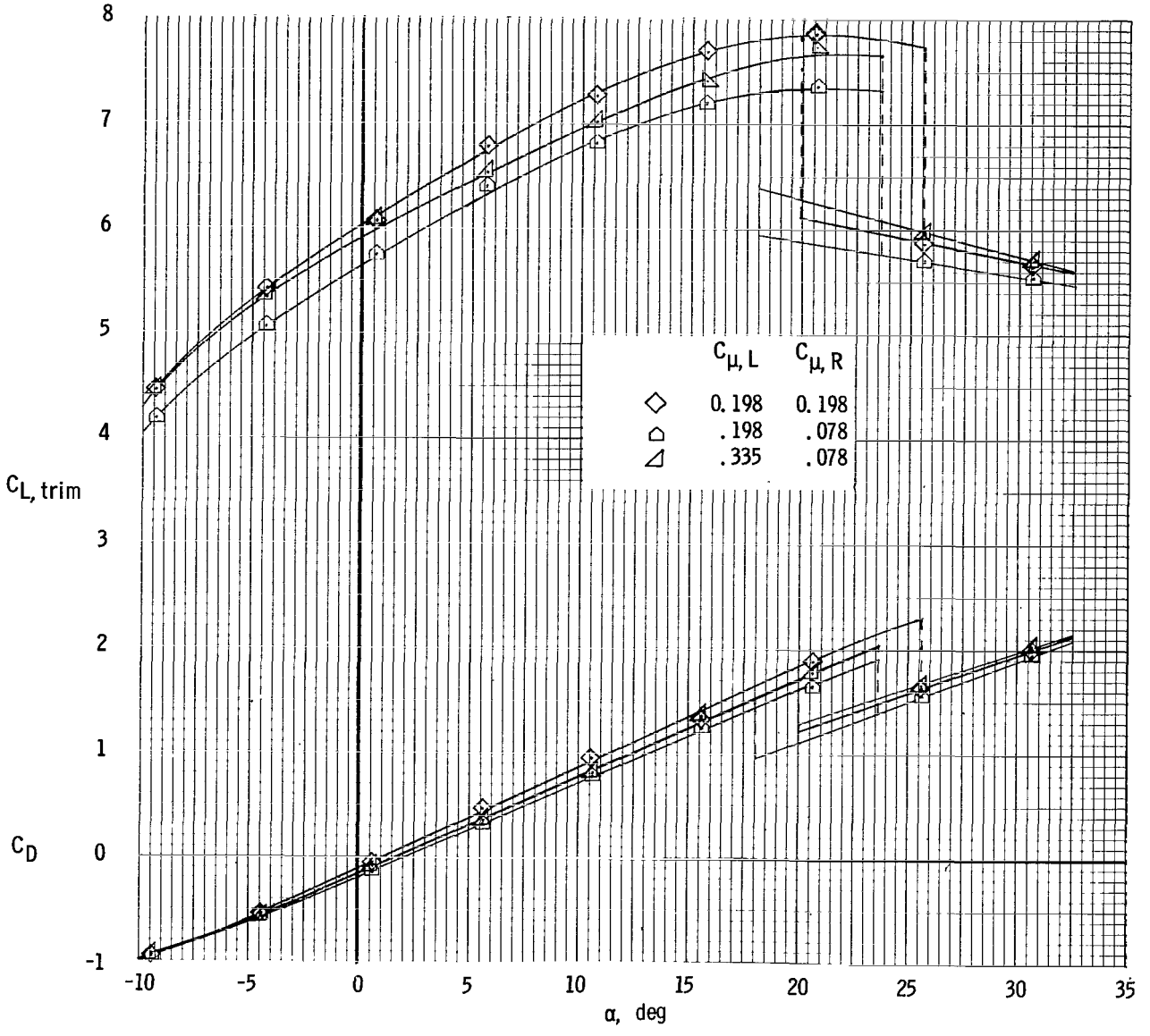

(b) Longitudinal characteristics.

Figure 22.- Concluded.

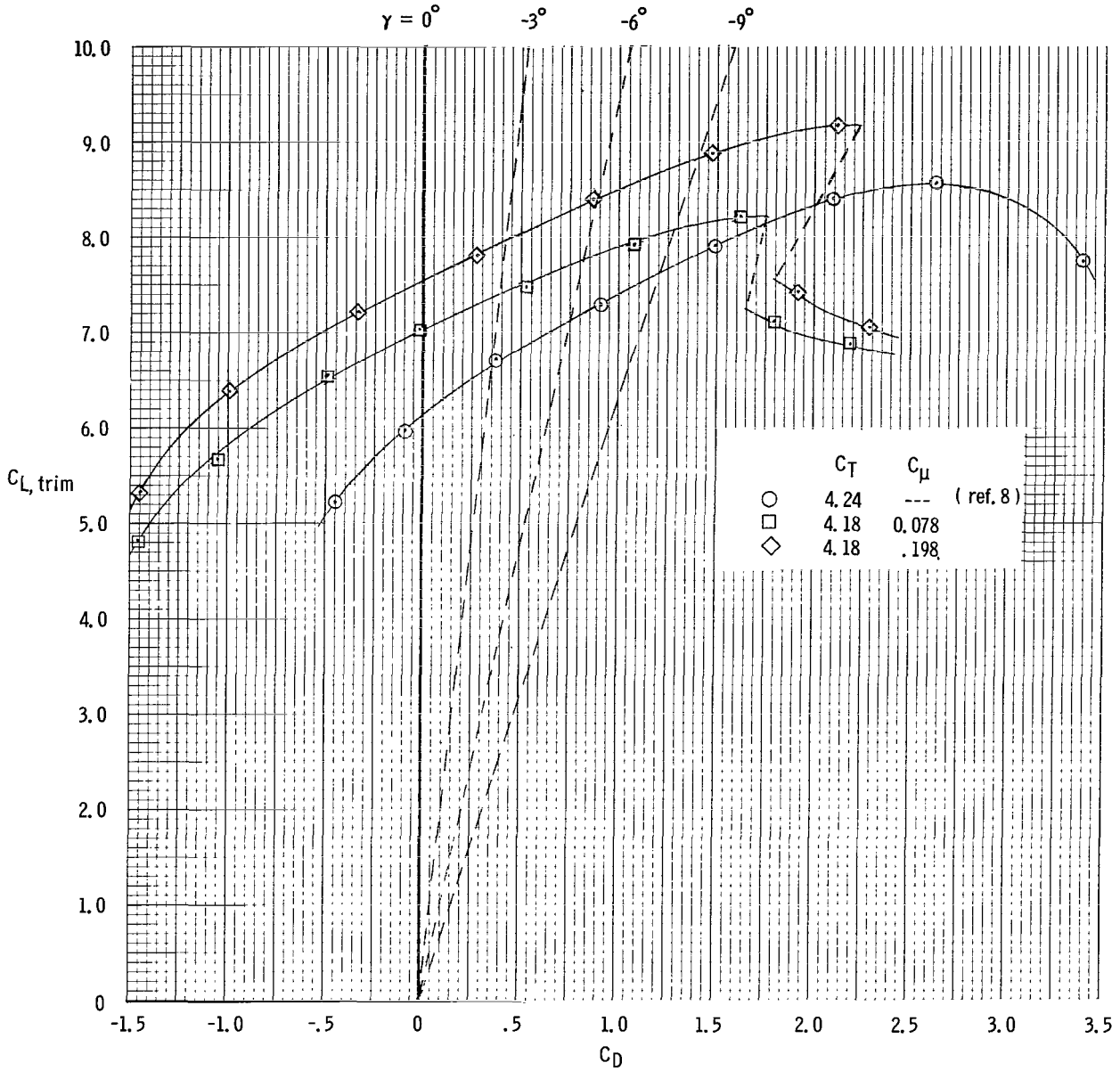

(a) Four engines operating.

Figure 23.- Drag polars for two high-lift models.

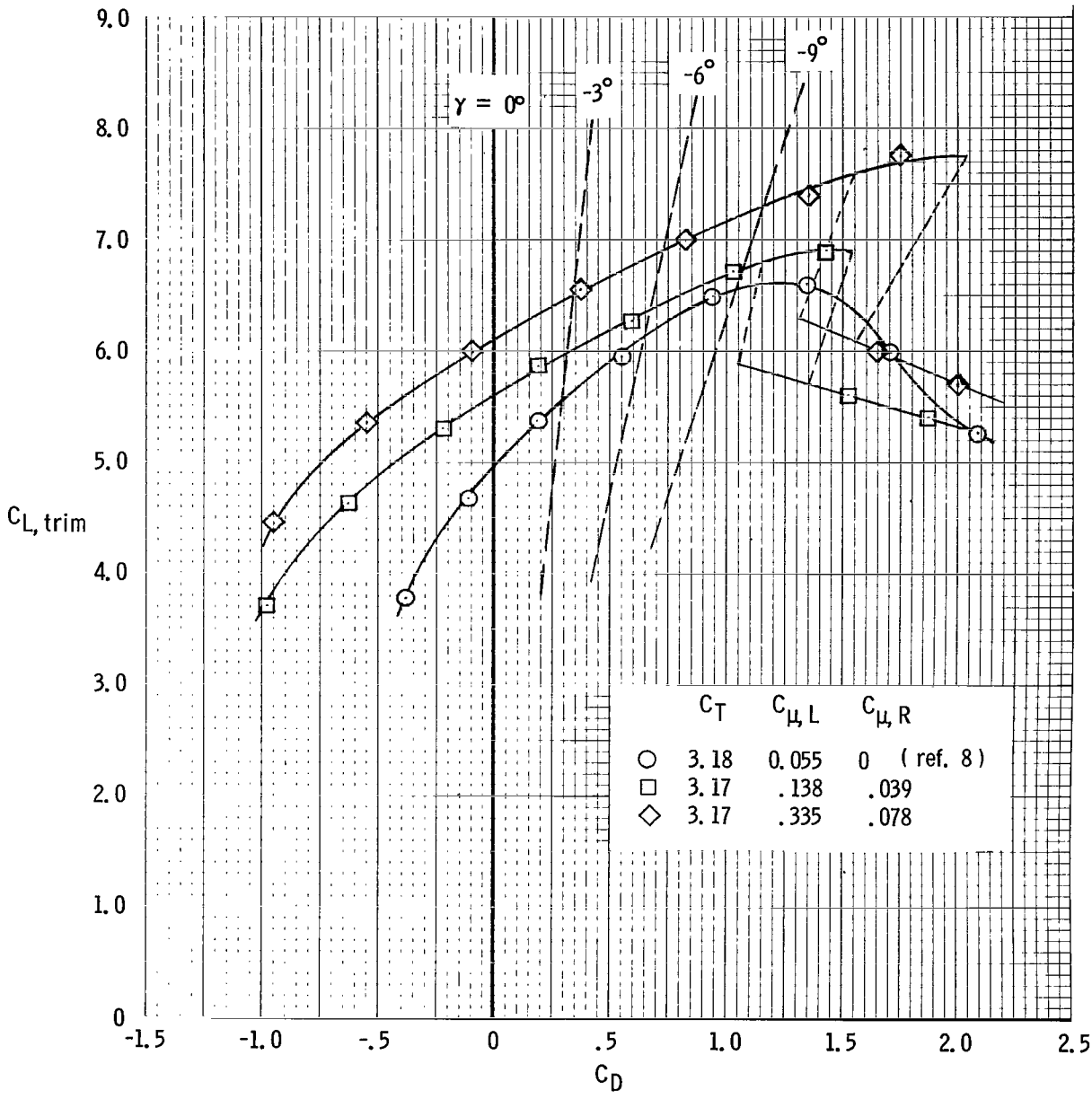

(b) Three engines operating.

Figure 23.- Concluded.

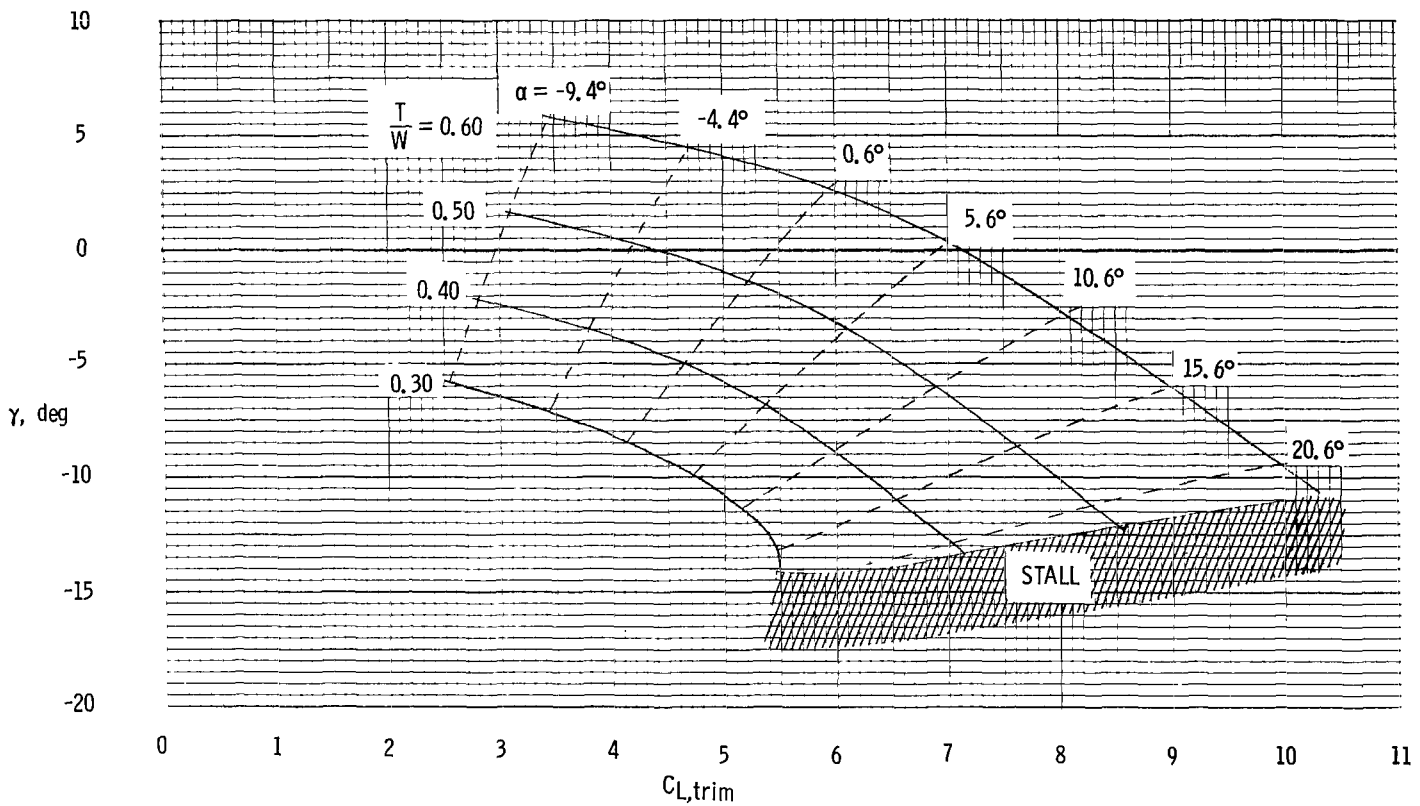

Figure 24.- The flight envelope for $C_{\mu} = 0.078$ (from data of fig. 4(b)).

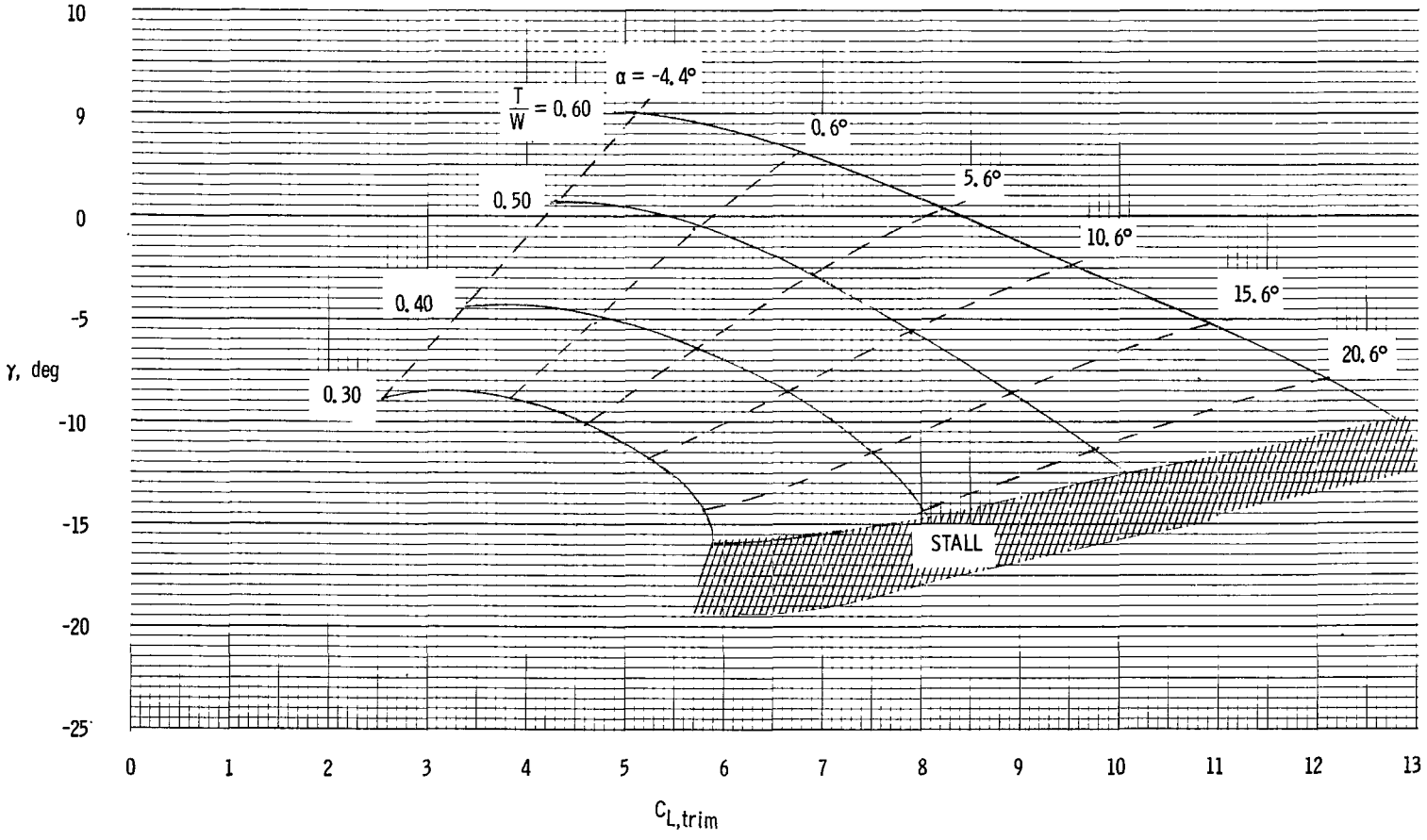

Figure 25.- The flight envelope for $C_\mu = 0.02C_L$ (from data of fig. 4).

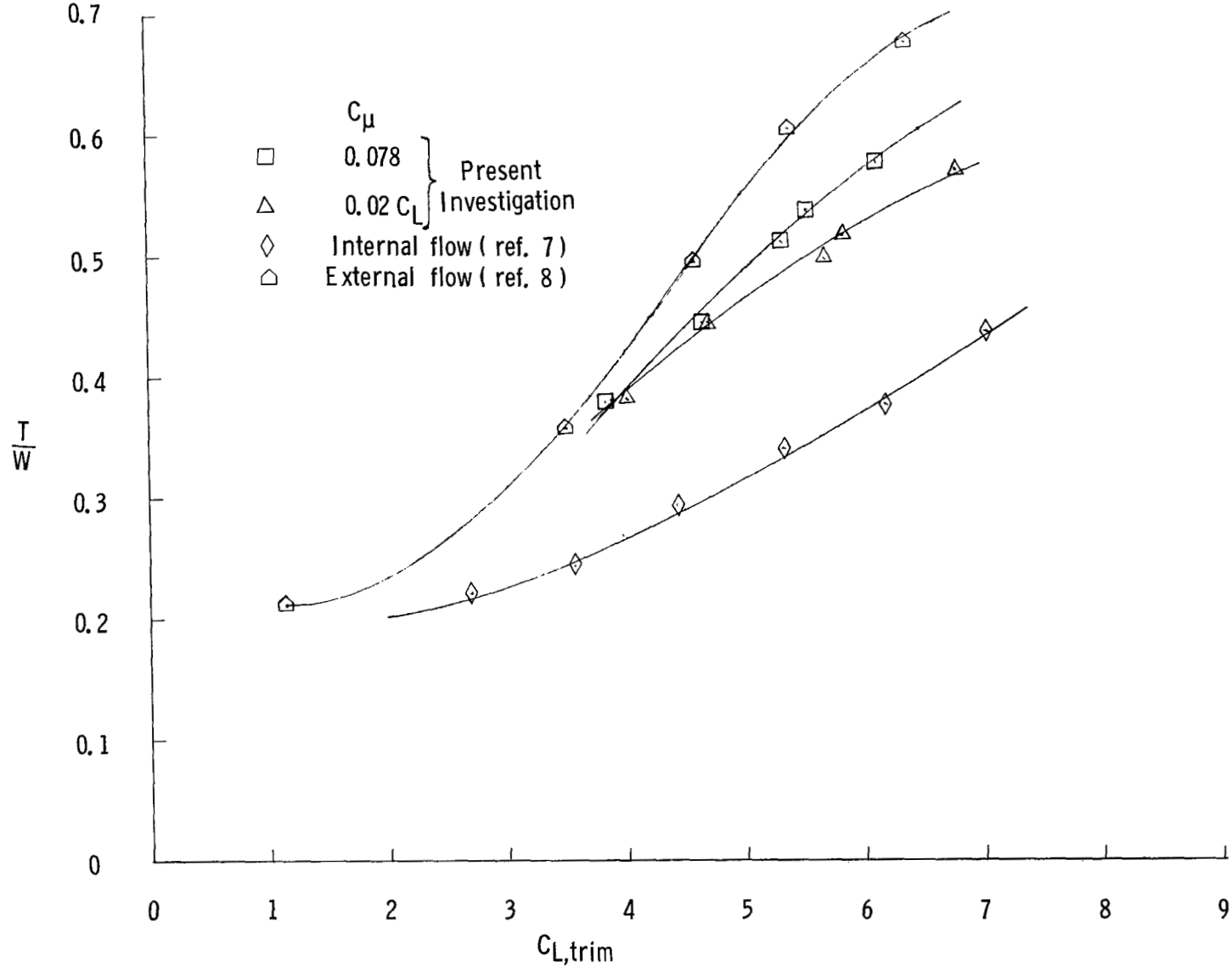

Figure 26.- Thrust-weight ratio required in level flight near $\alpha = 0^{o}$ for three high-lift models.